THE
PHYSICAL REVIEW

A journal of experimental and theoretical physics established by E. L. Nichols in 1893

SECOND SERIES, VOL. 64, NOS. 3 AND 4 AUGUST 1 AND 15, 1943

Neutron Polarization and Ferromagnetic Saturation

F. BLOCH, M. HAMERMESH, AND H. STAUB
Stanford University, Stanford University, California

(Received April 12, 1943)

The transmission of thermal neutrons through magnetized iron has been measured in its dependence upon the percentage deviation ϵ from saturation and upon the thickness d of the sample. In agreement with the theory of Halpern and Holstein it was found that the percentage increase of transmission caused by magnetization is given by $(n^2p^2d^2/2)f(\lambda/\epsilon d)$, where n is the number of iron atoms per unit volume. Writing for the scattering cross section of neutrons with parallel or antiparallel orientation of their spin with respect to the field, respectively $\sigma_0 \pm p$, we find $p=2.0\pm0.1\times10^{-24}$ cm². From the determined value of the length $\lambda=3.2\pm0.3\times10^{-3}$ cm, the linear dimensions of the microcrystals can be determined to be $\delta=1.4\times10^{-4}$ cm. For a thickness $d=3.8$ cm a transmission effect of almost 8 percent was observed if the magnetization was brought to within 2.5 per mille of its saturation value; more than twice this effect can be expected from the same thickness at complete saturation.

I. INTRODUCTION

IT is well known that the scattering cross section of a slow neutron in a magnetized substance depends upon the orientation of its spin with respect to the magnetization. This is due to the interaction of the magnetic moment of the neutron with that of the atoms in the substance.[1] A rigorous theory of the phenomenon is complicated by various factors: It requires a basic assumption concerning the magnetic interaction between a neutron and an electron and a good knowledge of the form factor for the magnetic shells in the atom. It is also necessary to take into account the interference of the neutron waves, scattered from different atoms.

For the purpose of the present paper it is sufficient, however, to note that the cross section for a neutron of given velocity v with its spin parallel or antiparallel to the direction of magnetization can always be written in the form

$$\sigma^+=\sigma_0+p, \quad \sigma^-=\sigma_0-p, \qquad (1)$$

respectively, where σ_0 stands for its value in the unmagnetized substance and where it is merely the theoretical evaluation of p in its dependence on v which is affected by the previously mentioned complications.

Consider now a monochromatic collimated beam of unpolarized neutrons with fixed primary intensity, which has passed through a layer of substance with thickness d: Let I be its intensity if the substance is unmagnetized, $I+\Delta I$ if the substance is homogeneously magnetized. An elementary consideration shows then that

$$\Delta I/I=\cosh npd-1, \qquad (2)$$

where n is the number of atoms per unit volume.

[1] F. Bloch, Phys. Rev. **50**, 259 (1936); **51**, 994 (1937). J. Schwinger, Phys. Rev. **51**, 544 (1937). O. Halpern and M. H. Johnson, Phys. Rev. **55**, 898 (1939). O. Halpern, M. Hamermesh, and M. H. Johnson, Phys. Rev. **59**, 981 (1941).

For $npd \ll 1$ this simplifies to

$$\Delta I/I \cong \tfrac{1}{2} n^2 p^2 d^2. \tag{2a}$$

Because of the smallness of p, Eq. (2a) represents for all practical thicknesses d a sufficiently good approximation; it seems desirable to verify experimentally the quadratic dependence of the "single transmission effect" $\Delta I/I$ upon d and thus to determine the interesting quantity p. This, however, meets with a characteristic difficulty. All neutron polarization experiments, including the ones reported here, have so far been carried out on polycrystalline iron where the condition of validity of (2) and (2a), that the magnetization of the substance be homogeneous, can never be reached ideally. Because of magnetic anisotropy the direction of magnetization will be slightly different in the various microcrystals of a polycrystalline sample, depending upon the orientation of their crystal axis. It would in principle require an infinite magnetizing field to turn the magnetization of each microcrystal completely into the direction of the field and thus to reach perfect saturation and thereby magnetic homogeneity. The first experimental evidence of a strong dependence of the polarization effects upon the degree of saturation of the iron was found by Powers.[2]

It was recently pointed out by Halpern and Holstein[3] that even small deviations from saturation can be understood to cause appreciable deviations from the ideal effect, described by (2). The magnetic moment of a neutron, passing through the polycrystal, will undergo a rapid precession around the direction of the magnetic induction B, which varies slightly from microcrystal to microcrystal, and on the average this will result in a depolarization, counteracting the polarization effect described by (2). It is convenient to introduce the percentage deviation from saturation

$$\epsilon = (M_\infty - M)/M_\infty, \tag{3}$$

where M is the total magnetization of the polycrystal and M_∞ the value which it would have if the magnetization of all the constituent single crystals were perfectly parallel to the magnetizing field. The whole transition from complete depolarization to full polarization will be found to occur in a state of almost complete saturation, and it is therefore sufficient to consider only the situation where $\epsilon \ll 1$. In the limiting case $\epsilon \ll 1$ and $npd \ll 1$, which is the only one of practical importance, the theory of Halpern and Holstein yields instead of (2a) the formula

$$\Delta I/I = \tfrac{1}{2} \cdot n^2 p^2 d^2 \cdot f(\lambda/\epsilon d), \tag{4}$$

where λ is a length, correlated to the linear dimensions of the single microcrystals and where

$$f(x) = 2x^2\left(e^{-(1/x)} + \frac{1}{x} - 1\right). \tag{5}$$

f is a monotonic function of its argument with the property $f(0)=0$, $f(\infty)=1$; it represents the reduction factor of the single transmission effect due to depolarization and reaches unity only asymptotically as ϵ vanishes, i.e., according to (3), as complete saturation is reached.

In the relation between λ and the linear dimensions of the microcrystals there enters the distance which a neutron travels during one full Larmor revolution. Let l be that distance, divided by 2π, i.e., the length of path of a neutron while its magnetic moment undergoes a precession by one radian. It is given by

$$l = v/Bg, \tag{6}$$

where g is the ratio of the magnetic moment of the neutron to its angular momentum, B the magnetic induction inside a microcrystal, and v the velocity of the neutron. Assuming v to be the thermal velocity at room temperature, i.e., $v = 2.5 \times 10^5$ cm/sec., taking $B = 20{,}000$ gauss and the measured[4] value $g = 1.86 \times 10^{+4}$ c.g.s. one obtains from (6)

$$l = 6.7 \times 10^{-4} \text{ cm}. \tag{7}$$

According to Halpern and Holstein one obtains a simple relation between λ and a length δ of the order of the linear dimensions of the microcrystals in the two limiting cases where δ is small or large compared to l. One has

$$\text{for } \delta \ll l: \qquad \lambda = l^2/\delta, \tag{8}$$

$$\text{for } \delta \gg l: \qquad \lambda = \delta/2, \tag{8a}$$

[2] P. Powers, Phys. Rev. **54**, 827 (1938).
[3] O. Halpern and T. Holstein, Phys. Rev. **59**, 960 (1941).
[4] L. Alvarez and F. Bloch, Phys. Rev. **57**, 111 (1940).

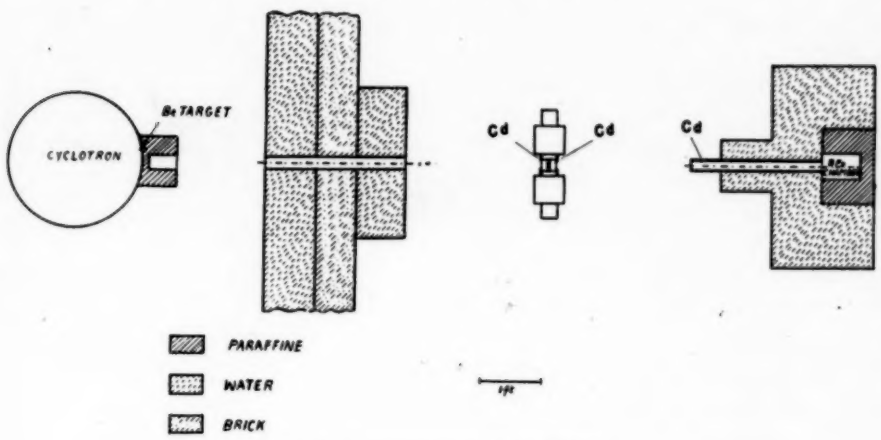

FIG. 1. Arrangement of apparatus.

and for $\delta \gtrsim l$: $\lambda \gtrsim \delta$. (8b)[5]

It is evident, from what has been said before, that a quantitative study of the single transmission effect requires not only the measurement of the percentage change of neutron transmission $\Delta I/I$ upon magnetization of the sample, but an equally accurate measurement of the percentage deviation from saturation, reached in the magnetized state, i.e., of the quantity ϵ, entering in Eq. (4). In the work presented here, we have determined $\Delta I/I$ for a series of values of ϵ and for two different thicknesses d of the same sample of hot rolled steel with the threefold objective:

1. To verify the depolarization theory of Halpern and Holstein.

2. To determine the "polarization cross section" p, defined by (1).

3. To obtain information about the characteristic length λ, entering in (4) and thereby through (8) about the linear dimension δ of the microcrystals in the sample under consideration.

II. MEASUREMENT OF THE SINGLE TRANSMISSION EFFECT

The method and arrangement to determine the single transmission effect were essentially the same as used by Alvarez and Bloch[4] in their determination of the neutron moment. The slow neutrons (see Fig. 1) emerged from a paraffin howitzer directly in front of the target chamber of the Stanford cyclotron[6] where a Be target was bombarded with 2.5-Mev deuterons. In a double screening wall of water-filled tin cans for the absorption of neutrons and of bricks for the absorption of γ-rays, there was in front of the howitzer a circular hole of 2-in. diameter to obtain a collimated neutron beam. This beam passed through a square plate of hot rolled steel between the poles of an electromagnet at right angles to the magnetizing field and from there through a Cd tube of 2-in. diameter and 26½-in. length which provided further collimation to the detecting BF_3 filled ionization chamber. In order

[5] It is clear that Eqs. (8) and (8a) are somewhat qualitative, insofar as δ, although doubtlessly of the order of the linear dimensions of the microcrystals, actually has to be obtained as a very complicated average value, not only over the sizes, but also over the varying geometrical shapes of the microcrystals; furthermore, as pointed out by Halpern and Holstein, there enters in the rigorous calculation the demagnetizing field from the surfaces of the microcrystals. It may be noted that the rigorous and general expression of the length λ entering in (4) can actually be written down as the average value of a certain double integral over the volume of a single crystal; assuming random orientation of the microcrystals it then appears that, due to the demagnetizing field, λ depends also upon the angle θ between the direction of the traversing neutrons and that of the magnetization. In the case corresponding to (8) one obtains

$$\lambda \sim (1+\tfrac{3}{8}\sin^4\theta)^{-1}.$$

In the case corresponding to (8a), the length λ is simply correlated to the total area of the surfaces of all microcrystals. In fact, if we denote by a the mean value of this area per unit volume of the sample, one obtains in this case

$$\lambda = \frac{1}{8a}\left(9+2\cos^2\theta-\frac{\cos^4\theta}{3}\right)^{-1}.$$

In view of the fact, however, that in our arrangement we had always $\theta=\pi/2$ and that the shape and size of the microcrystals are not known the simple formulae (8) and (8a) are quite sufficient for our purposes.

[6] The construction of this 27¾-in. cyclotron by Bloch, Bradbury, Staub, and Stephens was made possible by grants from the Rockefeller Foundation, the Research Corporation, and from various private sources. It was completed in the autumn of 1941, giving under normal operation a beam of about 10 μamp. of 2.5-Mev deuterons.

to prevent neutrons, scattered on the material of the magnet from entering the chamber, Cd diaphragms were placed across the neutron beam both on the front side and on the back side of the magnet. Except for a circular hole of 2-in. diameter in front, the ionization chamber was completely shielded with Cd and embedded in a large block of paraffin, surrounded by a layer of water-filled tin cans, leaving only its front side open. All these precautions were necessary in order to obtain conditions where the majority of the recorded neutrons were of thermal energy and had actually passed through the strongly magnetized region of the steel sample; even with a thickness of steel traversed of as much as 3.8 cm we found that 67 percent of the neutrons recorded were thermal and had passed through the steel. This was ascertained by shielding just the steel sample with Cd and counting as background the remaining neutrons, partly coming from elsewhere and partly consisting of those collimated neutrons above the thermal region which were still able to pass the Cd shield.

The boron trifluoride ionization chamber which was similar to the one used by Powers[2] had an active volume of 2-in. diameter and 6-in. length. It was filled with 2 atmos. of BF_3. The aluminum electrodes consisted of three concentric cylinders. The most inner and outer electrodes were connected to a potential of 3500 v and the intermediate one to the grid of a 38 tube. Porcelain was used as an insulator and during a full year did not seem to cause any trouble. Both leads were brought out of the chamber by spark plugs. The bottom of the chamber was sealed by an ordinary rubber gasket.

The boron-disintegration pulses in the ionization chamber were amplified in a Wynn-Williams type amplifier and, through a scale of 8 or 16 scaling circuit, were recorded by a Cenco counter. Since the collection time for the ions is by no means very small compared to the characteristic time of the amplifier, the number of pulses recorded would strongly depend on the voltage applied to the chamber. This effect can be reduced if one sets the bias of the recording device so that it is below the size of the great majority of the pulses which, due to the imperfect collection, consist of a rather broad group tailing off toward lower energies. The runs were taken with good steady conditions of the cyclotron, and we always operated the beam at such an intensity as to give us a rate of about one count per second on the Cenco counter. In order to be independent of fluctuations of the neutron intensity, we used the monitor of Fryer and Staub,[7] consisting of another small BF_3 ionization chamber and an electronic circuit which periodically recorded intervals of an equal amount of charge having been collected in this chamber. The monitor chamber was surrounded with paraffin and placed at a distance of about one foot from the Be target of the cyclotron. If the monitor would be ideal and no changes in the recording apparatus would occur, one should obviously record the same number of neutrons per monitor interval, independent of the intensity of the cyclotron beam. Actually, we found in the course of our measurements that this number fluctuated by about 1 percent; this may have been due to a slight dependence of the monitor performance upon the position of the target spot or to variations of the line voltage and, therefore, of the collecting voltage of the ionization chamber (which would affect the rate of recorded pulses). In order to eliminate the influence of these slow variations upon the accuracy of our measurements, the magnetizing current was turned on and off in alternate monitor intervals, and the percentage difference of the total number of counts, obtained under the two different conditions was then taken as a measure of the transmission effect.

By a suitable choice of the condenser, discharged by the ionization current in the monitor chamber, the monitor intervals were made of an approximate duration of $1\frac{1}{2}$ min. At the end of each monitor interval conditions were automatically changed through a telephone selector relay, which at the same time switched alternatingly over from one to the other of the two Cenco counters, thus allowing one counter to read all counts taken with and the other counter all those without magnetizing current. Measurements were performed on two samples of hot rolled steel of identical material. They were made of machined square plates of 5×5 cm, one sample having a total thickness of 1.91 cm, the

[7] E. Fryer and H. Staub, Rev. Sci. Inst. 13, 187 (1942).

other of 3.81 cm. Two opposite sides of the square were clamped between the poles of the magnet, its face perpendicular to the neutron beam and carefully centered with respect to it. The runs were taken by setting the magnetizing current to a certain value and then taking counts with this current alternatingly on and off; the setting of the current was frequently changed to ascertain that independent runs with the same value of the current gave statistically consistent results. A sufficiently large number of counts was taken for each setting to obtain the difference of the neutron intensity with and without magnetizing current to within an accuracy of about $\frac{1}{4}$ percent and $\frac{1}{2}$ percent of the intensity for the thin and the thick sample, respectively. The following tabulation gives the results for the two samples and for various values of the magnetizing current up to the maximum value of 15 amperes which we were allowed to pass permanently through our magnet. The transmission effect $\Delta I/I$ and its probable error tabulated here were obtained by dividing the directly observed difference of intensity by $I(1-b)$, where b is the percentage background, taking into account that the background is independent of the presence or absence of the magnetizing current.

Thin sample (1.91 cm). Percentage background $b=6.95\pm0.1$ percent.

Current (amperes)	0.50	0.70	1.0	2.0	3.0
$\Delta I/I$ (percent)	0.43±.13	1.76±.25	1.08±.19	1.65±.24	2.78±.26
Current (amperes)	5.0	9.0	15.0		
$\Delta I/I$ (percent)	3.33±.25	3.27±.25	3.67±.25		

Thick sample (3.81 cm). Percentage background $b=32.8\pm0.81$ percent.

Current (amperes)	1.0	1.2	2.0	3.0	4.0
$\Delta I/I$ (percent)	0.80±.76	−0.06±.72	2.79±.69	3.24±.76	3.27±.77
Current (amperes)	6.9	9.0	11.25	15.0	
$\Delta I/I$ (percent)	4.51±.69	6.39±.71	7.22±.75	7.70±.69	

It is of course important, when dealing with such small effects, that any small source of error be eliminated. Both before and between our runs various tests and blank runs were undertaken to ascertain carefully the reality of the observed effects. The test probably most severe consisted of runs where the iron sample was substituted by a brass sample with a thickness so as to transmit the same number of neutrons as the iron and under otherwise identical geometrical and physical conditions; the fact that we thus obtained well within the accuracy of our transmission effects no difference in the recorded counts, taken with and without the magnetizing current, shows particularly that the stray field of the magnet does not disturb the recording apparatus since it would be even stronger with brass than with iron between the poles.

III. MEASUREMENT OF THE MAGNETIZATION

As pointed out in Section I, it is not the dependence of the single transmission effect upon the magnetizing current, which is of physical interest, but its dependence upon the magnetization of the sample. After carrying out the measurements, described in the previous paragraph, we thus had to devise methods by which the small deviations from saturation reached in our experiments could be determined with fairly good accuracy.

We define the magnetization by

$$M=(B-H)/4\pi, \tag{9}$$

whereby its determination rests upon that of the difference of the magnetic induction B and the magnetic field H in a region where one can expect both to be uniform. The geometrical shape of the square plates used in the transmission measurements is rather inconvenient for such a determination; besides, since their linear dimensions are comparable to those of the poles of the magnet, B and H cannot be expected to be very uniform all over the sample. We had therefore first to determine ϵ in its dependence upon H on a sample of the identical material, but of such size and shape as to give more favorable conditions for the measurement of the magnetization. Such conditions were found in the so-called "isthmus method" which we have used, where a long and thin cylindrical piece of the material under test, the "isthmus," is mounted across the poles of

the magnet and where B and H are measured in its central region. The arrangement is schematically indicated in Fig. 2. The cylindrical isthmus is wound with a winding w_1, consisting of a certain number of turns. On a coaxial brass casing is wound a second winding w_2, consisting of the same number of turns. If we assume B and H to be parallel to the cylinder axis within the cylindrical sections, enclosed by w_1 and w_2, their changes ΔB and ΔH upon a sudden change of the magnetizing current can be determined from the ballistic throw of a galvanometer G, connected in series with the windings. Indeed, let A be the wound area of the isthmus, a_1 and a_2 the wound areas of the air space surrounded by the windings w_1 and w_2, respectively; let, further, D_1 be the ballistic deflection of the galvanometer if connected in series with w_1 and D_2 the deflection if G, w_1, and w_2 are all three connected in series, the latter two such that their induced electromotive forces oppose each other. Taking the galvanometer readings upon variation of the magnetizing current between the same two limits, one has then

$$\Delta H=\frac{D_2}{k(a_2-A-a_1)}, \tag{10}$$

$$\Delta B=\frac{1}{kA}\left(D_1-\frac{a_1}{a_2-A-a_1}D_2\right). \tag{10a}$$

The constant k depends upon the characteristics of the galvanometer and other elements of the circuit; we determined it in the usual way by calibration with an air coil. Its actual value, however, does not enter in the ultimate determination of ϵ.

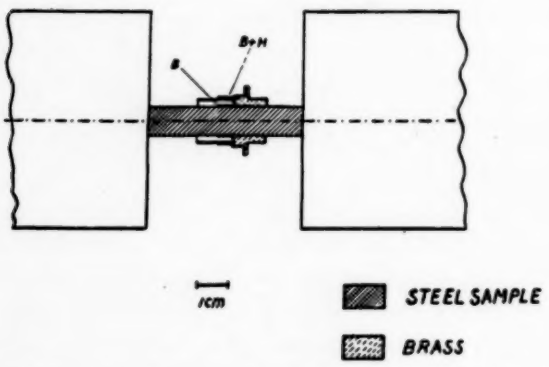

FIG. 2. Arrangement of windings and sample for the determination of H and B.

The requirement of accuracy in the determination of the quantities (10) and (10a) is evidently quite stringent since their difference $\Delta B-\Delta H$, which determines the change of magnetization, becomes increasingly smaller upon approach to saturation. Changing, for example, the magnetic H field in the neighborhood of 3000 gauss by 300 gauss, we found the corresponding change of $B-H$ to be about 10 gauss, or $\frac{1}{2}$ per mille of its saturation value. In order to ascertain this change to within 5 gauss or $\frac{1}{4}$ per mille of saturation, it requires therefore a determination of the deflections D_1 and D_2 and of the wound areas A and a_2 such that in the difference of (10) and (10a) they do not involve an error of more than 5/300 or about $1\frac{1}{2}$ percent, i.e., each of these quantities must be known with an accuracy of about 1 percent; a_1 which itself represents only a small correction, due to the finite thickness of wire and insulation of winding w_1, has to be known with correspondingly less accuracy. While it is true that the determination of these quantities with the required accuracy demands great care, it is not prohibitive, and we feel confident that we have succeeded. The determination of the wound areas requires merely well-machined cylindrical surfaces, the diameter of which can be easily measured with a micrometer; the correction for wire thickness and insulation must, of course, be applied after remeasuring the diameter when the wire has been wound on. A sufficient accuracy of the galvanometer reading can be ascertained by patient repetition.

The only remaining source of error can arise if B and H are appreciably non-uniform in the investigated central region of the isthmus. While it is true that in the absence of the isthmus the magnetic field in this region is sufficiently uniform and that its distortions by the isthmus become negligible if the isthmus is thin enough, one has nevertheless to make sure that this uniformity is maintained under the conditions of the experiment. We have considered as criterion for sufficient thinness of the isthmus that making the isthmus still thinner does not change the result. After carrying out the measurements with an isthmus of 5.1-cm length when its own diameter was 0.961 cm and that of the brass casing 1.430 cm, we have repeated them once more with another isthmus of the same length and the two

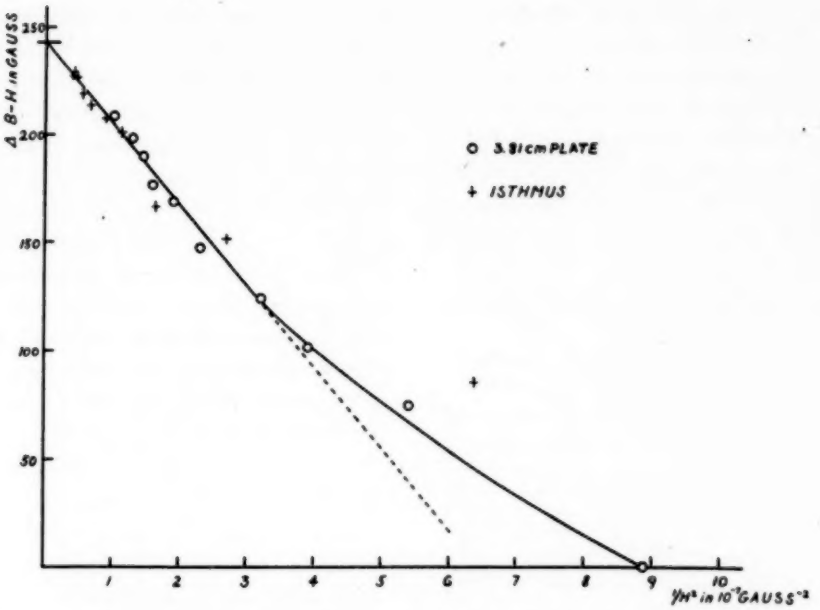

FIG. 3. Change of $B-H$ *versus* $1/H^2$. The actual value of $B-H$ is obtained by adding to the value of $\Delta(B-H)$ the constant value 19,800 gauss.

diameters, respectively 0.638 cm and 0.946 cm. Since the results, obtained for the approach to saturation, agreed in the two cases within the experimental error, it seems safe to assume that the error involved from non-uniformity was negligible.

There is another independent and rather severe test for the correct determination of the wound areas and for the uniformity of H and B. If the magnetizing current is more and more increased, and the corresponding increases of B and H are computed from (10) and (10a), it must turn out that while both B and H keep on increasing, their difference must converge towards a finite value, which through (9) determines the saturation value of the magnetization M. Both non-uniformities and errors in the wound areas would manifest themselves in an unlimited increase or decrease of the computed value of M. Unless there is an accidental cancellation of these errors, the very fact of the computed value of M converging towards a finite saturation value indicates the correctness of the performed measurement.

From the theoretical side one can predict the law of approach to saturation as long as one assumes that in the magnetization process of a macroscopic sample the magnetic moment of each microcrystal is changed only in its orientation but not in its magnitude. One obtains then for strong fields

$$M = M_\infty - a/H^2, \tag{11}$$

where a depends upon the material[8] and is a slowly varying function of H.

This law has been verified with great accuracy by Czerlinsky;[9] the small deviations which he has observed for very strong magnetic fields indicate indeed a slow increase of a with H. Within the experimental error we were able for high magnetic fields to represent our results by a law of the form (11) with a constant a, indicating that for the material and the fields used by us, the above-mentioned deviations were of no importance. In evaluating the percentage deviation ϵ of Eq. (3), we have used the deviation of the magnetization from that value, obtained by (11), upon extrapolation to $H=\infty$ with constant a.[10]

[8] R. Becker and W. Doring, *Ferromagnetismus* (Springer, Berlin, 1939), p. 167. T. Holstein and H. Primakoff, Phys. Rev. **59**, 388 (1941).

[9] E. Czerlinsky, Ann. d. Physik **13**, 89 (1932).

[10] It should perhaps be mentioned that it is essential to use (11) for extrapolation; the increase of magnitude of the microcrystalline magnetization, which will actually occur in very strong fields and which is omitted in that formula, has no effect upon the depolarization and on the value of ϵ, to be used in the sense of the theory. Our

In Fig. 3 we have plotted $\Delta(B-H)$ and its percentage deviation from saturation ϵ in their dependence on the magnetic field H, as obtained by the isthmus method for hot rolled steel. Although deviations of the order of one-tenth of a percent are to be considered significant in this plot, we do not claim nearly such an accuracy for the absolute determination of the extrapolated value of the magnetic saturation.

Once we have established the relationship between ϵ and H by the isthmus method, the problem of assigning the proper value of ϵ to a given magnetization current in the single transmission experiments, described in Section II, becomes comparatively simple. It reduces to the determination of the magnetizing field H for a given value of the current, the percentage error in ϵ thus involved being merely of the order of that of H. To determine the field in the central region of the plate, through which the neutrons pass in the transmission experiment, we used a thin rectangular search coil, placed right alongside the face of the plate. Its wound area was again effectively determined by calibrating the ballistic throw of the galvanometer against that produced by the known field at the center of a current solenoid. The position of the search coil was not very critical since, moving it over the whole area through which neutron passage occurs, we did not find the field to vary by more than about 3 percent; with the same accuracy we found the field along the entrance and exit face of the plate to be the same. In addition, we had to convince ourselves that between these two faces there were no appreciable deviations of H; since the thicker sample consisted actually of three, the thinner of two separate plates, this could be done by spacing these plates just enough to insert other rectangular search coils between them. It was thus easy to determine any possible difference of H between the plates and along their outside faces. Having found no such difference within the accuracy of our measurements of a few percent, we see no reason to doubt that the field H was sufficiently uniform throughout the passage region of the neutrons, and that for a given magnetizing current we had that percentage deviation from saturation which from the previous isthmus measurements corresponded to the field measured for this current.

TABLE I. Percentage deviation (ϵ) from saturation.

Thin sample (1.91 cm) Current (amp.)	H (gauss)	ϵ (percent)	Thick sample (3.81 cm) Current (amp.)	H (gauss)	ϵ (percent)
0.50	592	2.50	1.0	570	2.56
0.70	795	1.70	1.2	678	2.01
1.0	1100	1.16	2.0	1060	1.21
2.0	1690	0.63	3.0	1360	0.87
3.0	2140	0.41	4.0	1590	0.69
5.0	2710	0.25	6.9	2060	0.44
9.0	3370	0.17	9.0	2280	0.38
15.0	3980	0.12	11.25	2480	0.30
			15.0	2770	0.24

Table I gives the values for H and the corresponding ϵ for those currents for which the transmission effect was measured.

While measuring the magnetizing field for these samples, we measured at the same time the induction by winding the plates in the central region and observing the induced current pulse in the galvanometer. The values for the magnetization thus obtained agreed with those of the isthmus measurements for percentage deviations from saturation above about 0.5 percent. For smaller deviations we found systematic and ever-increasing differences, evidently arising from the fact that under the unfavorable geometrical conditions, presented by the square plates, the knowledge of the wound areas and the uniformity of B and H became insufficient to make the determination for the smaller deviations reliable. The agreement was, however, sufficient to indicate that there were no accidental differences in the material used for the isthmus and the square

TABLE II. Dependence of single transmission effect $\Delta I/I$ upon ϵ.

Thin sample (1.91 cm) ϵ (percent)	$\Delta I/I$ (percent)	Thick sample (3.81 cm) ϵ (percent)	$\Delta I/I$ (percent)
2.50	0.43±.13	2.56	0.80±.76
1.70	1.76±.25	2.01	−0.06±.72
1.16	1.08±.19	1.21	2.79±.69
0.63	1.65±.24	0.87	3.24±.76
0.41	2.78±.26	0.69	3.27±.77
0.25	3.33±.25	0.44	4.51±.69
0.17	3.27±.25	0.38	6.39±.71
0.12	3.67±.25	0.30	7.22±.75
		0.24	7.70±.69

extrapolation with constant a is very nearly correct, since variations would make themselves noticeable only in considerably higher fields.

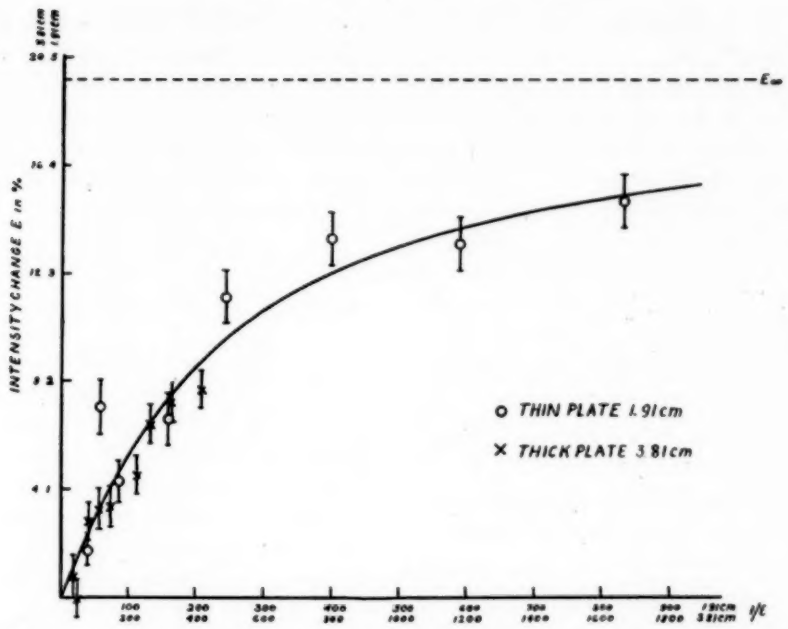

FIG. 4. Single transmission effect for both plate thicknesses as a function of deviation from saturation. Heavy line represents best fitting theoretical curve with corresponding saturation effect E_∞.

plates, and that we could indeed expect the same relation between ϵ and H for both.

IV. DISCUSSION OF THE RESULTS

From the measurements, reported in Section II and Section III, we are now able to give the final results in Table II, which represents the dependence of the single transmission effect $\Delta I/I$ upon the percentage deviation from saturation ϵ for our two samples.

These results are plotted in Fig. 4; the ordinates are the single transmission effects $E=\Delta I/I$, the abscissae the corresponding values of $1/\epsilon$. Since the ratio of the thicknesses d of the two samples is just about 1 : 2, we have chosen a representation in which for the thick sample the scale of the abscissae is reduced by a factor 2, that of the ordinates by a factor 4.

One can see that by this transformation the points obtained for the two samples fall within the statistical error into the same pattern; this shows that in agreement with Eq. (4) the polarization effect is proportional to the square of the thickness and that the depolarization factor f depends merely upon the product ϵd. Quite independent of the special form (5) of the function f, we consider this agreement as a first important test for the correctness of the theory of Halpern and Holstein.

The complete quantitative test of this theory is evidenced by the drawn out curve of Fig. 4. It represents the best fitting member of the two-parameter family of curves which one obtains from (4) and (5) by varying the two unknown constants p and λ. The thus experimentally determined values of these two constants are with their estimated errors

$$p=2.0\pm.1\times10^{-24}\ \text{cm}^2, \tag{12}$$

$$\lambda=3.2\pm.3\times10^{-3}\ \text{cm}. \tag{13}$$

The best theoretical evaluation of p is given by Hamermesh;[11] actually he finds for the quantity $w=np$ (n = the number of iron atoms per cc) $w=0.090\ \text{cm}^{-1}$ from which it would follow with $n=8.2\times10^{22}$/cc

$$p=1.1\times10^{-24}\ \text{cm}^2; \tag{14}$$

this is smaller by a factor 1.8 than the observed value, and therefore from (4) would lead to about three times too small transmission effects. The results of Powers[2] for thin iron agree with our experimental determination of p, indicating

[11] M. Hamermesh, Phys. Rev. 61. 17 (1942).

that his iron was sufficiently magnetized to reach the saturation value.

In comparing the theoretical and experimental values of p, it has to be remembered that the calculation of the former is based upon the not-too-well-known wave functions for the $3D$-shell of Fe. A qualitative description of the disagreement in terms of the wave functions can be given by stating that all their linear dimensions would have to be contracted by a factor $1\frac{1}{2}$ in order to reestablish agreement. It is true that so big an error in the scale of wave functions, calculated by the Hartree method, is surprising and that it is by no means certain that this is the cause of the observed discrepancy. On the other hand, the neutron polarization depends on the atomic form factor of the $3D$-shell alone and represents a rather more severe experimental test on the Hartree method than the spectroscopic and x-ray measurements by which it has been tested before.

As another alternative, Halpern and Johnson[12] have suggested the possibility of the neutron having the spin $\frac{3}{2}$, instead of the usually accepted value $\frac{1}{2}$. In view of the difficulties which such an hypothesis would introduce in the interpretation of nuclear phenomena, the sole support from the above discrepancy in the single transmission of neutrons does not seem to us sufficient to make it appear probable.

[12] O. Halpern and M. H. Johnson, Phys. Rev. **57**, 160 (1940).

As mentioned in Section I, the determination (13) of λ is connected with the linear dimension δ of the microcrystals. According to (8) and (8a) two values of δ are possible for a given λ, depending upon whether δ is small or large compared to the length l, given in (7). Depending upon the choice we get

$$\text{from (8)} \qquad \delta = 1.4\times10^{-4}\ \text{cm}, \tag{15}$$

$$\text{from (8a)} \qquad \delta = 6.4\times10^{-3}\ \text{cm}. \tag{15a}$$

The value (15a) is far too big to be plausible, and we consider the value (15) as a fair determination of the microcrystalline dimensions by means of this method.

In view of our results we foresee no essential experimental difficulties to overcome the rather strong depolarizing influences and thus to obtain considerably higher polarization effects than the ones obtained so far. It is true that in the case of thin iron we were able to obtain almost the complete effect, but for obvious reasons we were far from doing so with the thick sample. This could be helped, no doubt, by raising the magnetizing field to the order of 10,000 gauss which would merely require a somewhat larger electromagnet than the one at our disposal. Besides, however, it may well turn out that hot rolled steel is by no means the ideal material in the sense that other grades of iron will consist of smaller microcrystals or may be found easier to saturate, both desirable features to keep the necessary magnetizing field as low as possible.

PHYSICAL REVIEW VOLUME 64, NUMBERS 3 AND 4 AUGUST 1 AND 15, 1943

Determination of the Nuclear Spin of Cl^{37}

E. F. SHRADER*
Sloane Physics Laboratory, Yale University, New Haven, Connecticut
(Received December 11, 1942)

The nuclear spin of the chlorine atom was determined by observing the line intensities in the band spectrum of the homonuclear diatomic molecule of that atom. The lines of even J values show a different intensity from those of odd J values, the ratio of intensities being given by $(I+1)/I$ where I is the nuclear spin of the atom in question. In the band absorption spectrum of chlorine the intensity ratio of lines of the $Cl^{35}Cl^{35}$ molecule has been measured and compared with the value found by Elliott. These values are in substantial agreement and yield a value of 5/2 for the nuclear spin of Cl^{35}. In this spectrum no lines of the molecule $Cl^{37}Cl^{37}$ were observed due to the low concentration of Cl^{37} in the gas. By the method of thermal diffusion 200 cm³, S.T.P., of chlorine gas was obtained containing 45 percent Cl^{37}. The absorption spectrum of this gas showed lines of the $Cl^{37}Cl^{37}$ molecule in the 1→12 band of the $^1\Sigma\rightarrow{}^+0$ band system of Cl_2. For this band the alternating intensity ratio for the $Cl^{37}Cl^{37}$ molecule (1.28) was the same, within the experimental error, as for the $Cl^{35}Cl^{35}$ molecule (1.26), indicating that the nuclear spin of Cl^{37} is probably also 5/2. In interpreting the intensity ratios one must take into account the overlapping of lines and general background present.

1. INTRODUCTION

IT is a well-known fact that homonuclear diatomic molecules and certain linear polyatomic molecules exhibit the phenomenon of alternating intensities in their band spectra. This intensity ratio arises from the fact that the statistical weights of rotational levels with (+) symmetry are different from the statistical weights of levels with (−) symmetry. This ratio can be shown to be

$$(I+1)/I$$

for homonuclear diatomic molecules where I is the nuclear spin of the nucleus of the element in the molecule. For polyatomic molecules the intensity ratio is more complicated. The nuclear spin of a nucleus may therefore be determined by observing and measuring the alternating intensity ratio in the band spectrum of its homonuclear diatomic molecule. Elliott[1] analyzed the $^1\Sigma\rightarrow{}^+0$ band system of Cl_2 in absorption and made a determination of the alternating intensity ratio of the molecule $Cl^{35}Cl^{35}$. The value of this ratio was 1.35 from which he concluded that the most probable value of the nuclear spin of Cl^{35} is 5/2. In several bands he was able to identify the lines of the molecule $Cl^{35}Cl^{37}$ but due to the small concentration of Cl^{37} (24.2 percent) he was not able to identify lines of the homonuclear molecule $Cl^{37}Cl^{37}$. Elliott found no evidence of alternating intensities in the spectrum of $Cl^{35}Cl^{37}$. This agrees with theoretical predictions.

It is now possible, having obtained chlorine enriched in the heavy isotope, to obtain the band spectrum of $Cl^{37}Cl^{37}$ and make a determination of the nuclear spin of Cl^{37}.

2. EXPERIMENTAL

The spectrum of Cl_2 was obtained in absorption using a 21-foot concave reflection grating ruled 30,000 lines to the inch. An Eagle mounting was used which gave a dispersion of about 1.25A per millimeter in the first order.

Only a limited amount, approximately 200 cm³ S.T.P., of "enriched" chlorine containing 45 percent Cl^{37} was available. For this reason an absorption tube was constructed to give the greatest absorption for this small volume of gas. The optical arrangement is shown in Fig. 1. The absorption tube was 2.5 meters long and 1.2 cm

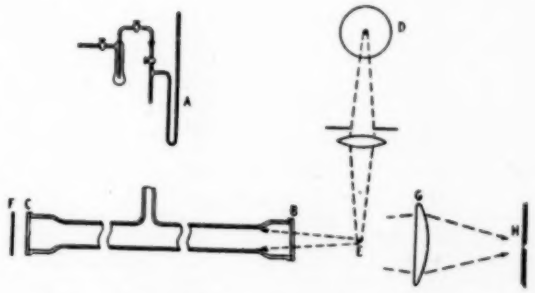

FIG. 1. Optical arrangement of apparatus.

* Now at Case School of Applied Science, Cleveland, Ohio.

[1] A. Elliott, Proc. Roy. Soc. **123**, 629 (1929); **127**, 638 (1930).

inside diameter. After cleaning thoroughly with nitric acid and washing, windows were sealed on the previously ground ends of the tube. Chlorine was admitted to the evacuated tube. The pressure in the tube was measured by means of a mercury manometer protected by a thin layer of concentrated sulphuric acid. The tube was filled with Cl_2 to a pressure of 50 cm of mercury.

Light from a 100-candlepower Point-O-Lite lamp was focused on the small mirror E which reflected the light into the tube. A second aluminized mirror at the far end reflected the light back down the tube past mirror E, through cylindrical lens G, and onto the slit of the grating spectrograph. The plane glass window at the grating end of the tube was placed at a slight angle to prevent light from being directly reflected into the slit. This arrangement necessarily sacrifices light intensity in order to obtain sufficient absorption. An exposure time of 48 hours was required using a slit width of 0.03 mm.

The standard photometric technique using a step filter for plate calibration was employed. The step filter was calibrated by means of a photronic cell and a quartz monochromator. A Koch and Goos photographically recording microphotometer was used to reduce the spectographic plate into an intensity curve. Each line was resolved graphically from its neighbors and its intensity calculated from plate calibration.

TABLE I. Wave-lengths, etc., of band lines in $Cl^{35}Cl^{35}$. Band 1→12. P and R branches.

J_P	J_R	λ in A	ν in cm^{-1}	α(max.)
15	17	5164.77	19356.57	0.019
16	18	5165.86	19352.47	0.014
17	19	5167.03	19348.11	0.017
18	20	5168.26	19343.50	
19	21	5169.53	19338.74	0.016
20	22	5170.88	19333.69	0.019
21	23	5172.29	19328.42	0.020
22	24	5173.76	19322.93	0.013
23	25	5175.33	19317.06	0.015
24	26	5176.92	19311.13	0.013
25	27	5178.62	19304.80	0.014
26	28	5180.39	19298.22	0.013
27	29	5182.19	19291.49	0.014
28	30	5184.08	19284.46	
29	31	5186.03	19277.22	0.017
30	32	5188.04	19269.76	0.009
31	33	5190.14	19361.97	0.016
32	34	5192.21	19253.96	0.012
33	35	5194.51	19245.73	0.017

3. RESULTS AND DISCUSSION

a. Analysis of Spectrum of "Enriched" Chlorine

The strongest discrete absorption of chlorine is the band progression 1→11, 1→12, and 1→13, which lies between 5130A and 5230A. The electronic transition is $^1\Sigma \rightarrow {}^+0$ and consequently each band consists of single P and R branches only.

TABLE II. Wave-lengths, etc., of band lines in $Cl^{35}Cl^{37}$. Band 1→12. P and R branches.

J_P	J_R	λ in A	ν in cm^{-1}	α(max.)
11	13	5163.66	19360.72	0.020
12	14	5164.40	19357.97	0.020
13	15	5165.31	19354.55	0.020
14	16	5166.25	19351.03	0.024
15	17	5167.25	19347.29	0.026
16	18	5168.27	19343.47	
17	19	5169.40	19339.24	0.029
18	20	5170.58	19334.83	0.023
19	21	5171.86	19330.03	0.032
20	22	5173.14	19325.23	0.026
21	23	5174.53	19320.04	0.019
22	24	5175.94	19314.82	0.024
23	25	5177.44	19309.20	0.017
24	26	5179.02	19303.33	0.016
25	27	5180.64	19297.26	0.016
26	28	5182.38	19290.81	0.015
27	29	5184.09	19284.44	
28	30	5185.92	19277.62	
29	31	5187.78	19270.73	0.017
30	32	5189.77	19263.34	0.026
31	33	5191.79	19255.82	0.022
32	34	5193.88	19248.09	0.026

TABLE III. Wave-lengths, etc., of band lines in $Cl^{37}Cl^{37}$. Band 1→12. P and R branches.

J_P	J_R	λ in A	ν in cm^{-1}	α(max.)
7	9	5163.85	19360.00	0.010
8	10	5164.25	19358.52	0.012
9	11	5164.91	19356.01	0.015
10	12	5165.57	19353.57	0.013
11	13	5166.41	19350.43	0.010
12	14			
13	15	5167.83	19345.12	0.013
14	16	5168.76	19341.25	0.011
15	17	5169.65	19338.39	0.016
16	18	5170.73	19334.26	0.009
17	19	5171.68	19330.71	0.0012
18	20	5172.79	19326.48	0.009
19	21	5174.12	19321.58	0.010
20	22	5175.33	19377.06	
21	23	5176.77	19311.68	0.013
22	24	5177.89	19307.44	0.008
23	25	5179.52	19301.46	0.010
24	26	5181.00	19296.00	0.005
25	27	5182.67	19289.73	0.008
26	28	5184.27	19283.75	0.005
27	29			
28	30	5187.58	19271.43	
29	31	5189.53	19264.20	0.007
30	32	5191.35	19357.47	0.008
31	33	5193.38	19249.93	0.010
32	34	5195.26	19242.98	0.008

In band 1→12 the P and R branches fall one on top of the other, the lines of one branch lying on the lines of the other whose J values are two removed. Hence even J values fall on even and odd on odd and the alternating intensity phenomenon is retained, not obliterated, as would be the case if even J value fell on odd J value.

From a spectrogram taken with the enriched chlorine it has been possible to identify 24 lines which belong to the molecule $Cl^{37}Cl^{37}$ in the 1→12 band. Due to the increased complexity and over-lapping of lines it has been impossible to identify any lines in the 1→11 and 1→13 bands as belonging to the molecule $Cl^{37}Cl^{37}$.

TABLE IV. Rotation constants of band 1→12 of $Cl^{37}Cl^{37}$.

B''	B'
0.1115 cm^{-1}	0.2228 cm^{-1}

Tables I, II, III give wave-lengths, etc., for the lines of the three molecules. The rotational constants are given in Table IV. The general appearance of the spectra of normal and enriched chlorine may be seen in Fig. 2.

The maximum value of the absorption coefficient, α(max.), for a given line is calculated from the expression

$$I = I_0 e^{-\alpha\rho x},$$

where I is the intensity at the center of the absorption line, ρ is the chlorine concentration in gram molecules per liter, and x is the thickness of chlorine in cm. Elliott[2] studied the relations of slit widths and line shapes to the line intensities and found no appreciable error was introduced in neglecting their effect.

b. Alternating Intensity Measurements

Elliott's measurements on the alternating intensity ratio of $Cl^{35}Cl^{35}$ in band 1→12 of "normal" chlorine were repeated by the author. The value obtained was 1.31 as compared to Elliott's value of 1.34 for this band. The relative intensity of lines of the $Cl^{35}Cl^{35}$ molecule to lines of the $Cl^{35}Cl^{37}$ molecule was found to be 1.32 as against Elliott's value of 1.35 for the same ratio. These values are in agreement with each other within experimental error.

[2] A. Elliott, Proc. Roy. Soc. **127**, 638 (1930).

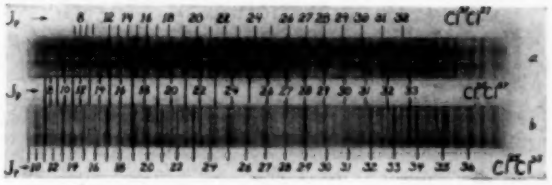

FIG. 2. Absorption spectrum of Cl_2 (band 1→12 of the $^1\Sigma \rightarrow {}^+0$ system). a is the spectrum of Cl_2 containing 45 percent Cl^{37}. b is the spectrum of Cl_2 containing 24.2 percent Cl^{37}. The rotational quantum numbers of the P branch are given for each molecule.

The alternating intensity ratios for the two homonuclear molecules were obtained from the spectrum of the "enriched" chlorine. These ratios were found to be 1.26 for $Cl^{35}Cl^{35}$ and 1.28 for $Cl^{37}Cl^{37}$. This ratio may be calculated in two ways. The first way consists of comparing the average intensity of all the strong lines to the average intensity of the weak lines. The second method consists of finding the intensity ratio of each line to its immediate neighbors and then averaging over all lines. These two methods give the same result in this particular case.

As was pointed out by Elliott the experimental values of the ratios should be regarded as lower limits since any background due to overlapping lines, etc., will make the measured ratio smaller than the true value. A background of less than 20 percent will raise Elliott's value 1.34 to 1.40 which is the theoretical value for a nuclear spin of 5/2.

One would expect this background effect to be greater in the spectrum of the "enriched" chlorine since the intensity of all the lines is relatively less. This seems to be in accord with the measured values of 1.26 and 1.28 as the alternating intensity ratios in the spectrum of "enriched" chlorine. However since the intensity of the spectrum of $Cl^{37}Cl^{37}$ is comparable to the intensity of the spectrum of $Cl^{35}Cl^{35}$ the relative effect of the background may be neglected. It would appear then that the nuclear spin of Cl^{37} is the same as the nuclear spin of Cl^{35}. The most probable value of the nuclear spin of Cl^{35} is 5/2 as determined by Elliott[2] and by the author from the spectrum of "normal" chlorine.

The author is indebted to Professor W. W. Watson, who suggested this problem, for his guidance and helpful suggestions.

PHYSICAL REVIEW VOLUME 64, NUMBERS 3 AND 4 AUGUST 1 AND 15, 1943

Conduction of Electricity in Highly Insulating Liquids*

CHIA-SHAN PAO†
Department of Physics, Washington University, St. Louis, Missouri
(Received June 21, 1943)

Investigations have been made on the natural conductivity, and on the conductivity induced by gamma-rays in isooctane and liquid oxygen. The characteristics of the two types of conductivity are so very different that it may be concluded that the natural conductivity is not due to stray radiation or to cosmic rays. The curves for the natural conductivity are such that the current increases much faster than the field. Evidence is presented supporting Plumley's theory that the observed conductivity is due to dissociation of the liquids by the field, and against the view that it has a thermionic origin at the cathode, or the view that it is due to radiation. The prediction that the logarithm of the current should be a linear function of the square root of the field is verified. The much larger currents induced by gamma-rays rise at first rapidly and then more slowly in a manner indicating a slow approach toward saturation. The results fit Jaffé's formula satisfactorily.

INTRODUCTION

RELATIVELY few investigations on the electrical conductivity of highly insulating liquids have been made. In comparison with the immense amount of work which has been done on the electrical conductivity occurring in, and imparted to, gases, it is evident that much remains to be done in accumulating information about the corresponding phenomena in highly insulating liquids. The first publication in this field was that of P. Curie,[1] who found that the electrical conductivity of petroleum ether, carbon tetrachloride, carbon disulphide, and benzene was increased by exposure to gamma- or x-rays, an investigation suggested, of course, by the effect of these rays on air. Later, other investigators studied the current-voltage characteristics of hexane and similar liquids when exposed to gamma-rays,[2] the mobilities,[3] the coefficient of recombination,[4] and the coefficient of diffusion of the ions. Jaffé[2] made an important contribution to the understanding of the current-voltage characteristics of hexane when irradiated by gamma-rays. In his 1908 paper he considered the current to be accounted for as the sum of two separate currents; one of these rising to a saturation value like the current in a gas, while the second is an ohmic current. In 1913 he discarded this view in favor of a theory according to which the ions are produced in very densely packed columns isolated from each other. These columns are the tracks of the photoelectrons ejected by the gamma-rays. An important feature of this theory was that it gave a quantitative relationship between the current and the field, a relationship which expressed the great difficulty of securing saturation, as a result of the ease with which recombination occurs in the tightly packed columns of ions. This theory has been extended successfully to cases of ionization in compressed gases.[5] The most recent application of Jaffé's theory is that of Mohler and Taylor,[6] and later Taylor[7] alone, who used it successfully in their work on ionization in carbon disulphide by x-rays. While there is no reason to suppose that Jaffé's theory is inadequate, it is certainly desirable to extend the scope of investigations on the conductivity imparted to liquids by ionizing radiations.

When all ionizing agents such as x-rays and radium are removed, it is found that there still exists a residual or natural conductivity in these liquids. However, there is no general agreement as to its characteristics. In the first place, the

* From a dissertation submitted in partial fulfillment of the requirements for the Ph.D. degree at Washington University.

† Now at the Radiation Laboratory, Massachusetts Institute of Technology, Cambridge, Massachusetts.

[1] P. Curie, Comptes rendus **134**, 420 (1902).

[2] G. Jaffé, J. de Phys. **5**, 263 (1906); Ann. d. Physik **25**, 257 (1908); Le Radium **10**, 126 (1913); Ann. d. Physik **42**, 303 (1913).

[3] I. Adamczewski, Acad. Polonaise Sci. et Lettres, Bull. **5–7A**, 217 (1934); Acta Phys. Polonica **3**, 235 (1934); Ann. de physique **8**, 309 (1937).

[4] H. J. Van der Bijl, Ann. d. Physik **39**, 1, 170 (1912); C. Bialobrzeski, J. de phys. et rad. **7**, 329 (1936).

[5] J. W. Broxon and G. T. Meredith, Phys. Rev. **54**, 9 (1938); J. Clay, Rev. Mod. Phys. **11**, 123 (1939).

[6] F. L. Mohler and L. S. Taylor, J. Research Nat. Bur. Stand. **13**, 659 (1934).

[7] L. S. Taylor, J. Research Nat. Bur. Stand. **17**, 557 (1936).

residual conductivity of a supposedly pure insulating liquid can be reduced by a factor of a thousand or more by treating it in such a way as to remove traces of water. Such treatment may be prolonged refluxing with an agent like sodium or phosphorus pentoxide, or exposure to a high electric field. When a reasonably low limiting value of the conductivity has been reached, the next question is to find how it originates. Some authors[8] believe that the residual conductivity should be attributed to cosmic and similar radiations. Other physicists[9] interpret their investigations to mean that the conductivity is due to a thermionic emission from the cathode combined with a Schottky effect. This has been criticized by LePage and DuBridge.[10] The most recent work is that of Plumley[11] who interprets his experiments to support the potential dissociation theory, which was originally proposed by Onsager[12] for very weak electrolytes. According to Plumley's view there are even in the purest hydrocarbons such as hexane a very small number of ions resulting from the spontaneous dissociation of molecules. A favorable orientation of the molecules with respect to the field increases the number of dissociations, the number increasing rapidly with the strength of the field. The investigations, while often supporting the point of view of the various authors, are seldom complete enough to decide definitely against alternative theories. For example, in the experiments for which the thermionic point of view was suggested, there was no systematic investigation of how the current depended on the volume of the liquid between the electrodes. For a given field, the thermionic theory would imply no dependence on the volume of the liquid, whereas all other theories would require for a given field a larger current, the greater the amount of liquid involved. However, it must be recorded that all who have worked on the residual conductivity of highly insulating liquids have found great difficulty in securing reproducible results. Frequently, for no apparent reason at all, the value of the observed current will change by a factor of two or so. Getting the liquid into a state where it will retain reasonably constant characteristics is often a tedious trial and error process.

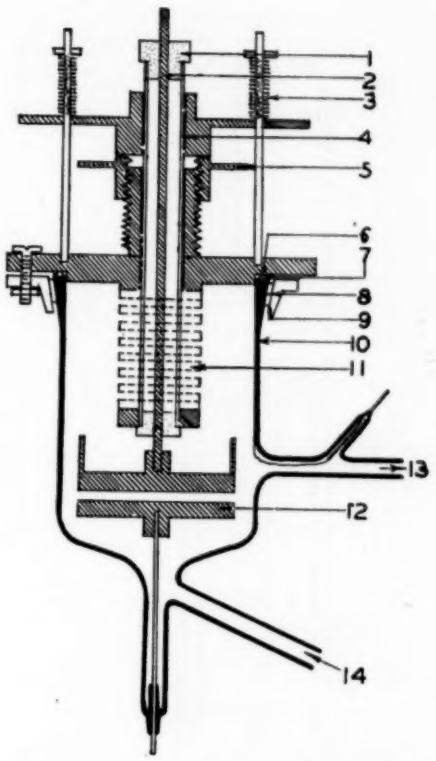

FIG. 1. Experimental cell I: (1) amber plug, (2) brass rod, (3) spring, (4) brass tube, (5) graduated brass disk, (6) 20-ampere Buss fuse wire, (7) mixture of paraffin and stopcock greases, (8) packing, (9) metal flange, (10) silvered glass jar, (11) sylphon, (12) brass electrode, (13) outlet for the liquid, (14) inlet for the liquid.

This investigation was undertaken to study both the natural and induced conductivities under as varied conditions as possible in the hope that some of the ambiguities now existing as to interpretation could be removed. The liquids chosen for investigation were isooctane and liquid oxygen. The reason for choosing isooctane was that we were fortunate to secure a supply of very pure liquid through the courtesy of Dr. G. W. Waters of the Shell Oil Company at Wood River, Illinois. The conductivity was investigated not only as a function of the field but also as a function of the spacing between the electrodes, or what amounts to much the same

[8] G. Jaffé, Ann. d. Physik **28**, 326 (1909); M. C. Bialobrzeski, J. de phys. et rad. **7**, 329 (1936); A. Rogozinski, *Ibid.* **8**, 128S (1937); A. Rogozinski, Phys. Rev. **60**, 148 (1941).
[9] E. B. Baker and H. A. Boltz, Phys. Rev. **51**, 275 (1937).
[10] W. R. LePage and L. A. DuBridge, Phys. Rev. **58**, 61 (1940).
[11] H. J. Plumley, Phys. Rev. **59**, 200 (1941).
[12] L. J. Onsager, J. Chem. Phys. **2**, 509 (1934).

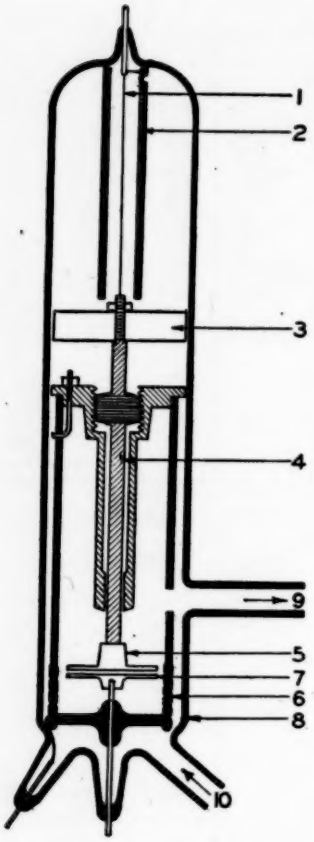

FIG. 2. Experimental cell II: (1) fine nickel wire, (2) brass cylinder, (3) soft ion bar, (4) brass rod, (5) brass electrode, (6) fine nickel screen, (7) copper electrode, (8) guard ring, (9) outlet for the liquid, (10) inlet for the liquid.

thing, the volume of the liquid. Measurements were also carried out at different temperatures.

APPARATUS

The apparatus and methods employed may be conveniently discussed under several headings.

1. The Conductivity Cells

In all, four cells were used in this investigation. Two of them had parallel plate electrodes, the spacing between which could be adjusted so that the effect of distance between the electrodes on the observed current could be investigated. Two others had concentric cylindrical electrodes. One of these cells was easy to shield with lead for investigating a possible cosmic-ray origin, and the other was specially designed for investigating the effect of temperature.

Cell I: A diagram of this cell is shown in Fig. 1; the dimensions of interest are the radius of the electrodes, 2.4 cm, the pitch of the screw, 1/24th of an inch. By means of the sylphon it is possible to vary the distances between the electrodes from zero to 6 mm. The insulation of the upper electrode, which is the one connected to the electrometer, consists of two pieces of amber. The upper piece is made vacuum tight by Sealstix. The glass part of the apparatus is made from standard Pyrex glass pipe. The junction between its flange and the brass disk is made vacuum tight by a gasket of fuse wire fitted into the groove in the flange in place of the more usual rubber gasket. Care was taken to ensure that the faces of the two electrodes were accurately parallel. The inside of the glass was coated with evaporated silver, which was electrically grounded to act as a shield for the upper electrode. The liquid did not rise above the level of the side tube (*13*).

Cell II: This all glass cell is shown in Fig. 2. The upper electrode, in this cell connected to the

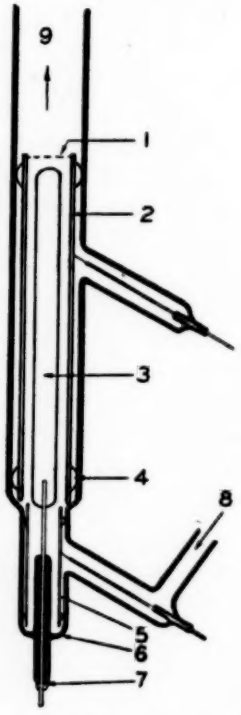

FIG. 3. Experimental cell III: (1) nickel screen, (2) monel cylinder, (3) dural rod, (4) blobs of solder, (5) brass cylinder, (6) guard ring, (7) Dennison's "number 4 express" sealing wax, (8) inlet for the liquid, (9) outlet for the liquid.

high voltage, is a brass disk 2.88 cm in diameter which can be moved up or down by manipulating a magnet in the vicinity of the soft iron bar (*3*). The lower electrode (connected to the electrometer) is a copper disk supported by a strong tungsten wire which is sealed into a glass spider at the end of the inner glass tube (*6*); on the surface of the glass tube (*6*) is a grounded nickel screen. The metal cylinder (*2*) prevents a corona discharge from the fine wire (*1*) from giving trouble. Great care was taken to ensure parallelism between the electrodes.

Cell III: This cell, designed to study the effect of external radiation, is shown in Fig. 3. It has two concentric cylindrical electrodes, the outer one of monel 9.6 cm long, 1.11-cm internal diameter, and the inner one of dural 9.2 cm long and 0.635-cm outside diameter. Blobs of solder serve to center the monel tube. Care was taken to secure exact centering. Cylinder (*5*) serves as a guard ring. The end (*7*) is covered with a good grade of sealing wax to ensure high insulation. The outside of the tube, above the sealing wax, is painted with Aquadag which is grounded. When the liquid is circulating in the system, it flows in through the tube (*8*) and leaves the tube through (*9*).

Cell IV: The cell (Fig. 4) is designed to be inserted in a thermos jar to allow investigations to be made at different temperatures. The dural rod (*6*) is 8.62 cm long and 1.68 cm in diameter. The monel cylinder (*7*) has an inside diameter of 2.42 cm. There are guard rings both inside and outside the cylinder (*4*) which is evacuated. At (*1*) there is amber insulation. Continuous circulation of the liquid is not possible with this cell. The liquid is distilled into the cell through (*8*); it can be tipped back into the distilling flask and the process repeated.

2. Treatment of the Isooctane

In order to secure low and reasonably steady residual currents, it is necessary to remove the constituents (whatever they may be) which are associated with a high conductivity (say 10^{-16} mho/cm) which is to be found even in the purest liquid obtainable commercially. The method finally adopted was to reflux the liquid over metallic sodium for a long time in a closed system including the conductivity cell. A simple design of the distilling and refluxing system is shown in Fig. 5. By increasing the heat input to the distilling flask, it was possible to arrange for the newly distilled liquid to pass through the conductivity cell back into the flask in a continuous cycle. In this way any suspended matter that might have been present in the cell initially was eventually removed. The conductivity sometimes obtained in this work is the lowest on record, 3×10^{-20} mho/cm. (Since the relationship between current and voltage is not linear, no precise meaning can be attributed to this unit; it is, however, a short and convenient unit for comparing results.)

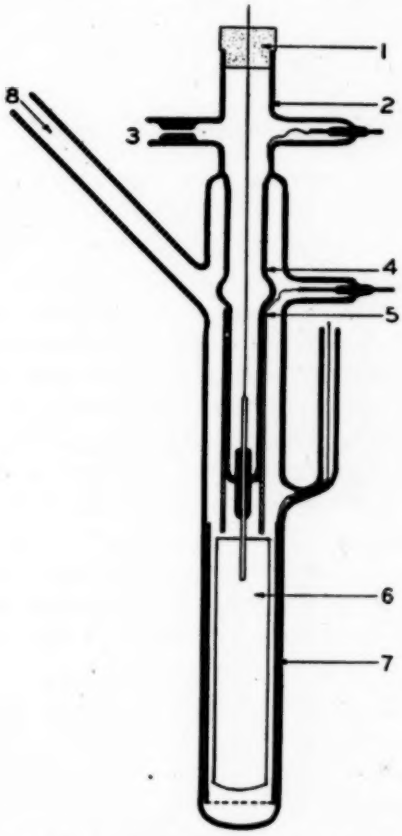

FIG. 4. Experimental cell IV: (1) amber plug, (2) Aquadag film, (3) to diffusion pump, (4) Hanovia "Liquid Bright Platinum" paint serving as a guard ring, (5) brass cylinder, (6) dural rod, (7) monel cylinder, (8) glass tube connected to a two-way stopcock.

3. Use of Liquid Oxygen

Investigations of liquid oxygen were carried out only with cell IV. The apparatus was very carefully washed and then dried thoroughly.

The tube (*8*) was connected through a suitable two-way stopcock which allowed one first to produce a vacuum in the apparatus and then to admit oxygen through a filter from a tank at a pressure of about 12 lb./in.^{2} above atmospheric pressure. On immersing cell IV in a thermos bottle of liquid air it was possible to fill it with liquid oxygen. It is believed that, though traces of water may be responsible for the conductivity in isooctane above the limiting value finally reached, they cannot be a cause of trouble in liquid oxygen for traces of water would be frozen to the walls and unavailable to form ions.

4. Measurement of Current

The currents measured ranged all the way from 10^{-11} down to 10^{-16} ampere. They were measured by means of the Western Electric D-96475 electrometer tube mounted in a vacuum. The grid of the tube was grounded through one of a set of S. S. White resistors whose values ranged from 4.06×10^{11} to 2.4×10^{9} ohms. The tube was used in the well-known balanced circuit set-up described by Penick.[13] A sensitivity of 200,000-mm divisions per volt was obtained, so that with a resistor of 4.06×10^{11} ohms, a deflection of 1 mm indicated a current of 1.2×10^{-17} amp. This sensitivity was seldom used except when the current to be measured was extremely low. For high currents care was taken to use a resistor between the grid and the cathode which limited the voltage change on the grid to less than 0.05 volt. This was necessary to secure linearity in the system.

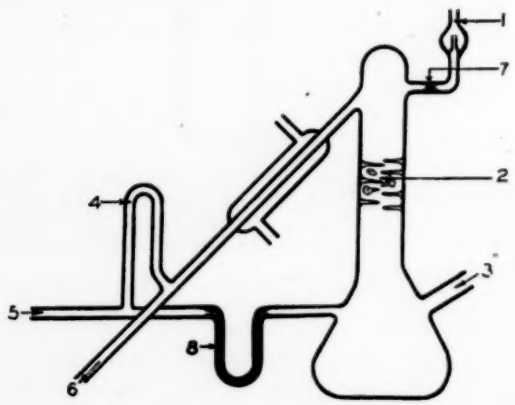

FIG. 5. Distillating system: (1) to Wood's metal seal off device, (2) indentations, (3) entrance for the liquid and sodium, (4) glass tube for equalizing the pressures between the cell and the reservoir, (5) inlet for the liquid from the cell, (6) outlet for the liquid to the cell, (7) constriction, (8) capillary.

[13] D. B. Penick, Rev. Sci. Inst. **6**, 115 (1935).

5. High Voltage Supply

The investigation included measurements on the current through the liquids with voltages as high as 6000 volts. Slight fluctuations in the voltage applied to the cells can produce effects which will completely mask a small current. Constant voltage can be secured by means of a sufficient number of B batteries. In this investigation voltages as high as 1485 volts were provided by means of B batteries. It was impracticable to use B batteries for higher voltages. An electronic high voltage supply was designed and constructed which had the following characteristics: (1) Constant voltages up to 5500 volts could be produced at will. The constancy was comparable to that of a bank of B batteries. Tests showed that the output voltage changed by less than 0.1 volt in a time interval of ten minutes. The fluctuations were often considerably less than this. (2) The device gave high voltages of either sign with no difference in the constancy of the output. (3) No detectable ripple could be observed. An account of the high voltage supply will be published elsewhere.

EXPERIMENTAL RESULTS

Induced Conductivity (Isooctane)

1. Dependence on Field and Volume

The conductivity induced by gamma-rays in highly purified isooctane was investigated in all the cells. Only with cells I and II was it possible to study the way in which the current depends on the spacing for any given electric field. (It was possible of course to investigate the dependence on field with all four cells.) Typical results for the current obtained with isooctane in cell II irradiated by gamma-rays are shown in Fig. 6. It is clear that the current is almost, but not quite, independent of the direction of the electric field. This asymmetry is a spurious effect and is to be attributed to the small contribution to the observed current from the "dead" region around the back of the electrode which is connected to the electrometer. The direction of the current in

this region is not affected by the sign of the voltage on the other electrode; hence, the small asymmetry. This interpretation was verified by using one cell with a lead shield so arranged that the direct ionization of the "dead" region by the radium is greatly reduced; it was found that this shielding reduced the small asymmetry very greatly. The current increases noticeably with the field showing that saturation calls for much higher fields. Results of this kind were obtained by Jaffé[2] with hexane many years ago.

He proposed an interpretation according to which the ionization due to the photoelectrons ejected here and there in the liquid by gamma-rays takes place in very short columns densely packed with ions. The difficulty of obtaining saturation is due to the strong initial recombination within the columns. Jaffé developed a formula expressing the value of the current at any field in terms of the mobility, diffusion, and recombination coefficients of the ions. The formula is

$$\frac{1}{I_A}=\frac{1}{I_\infty}\left[1+\frac{\alpha N}{7.85bw}\frac{1}{X}F\left(\frac{b^2w^2X^2}{2D^2}\right)\right], \qquad (1)$$

where I_A is the current per unit area at a field X, I_∞ the saturation current at infinite field, N the number of ion pairs produced per cm length of a column, b the initial diameter of the column within which the ions are found, and α, w, and D are the recombination, mobility, and diffusion coefficients, respectively, of the ions. $F(b^2w^2X^2/2D^2)$ is a complicated function of the argument which approaches unity when the argument is sufficiently large. In practice this is secured by using a high enough field so that Eq. (1) becomes

$$\frac{1}{I_A}=\frac{1}{I_\infty}\left(1+S\frac{1}{X}\right). \qquad (2)$$

Here S is $\alpha N/7.85bw$. The validity of this theory may be tested by plotting $1/I_A$ against $1/X$. If the plot results in a curve which is practically straight for all values of X above a certain value then one can infer that the theory applies. Moreover, the intercept of this line (when extrapolated) on the ordinate through the origin gives the value of $1/I_\infty$. It is thus possible,

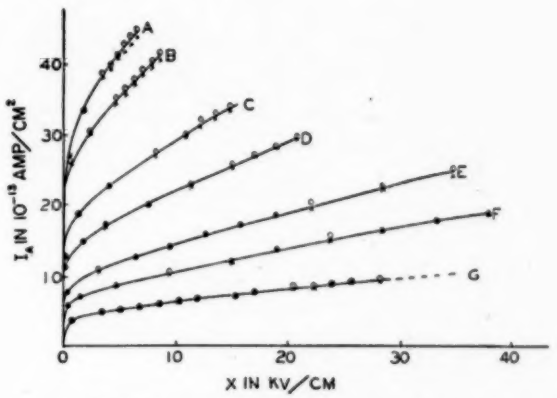

FIG. 6. Variation of induced current with field strength in isooctane irradiated by constant radiation from 2000 μg radium. Curves *A*, *B*, *C*, *D*, *E*, *F*, and *G* represent results when $d=0.848$, 0.636, 0.371, 0.265, 0.159, 0.106, and 0.053 cm. Open circle and cross represent the respective results for positive and negative voltages applied to the high voltage electrode of cell II.

assuming the validity of Jaffé's theory, to calculate the value of the saturation current. The slope of the line in such a graph has the value S/I_∞.

The directly observed experimental results collected in Fig. 6 are replotted in Fig. 7. It is clear that these "Jaffé plots" have straight portions which can be extrapolated back to the ordinate at the origin which corresponds to an infinite field. The characteristics of this family of curves are presented in Table I. Here d is the spacing between the electrodes. The fourth column is quite significant for it shows that I_∞ is almost exactly proportional to d, as it should be if the total number of ion pairs is proportional to the available volume. On the other hand, the fifth column shows that the currents observed for an experimentally obtainable field $X=20$ kv/cm are not quite proportional to the spacing between the electrode. It is to be expected that with the larger spacings, the currents would deviate further from the saturation value, as is found to be the case.

2. *Dependence on the Intensity of Radiation*

In order to determine the intensity variation of the current induced in the liquid at room temperature, current-intensity runs were taken for different fields in a cell of concentric cylinder type, whose construction is similar to that of cell III. The intensity of radiation was varied by

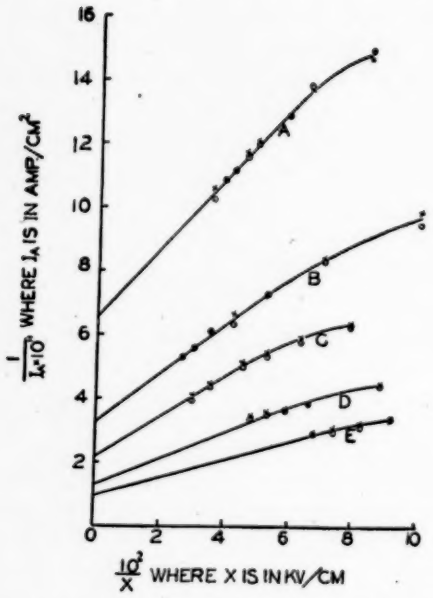

FIG. 7. Inverse current and inverse stress (field strength) relationship for isooctane irradiated by constant radiation of 2000 μg radium. Curves *A*, *B*, *C*, *D*, and *E* represent the results when $d=0.053$, 0.106, 0.159, 0.265, 0.371 cm, respectively. Open circle and cross represent the results when positive and negative voltages are applied to the high voltage electrode of cell II.

using different calibrated gamma-ray standards supplied by the Bureau of Standards. Figure 8 shows what one obtains when the intensity of radiation is selected and the current measured at various fields. It is clear that the present results agree with those obtained by Adamczewski,[14] who measured the ionization current through hexane with various intensities of x-rays.

With a fixed value of field strength the induced current was measured as a function of the intensity of radiation. A typical curve is shown in Fig. 9. It is a rather remarkable phenomenon that the relationship between the induced current and intensity of radiation is quite linear, a fact which, in principle, enables us to use the ionization in such a liquid to indicate the intensity of radiation. If the radiation is sufficiently strong and if the liquid inside the ionization chamber is fairly pure, so that the induced current is much greater than the residual current, the author believes that this kind of measurement may be developed into a dependable and accurate method of measuring radiations.

[14] I. Adamczewski, Acta Phys. Polonica **3**, 246 (1934).

3. *Dependence on Temperatures*

The effect of temperature on the currents through isooctane as a function of the field was studied by means of cell IV. Figure 10 shows the results obtained when the field was set at some selected value and the temperature varied. Figure 11 shows what one obtains when the temperature is selected and the current measured at various fields. It is clear that for any given field the currents are larger the higher the temperatures. This can be explained qualitatively by the fact that viscosity decreases with increasing temperature and when viscosity decreases, the ions in the column are more readily separated from each other so that closer approach to the saturation current is obtained.

The results in Fig. 11, together with some others not shown, are replotted as Jaffé plots in Fig. 12. It is interesting to note that all the lines, when extrapolated, hit the ordinate at the origin at substantially the same place, indicating that for each curve we have the same I_∞. This is as it should be, for with the radium placed in a fixed position with respect to the cell, one would expect the same total number of ion pairs to be produced whatever the temperature may be. (It is true that a change in density with temperature could affect the absorption of gamma-rays slightly and this would change the total number of ion pairs produced per unit volume. However, this is probably too small an effect to make a noticeable change in I_∞.)

From Fig. 12 we find an empirical relation between the value of S and T to be $S=\text{const.}/T^{1.28}$. Since $S=\alpha N/7.85bw$ it is likely that N and b are but little affected by the temperature so that the principal factors varying with the temperature are α and w, the recombination and mobility coefficients, respectively. Thus measurements of the slopes of the straight lines in the Jaffé plots

TABLE I. Characteristics of curves of Fig. 7; d is the space between electrodes.

d	$\frac{10^{-11}}{I_\infty}$	$I_\infty \times 10^{-12}$	$\frac{I_\infty \times 10^{-12}}{d}$	$\frac{I_{20}}{I_\infty}$	$S \times 10^{12}$
0.053	6.6	1.51	2.85	0.550	10.9
0.106	3.3	3.02	2.845	0.465	7.3
0.159	2.2	4.53	2.845	0.412	6.2
0.265	1.33	7.51	2.83	0.397	4.03
0.371	0.96	10.04	2.81	0.405	2.83

can be used to indicate the way in which α/w changes with the temperature.

In cells containing electrodes of different materials, the magnitude of the current was quite independent of which electrode was the cathode, a result entirely in accord with the view that the conductivity due to gamma-rays is a volume effect in the liquid and not a surface effect at the electrodes.

No time lag in the value of the observed current was noticed when the field was changed. This result is not in agreement with that found by Taylor[7] for ionization of carbon disulphide by x-rays. Our statement is subject to the proviso that conclusions cannot be drawn as to time intervals less than about three minutes as the resistance condenser factor of our set-up was of this order.

It may be concluded that the phenomena observed when isooctane is irradiated by gamma-rays may be attributed to the formation of ions in the liquid and that the results are described adequately by Jaffé's theory.

Induced Conductivity (Liquid Oxygen)

Because of the experimental restrictions imposed by the low temperature of liquid oxygen, it was impracticable to use either cell I or II to determine the effect of changing the spacing.

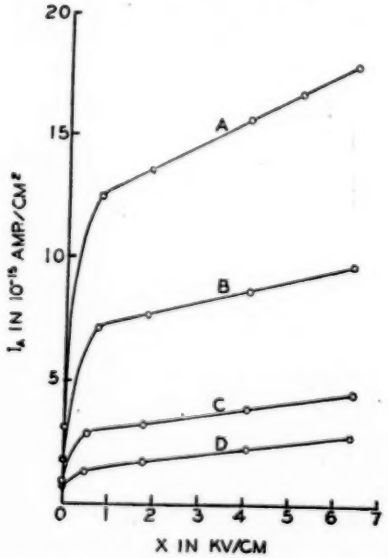

FIG. 8. Variation of induced current with field strength in isooctane at room temperature ($T=297°K$). Curves A, B, C, and D represent the respective results when the amounts of radium are 100, 50, 20, and 10 μg.

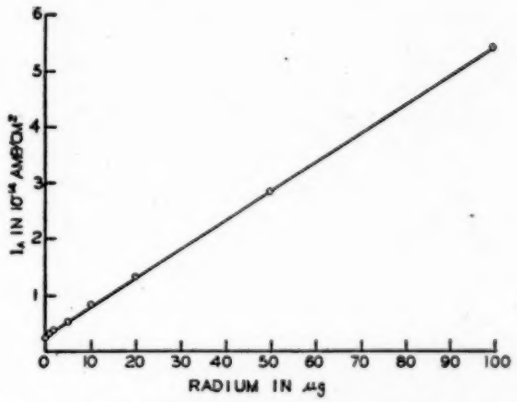

FIG. 9. Variation of induced current with intensity of radiation at $X=5830$ v/cm.

Cell IV was used for studies on liquid oxygen. The direct experimental measurements are plotted in Fig. 13. (To facilitate comparison, the light dotted line shows the curve for isooctane at 273°K in the same cell. The curves are adjusted arbitrarily to coincide at 10 kv/cm.) The curve for liquid oxygen indicates that saturation is much harder to attain in it than in isooctane. The corresponding Jaffé plot is shown in Fig. 14. The intercept on the ordinate at the origin is so small that it would be almost useless to use the curve to determine the value of I_∞. However, the value of I_∞ is of the order 30 times more than I_A at 10 kv/cm, whereas, in the case of isooctane, the value of I_∞ is only of the order 2 times more than I_A at 10 kv/cm (for $T=273°K$). If the 273°K curve for isooctane is transferred to Fig. 14 and adjusted so that I_∞ is the same for both, we find that the Jaffé plot for isooctane is the lower curve. The S for liquid oxygen is thus much larger than the S for isooctane.

The high value of S can be attributed principally to the factors $\alpha N/w$. N may well be considerably larger for liquid oxygen than for isooctane because the oxygen molecules offer a larger cross section to the gamma-ray photoelectrons than do the isooctane molecules. Little can be said as to the quotient α/w since no measurements have been made to determine these constants in liquid oxygen.

Natural Conductivity (Isooctane)

1. Dependence on Field and Volume

The investigation of the natural conductivity in isooctane and similar liquids, that is, the

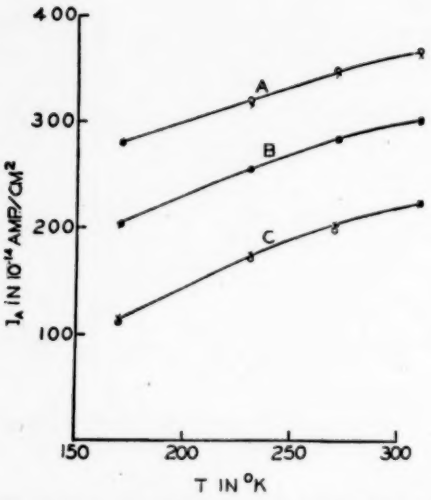

FIG. 10. Variation of induced current with absolute temperature in isooctane irradiated by constant radiation from 4000 μg radium. Curves *A*, *B*, and *C* represent the results when $X=14{,}850$, 8088, and 1348 v/cm, respectively. Open circle represents the results when positive voltages are applied to the high voltage electrode of cell IV, and cross represents the results when negative voltages are applied to the high voltage electrode.

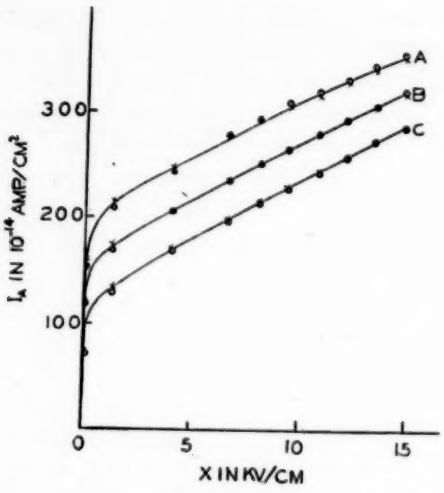

FIG. 11. Variation of induced current with field strength in isooctane irradiated by constant radiation from 4000 μg radium. Curves *A*, *B*, and *C* represent the results when $T=315.3$, 260.6, and 210°K, respectively. Open circle represents results when positive voltages are applied to the high voltage electrode of cell IV, and cross represents results when negative voltages are applied to the high voltage electrode.

residual conductivity to be found in the absence of ionizing agents such as radium, is full of experimental difficulties. The currents to be measured are so small that it is difficult to secure reproducible results. This is also accentuated by the need for measurements at high voltages as well as at low voltages. Slight variations in the absolute value of the high voltage, which may be quite insignificant in a relative sense, often produce electrostatic induction effects of a magnitude comparable with the current being measured. There is no agreement among previous investigators as to the nature and origin of the natural conductivity. It has been attributed to (1) radiation, probably cosmic rays, (2) thermionic emission from the cathode, (3) cold emission from the cathode,[15] and (4) dissociation induced by the field. In order to effect a discrimination between these views it is desirable to study the conductivity as a function of several variables in one and the same investigation. Thus for a given field, the current should be independent of the spacing between the electrodes, if the explanation be either (2) or (3). The supporters of these theories have not made this particular test.

The dependence of the current through isooctane on spacing was investigated in cells I and II. Although the same amount of effort was spent on the experiments involving these two cells, the ultimate conductivity (at the same field) ob-

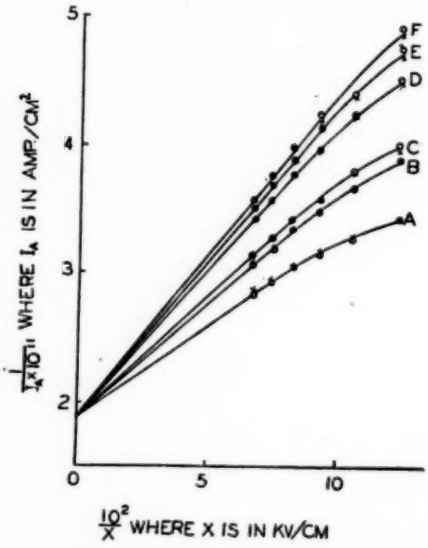

FIG. 12. Variation of inverse current and inverse stress (field strength) curves with the absolute temperature in isooctane irradiated by constant radiation from 4000 μg radium. Curves *A*, *B*, *C*, *D*, *E*, and *F* represent the results when $T=313.3$, 273, 260.6, 230, 210, and 191°K, respectively. Open circle and cross represent the results when positive and negative voltages are applied to the high voltage electrode of cell IV.

[15] R. W. Dornte, Ind. Eng. Chem. **32**, 1529 (1940).

tained after prolonged refluxing and circulation was about 20 times less in II than in I. This is typical of much of the work in the field. Many cells with refluxing and circulating systems have been tried out. Often two systems, substantially identical, yield widely different ultimate conductivities. Figures 15 and 16 give directly the values of the currents per unit area as a function of both the spacing and the field. It is to be noted that the current is independent of the sign of the potential applied to the high voltage electrode. This was also found later with cells III and IV where the electrodes are made of different metals. Had the current been due to a thermionic emission at the cathode, it would have depended very greatly on the nature of the cathode. We may conclude, therefore, that these experiments give no support to explanations (2) nor indeed to (3). Another characteristic to be noted is that the curves for the natural conductivity are entirely different in shape from the curves for the conductivity induced by gamma-rays. This result makes it extremely unlikely that one can attribute the residual conductivity to feeble radiations of the gamma-ray type. Figure 17 shows that the currents observed in cell I are strictly proportional to the spacing between the electrodes, or what amounts to the same thing, to the volume of the liquid between the electrodes. Figure 18 shows how the currents in cell II depend on the spacing. While it is clear that these currents also definitely increase with the spacing, they are not strictly proportional to the spacing. It may be that this is to be attributed to the great difficulty in making measurements in this region. (Over one-half of points in Fig. 18 correspond to I_A less than 10^{-15} amp./cm².) On the other hand, since the currents in Fig. 18 are so much smaller than those in Fig. 17 it may well be that the way in which the lines pass above the

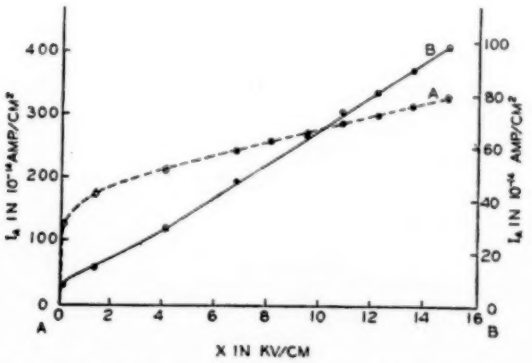

FIG. 13. Variation of induced current with field strength. Curve *A* (dotted curve) represents the results when isooctane was irradiated by 4000 μg radium at $T=273°K$. Curve *B* (solid curve) represents the results when liquid oxygen was irradiated by 4500 μg radium at $T=90°K$. Open circle and cross represent the respective results for positive and negative voltages applied to the high voltage electrode of cell IV.

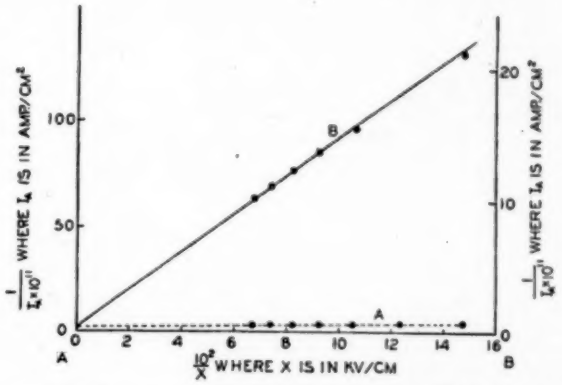

FIG. 14. Inverse current and inverse stress (field strength) curves. Curve *A* (dotted curve) represents the results when isooctane was irradiated by 4000 μg radium at $T=273°K$. Curve *B* (solid curve) represents the results when liquid oxygen was irradiated by 4500 μg radium at $T=90°K$. Open circle and cross represent the respective results for positive and negative voltages applied to the high voltage electrode of cell IV.

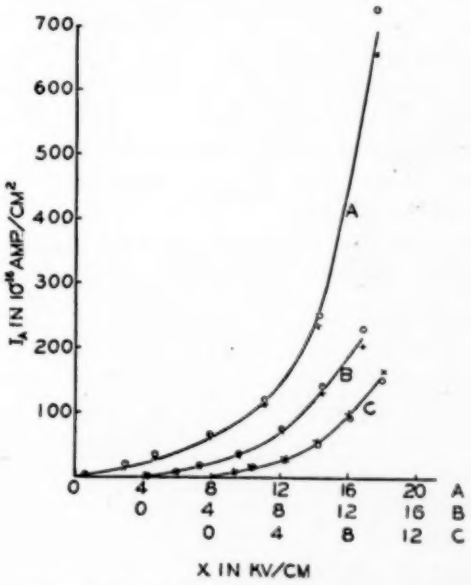

FIG. 15. Variations of residual current and field strength curves for isooctane. Curves *A*, *B*, and *C* represent the results when $d=0.318$, 0.424, and 0.530 cm. Open circle and cross represent the results when positive and negative voltages are applied to the high voltage electrode of cell I.

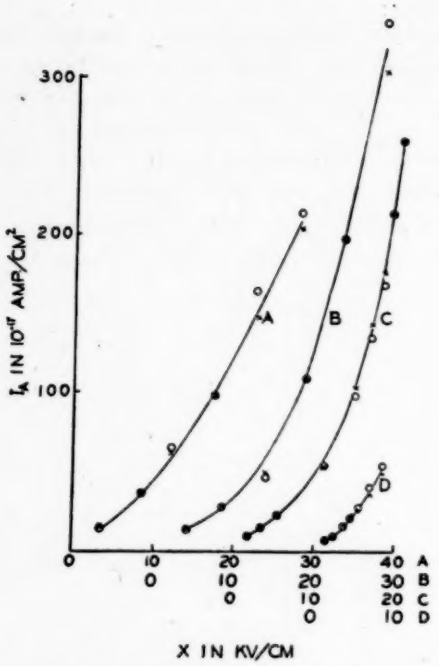

FIG. 16. Variation of residual current and field strength curves for isooctane. Curves A, B, C, and D represent the results when $d=0.053$, 0.106, 0.265, and 0.636 cm, respectively. Open circle and cross represent the results when positive and negative voltages are applied to the high voltage electrode of cell II.

origin indicates the superposition of two effects, a small one (possibly due to radiation) whose characteristic curve cuts the zero ordinates above the origin and a larger one which is proportional to the spacing. In Fig. 17 the larger effect is possibly so enhanced that the small effect is swamped. It is perhaps unprofitable to speculate further on the point. Clearly more experimental work should be done.

Plumley[11] has applied the potential dissociation theory to explain residual conductivity. According to this view a very small number of the molecules even in the purest hydrocarbons are dissociated into ions. Other molecules on the verge of dissociation will be dissociated by a field if their orientation be favorable. Plumley gave a formula for the number of dissociated molecules, which, therefore, also leads to an expression for the current in terms of the temperature T and the field X. The formula is

$$I_A = C \exp\left[(2e/kT)(eX/300D)^{\frac{1}{2}}\right]. \qquad (3)$$

Here C is proportional to the number of dissociated molecules at zero field. The exponential term describes the way in which a field X increases the degree of dissociation; k is Boltzmann's constant, e the unit charge, and D the dielectric constant. This theory can be tested by plotting $\log_{10} I_A$ against $X^{\frac{1}{2}}$. If it is correct, a straight line should be obtained and its slope should be $2e^{\frac{1}{2}}/2.3kT300^{\frac{1}{2}}D^{\frac{1}{2}}$. The "2" enters the equation through a particular assumption as to the nature of the force between the ions. If a straight line with a slope differing from the calculated value be obtained from the experimental results, it may be inferred that while the theory, in the main, is satisfactory, the correct form of the force between the ions has yet to be found.

In Figs. 19 and 20 we have re-plotted the results given in Figs. 15 and 16 for cells I and II, respectively. Insofar as the plots are straight lines one may infer that the potential dissociation theory is satisfactory. The slopes of the lines in Fig. 19 are substantially the same, a result which we should expect for there is nothing in the theoretical expression for slope which depends on the spacing between the electrodes. In these observations, however, the variation in spacing is not very great. When this variation is made large, the curves of Fig. 20 are obtained; here the slopes are very different for the different spacings. This cannot be accounted for by Plumley's

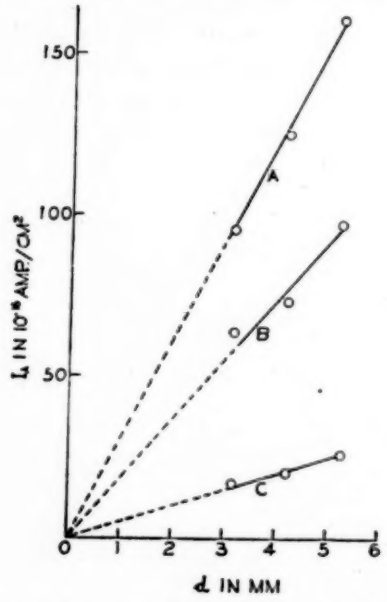

FIG. 17. Variation of residual current with electrode spacing at constant field strength. Curves A, B, and C represent the results when $X=10$, 8, and 4 kv/cm, respectively.

theory. The theoretical value of the slope $2e^{\frac{1}{2}}/2.3kT300^{\frac{1}{2}}D^{\frac{1}{2}}$ is 0.0092 at 297°K. For cell I (Fig. 19) the experimental value is 0.0215, while for cell II (Fig. 20) it ranges from 0.0105 to 0.0183.

2. *Dependence on Treatment of the Isooctane*

Observations were made on the residual current through cell II during a period of six weeks. This cell together with its distilling flask forms a closed system. The first observations were made after circulation for about twenty-four hours. Results about three times larger in magnitude than those represented in Figs. 16 and 18 were obtained. During the course of repeated distillation and circulation the current values slowly diminished to the limiting values shown in Figs. 16 and 18. The slope of the log I_A against $X^{\frac{1}{2}}$ lines also diminished by roughly 20 percent.

When the liquid had been "purified" by prolonged distillation over sodium, exposure to a high electrostatic field for an hour did not produce any further reduction.

3. *Time Lag*

Some investigators report hysteresis effects in the current when the field is charged. No time lags of this sort were found in this investigation larger than the purely instrumental ones associated with the resistance capacitance characteristics of the circuit.

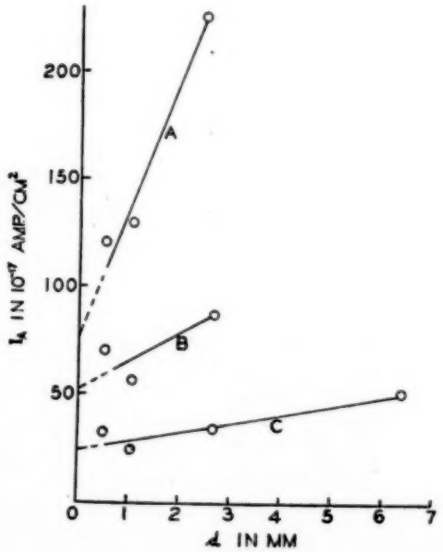

FIG. 18. Variation of residual current with electrode spacing at constant field strength. Curves A, B, and C represent the results when $X=20$, 14, and 8 kv/cm, respectively.

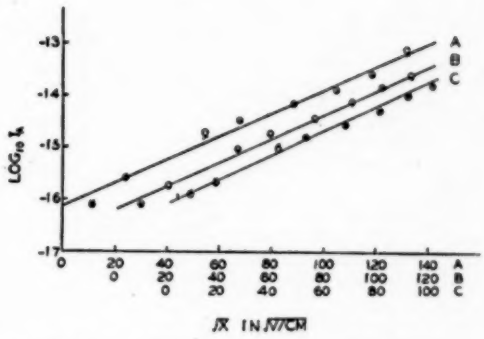

FIG. 19. Relation between $\log_{10} I_A$ and $X^{\frac{1}{2}}$ for isooctane. Curves A, B, and C represent the results when $d=0.318$, 0.424, and 0.530 cm. Open circle and cross represent the results when positive and negative voltages are applied to the high voltage electrode of cell I.

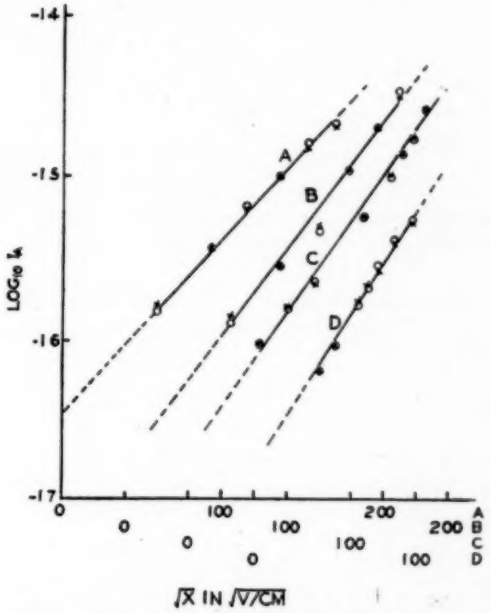

FIG. 20. Relation between $\log_{10} I_A$ and $X^{\frac{1}{2}}$ for isooctane. Curves A, B, C, and D represent the results when $d=0.053$, 0.106, 0.265, and 0.636 cm, respectively. Open circle and cross represent the results for positive and negative voltages applied to the high voltage electrode of cell II.

4. *Effect of External Radiation*

It was possible to surround cell III with 3 inches of lead and an extra inch on the top. No measurable change in the current at any field could be detected. On replacing cell III by a Geiger-Müller tube it was found that its response was cut down by 22 percent by the presence of

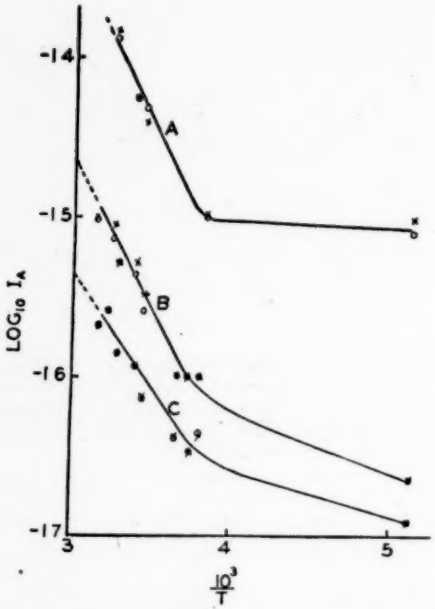

FIG. 21. $\log_{10} I_A$ against $1/T$ curves for isooctane. Curves A, B, and C represent the results when $X = 14{,}850$, 4010, and 1215 v/cm. Open circle and cross represent the respective results for positive and negative voltages applied to the high voltage electrode of cell IV.

the lead. It may, therefore, be inferred that little or none of the current through the isooctane in cell III could be attributed to cosmic radiations. Other investigators[8] have published results in support of the view that the residual conductivity in their experiments is due to radiation which can be reduced by shielding. The data are summarized in Table II.

It is difficult to understand why no evidence of an effect due to stray radiations was found in this investigation. The "conductivity" of the liquid was as low as that used by the other investigators. There is a difference which may perhaps be important. The volume of the cell used in this work was far smaller than in the cells used by the other investigators, while the field was larger. It is conceivable that had the current at fields below 1 kv/cm been large enough to measure accurately, a dependence on shielding would have been found.

Assuming that the residual conductivity of air is due to the formation of 3 ion pairs per cc per sec., and making reasonable assumption as to the method of predicting the ionization in isooctane, as suggested by Mohler and Taylor's work,[6] it may be concluded that the current to be expected in isooctane is 6×10^{-16} amp./cm³. This is of the order of magnitude of the observed current below about 1 kv/cm, but unfortunately it is not easy to make decisive measurements on the effect of shielding when the current is so small. To secure further evidence in this direction it would be helpful to use a cell containing a much larger volume of liquid.

5. *Effect of Temperature*

Equation (3) indicates theoretically how I_A should depend on the temperature. According to this equation the relation between $\log I_A$ and $1/T$ should be linear. The experimental results are shown in Fig. 21. The most noticeable thing about these curves is the change in slope for the lower part of the temperature range. This has the effect that the current at low temperatures is larger than theory predicts.

It should be pointed out here that in the temperature range from 318°K to 263°K the slopes of $\log_{10} I_A$ against $1/T$ are of the same order of magnitude as those for toluene measured by LePage and DuBridge.[10] The only difference is that the present slopes of these plots decrease with a decrease of field, while those obtained by LePage and DuBridge increase with decreasing fields, as actually required by the potential dissociation theory. Again this difference can be reconciled by assuming that the observed current is composed of two effects, one due to cosmic radiation and the other due to the potential dissociation. The current measured by LePage and DuBridge is about 50,000 times larger than the current measured in the present investigation (at the same X and the same T); thus, one would

TABLE II. Evidence for ionization of liquids by natural radiation.

	Jaffé	Bialobrzeski	Rogozinski	Pao
v	200	800	—	5.98
X	1500	900	—	19000
r_1	0.15	2	—	0.317
r_2	2.00	4	—	0.555
I_v	216	600	135	190000
l	3	5	7	8
R	0.66	0.61	0.28	0.00

In this table the following symbols are used: v = the effect volume of the liquid in cubic centimeters; X = the maximum field strength in volt/cm used in the investigation; r_1 = radius of the inner electrode in cm; r_2 = radius of the outer electrode in cm; I_v = the current density in number of ions/cc·sec. at X; l = thickness of the lead used in cm; R = effect of the external radiation.

expect that, in their measurements, the potential dissociation effect overrides the other to show a result in accordance with the theory, while in our measurement the two effects may be of the same order of magnitude. By calculating the number of ions per cubic centimeter per second at $T=273°K$ from Fig. 21, we found these values to be of the same order of magnitude as the value calculated for the cosmic ray alone, which is about 4240 ions/cc·sec. This tends to support the argument given above.

The relationship between I_A and X at different temperatures is shown in Figs. 22 and 23. As T decreases from 309°K to 195°K, the slope *decreases* almost 13 percent. Theoretically, if Eq. (3) applies, the slope should *increase* about 38 percent.

The assumption made in this method of testing Eq. (3) is that every ion pair produced finds its way to the electrodes, which is the same thing as saying that we have a saturation current. Plumley[11] has established a criterion for testing whether or not saturation conditions prevail. On applying this test it would appear that we actually do have saturation. However, as the temperature is lowered the mobility of the ions decreases while the coefficient of recombination increases. Both factors act so as to diminish the degree of saturation as the temperature is lowered. This explanation is still to be confirmed.

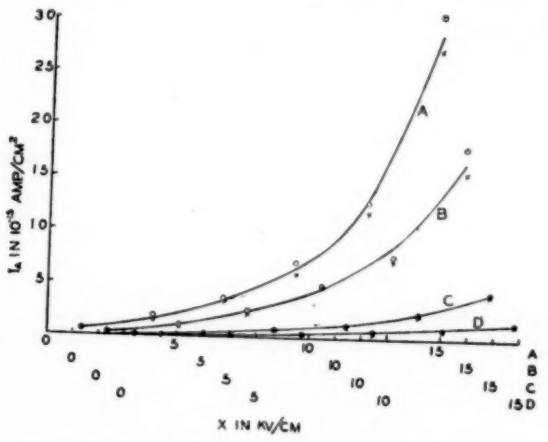

FIG. 22. Variation of residual current with field strength at constant temperature. Curves *A*, *B*, *C*, and *D* represent the results when $T=309.5$, 296.7, 273, and 195°K, respectively. Open circle and cross represent the results for positive and negative voltages applied to the high voltage electrode of cell IV.

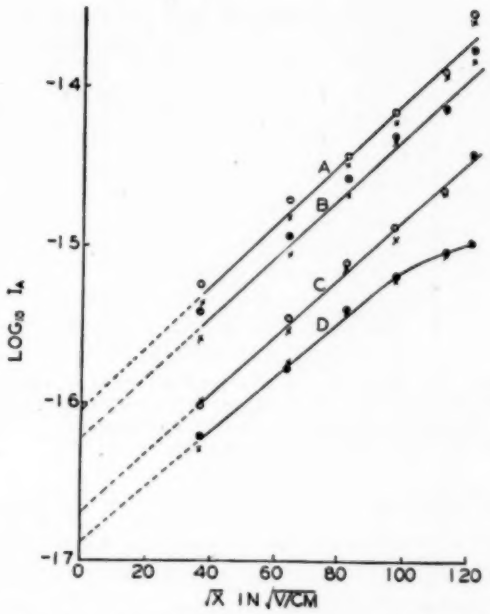

FIG. 23. $\log_{10} I_A$ against $X^{\frac{1}{2}}$ curves for isooctane. Curves *A*, *B*, *C*, and *D* represent the results when $T=309.5$, 296.7, 273, and 195°K, respectively. Open circle and cross represent the results when positive and negative voltages are applied to the high voltage electrode of cell IV.

Natural Conductivity (Liquid Oxygen)

The current passing though liquid oxygen as a function of the field in the absence of radium is shown in Fig. 24. Cell IV was used so that these results are directly comparable with those for isooctane in Fig. 22. The outstanding results here are that, when the same cell is used, the current in liquid oxygen is much less than that in isooctane for fields below about 5 kv/cm; for higher fields, say 15 kv/cm, the currents are of the same order of magnitude. As a matter of interest, we tabulate the conductivity of isooctane obtained from curve *C*, Fig. 22, and that of liquid oxygen in Table III.

TABLE III. Comparison of natural conductivities of isooctane and liquid oxygen.

Isooctane ($T=273°K$)		Liquid oxygen ($T=90°K$)	
X	σ_a	X	σ_a
1348	7.3	1214	0.252
4050	7.9	4010	0.307
6760	11.0	6760	2.495
9460	12.5	9460	4.52
12140	17.9	12140	7.61
14860	26.1	13520	9.84
		14860	14.70

X is the field strength in volt/cm; σ_a is the average of positive and negative conductivities in 10^{-20} mho/cm.

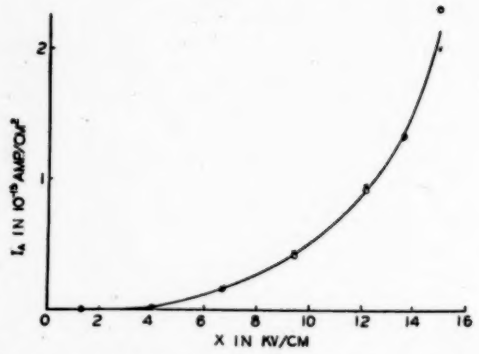

FIG. 24. Variation of the residual current with field strength in liquid oxygen. Open circle and cross represent the respective results for positive and negative voltages applied to the high voltage electrode of cell IV.

In order to compare the slopes of the straight lines representing $\log I_A$ against $X^{\frac{1}{2}}$ for liquid oxygen and isooctane the results shown in Fig. 24 are replotted. In Fig. 25 curve A represents the results for isooctane at $T=273°$K, curve B for liquid oxygen at $T=90°$K. It is noted that the liquid oxygen has a greater slope as predicted by the potential dissociation theory because of its lower temperature. The experimental slope for curve B is 3.56×10^{-2}, while the theoretical value is 3.03×10^{-2}.

In working with isooctane at ordinary temperatures there is always the slight possibility that the conductivity is due to the ions into which the last irremovable traces of water dissociate and not to charged molecules or fragments of molecules of isooctane. Such an explanation for the behavior of liquid oxygen cannot be sustained for it seems certain that any water that might happen to get into the apparatus would be firmly frozen to the solid surfaces.

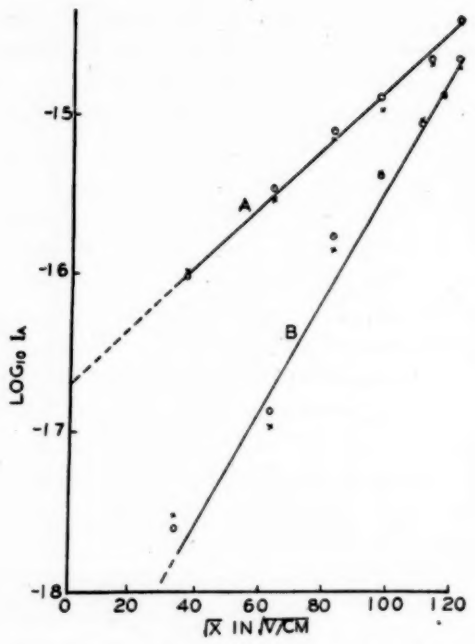

FIG. 25. Relation between $\log_{10} I_A$ and $X^{\frac{1}{2}}$. Curve A represents the results for isooctane at $T=273°$K and curve B represents the results for liquid oxygen at $T=90°$K. Open circle and cross represent the respective results for positive and negative voltages applied to the high voltage electrode of cell IV.

ACKNOWLEDGMENT

The writer wishes to thank Professor A. L. Hughes for suggesting this investigation and for his continued interest and help while the experimental work was in progress.

PHYSICAL REVIEW VOLUME 64, NUMBERS 3 AND 4 AUGUST 1 AND 15, 1943

Magnetic Rotatory Power of Crystalline Nickel Sulphate in the Short Infra-Red Spectrum

S. BREEN,* J. N. HUMPHREY, AND L. R. INGERSOLL
Department of Physics, University of Wisconsin, Madison, Wisconsin

(Received May 22, 1943)

The magneto-optical activity of thin crystals of nickel sulphate α-hexahydrate has been measured by means of the spectroradiometric method in the spectral range 0.7μ to 1.9μ and for ordinary and low (−125°C) temperatures. The curves showing the dispersion of the rotation have marked anomalies in the region of λ 0.69μ and particularly 1.16μ, matching the ones found in the optical rotation for these wave-lengths. The ratio of the rotations at low temperatures and room temperature is itself an anomalous curve. The effects can be qualitatively explained on the basis of the inverse Zeeman effect.

THE interesting anomalous optical properties of thin crystals of nickel sulphate α-hexahydrate have been studied at some length, particularly as regards optical activity, circular dichroism, and absorption in the wave-length range 0.25μ–2.3μ at ordinary[1] and low[2] temperatures. The magnetic rotation has also been measured in the visible[3] and ultraviolet[4] regions. The present work is a study of the magnetic rotatory power (Faraday rotation) in the short infra-red, particularly in the region of the absorption band at λ 1.16μ, where the optical activity shows such a striking anomaly. This has been done for both ordinary and low temperatures.

EXPERIMENTAL METHODS

The spectroradiometric method of measuring magnetic rotatory dispersion has been described[5] several times and need be only briefly mentioned. Light from a special tungsten strip filament lamp was concentrated by a spherical aluminized glass mirror into a narrow conical beam, polarized by passage through a double-image prism (only one image being used) with principal plane at 45° azimuth. This light traversed the conically bored polepieces of a large electromagnet, converging to a focus on the crystal specimen between the poles. It was then in turn focused by a second concave mirror, after passage through a large Wollaston calcite double-image prism (whose principal planes were vertical and horizontal) on the double slit of the spectrometer. The two slits were vertically above one another, and one of the two images from the Wollaston fell on each slit. After passage through the spectrometer, which used a 9-cm high heavy glass 45° prism with Wadsworth mirror mounting and two concave mirrors of 40-cm focus, the two beams fell on the two arms of a vacuum differential thermopile which was connected with a Kipp and Sons ZC galvanometer. When the system was balanced (i.e., the two beams of equal intensity), with no magnetic field, the galvanometer spot stood at zero, but exciting the magnet, with the crystal between the polepieces, caused a small Faraday rotation of the plane of polarization of the beam which fell on the Wollaston prism and the resulting unbalance gave a galvanometer deflection. To interpret this deflection in degrees or minutes of rotation, it was compared with that produced by the mechanical rotation of the polarizer through 1°. Measurements could be made in general for wave-lengths between 0.5μ and 2.3μ although the results in the present case are confined to the region 0.7μ–1.9μ.

* Now at Radiation Laboratory, Massachusetts Institute of Technology, Cambridge, Massachusetts.

[1] N. Underwood, F. G. Slack, and E. B. Nelson, Phys. Rev. **54**, 355 (1938) (see this article for earlier references); F. G. Slack and Philip Rudnick, Phil. Mag. **28**, 241 (1939); L. R. Ingersoll, P. Rudnick, F. G. Slack, and N. Underwood, Phys. Rev. **57**, 1145 (1940).

[2] P. Rudnick, F. G. Slack, and J. J. O'Connor, Phys. Rev. **58**, 1003 (1940); W. C. Knopf, Jr., and W. C. Gilmore, Jr., J. Opt. Soc. Am. **32**, 619 (1942); P. Rudnick and L. R. Ingersoll, J. Opt. Soc. Am. **32**, 622 (1942).

[3] F. G. Slack, R. T. Lageman, and N. Underwood, Phys. Rev. **54**, 358 (1938).

[4] J. J. O'Connor, C. Beck, and N. Underwood, Phys. Rev. **60**, 443 (1941).

[5] L. R. Ingersoll, J. Opt. Soc. Am. **5**, 157 (1921); Phil. Mag. [6] **18**, 74 (1909). For description of the thermopile-galvanometer system in use at present see L. R. Ingersoll and W. R. Winch, Phys. Rev. **44**, 401 (1933); L. R. Ingersoll, J. Opt. Soc. Am. **27**, 412 (1937).

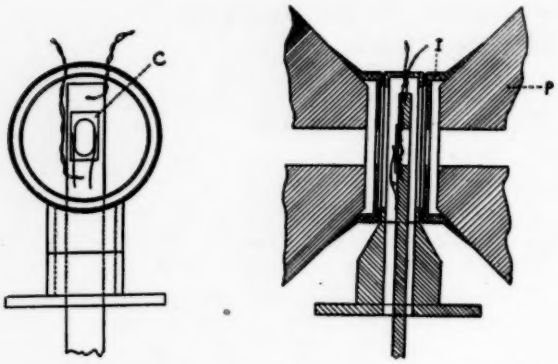

FIG. 1. Crystal holder and method of cooling. *C*, crystal; *P*, magnet polepieces; *I*, Inconel caps.

The method of keeping the crystal specimen at a suitable low temperature requires a little description. Preliminary experiments involving various ways of cooling the crystal by more or less intimate contact with liquid air in general proved unsuccessful, the chief difficulty encountered being the film of condensed moisture on the specimen or windows or both. The problem was finally solved by mounting the crystal (Fig. 1) on a flat brass bar, the end of which extended into a flask of liquid air and past which was flowing a stream of cold evaporated air. To avoid the disturbing effect due to the proximity of the relatively warm polepieces, these were sheathed with specially designed Inconel caps. The resulting temperature, which was measured by two small calibrated thermocouples in contact with the bar just above and below the crystal, could be maintained very steady at $-125°C$, and this was quite satisfactory for our purpose. The room temperature measurements were made at 25°C. Suitable water-cooling arrangements for the magnet helped in keeping this, as well as the lower temperature, satisfactorily constant.

All rotation measurements were made for a field of approximately 13,300 oersteds which was used throughout the experiments. The rotations were determined for reversal of this field in terms of the galvanometer deflections produced, as already described.

The cleaved crystal laminae varied in thickness from 0.4 to 0.9 mm; some eight different specimens were used altogether. Their diameter was only slightly larger than the 5-mm diaphragm hole over which they were mounted. The optic axis was, of course, perpendicular to the crystal surface. Both right and left crystals were used. Since it might conceivably be urged that the anomaly found in the magnetic rotation was a spurious effect connected with the great anomaly in the optical rotation[6] at λ 1.16μ, some measurements were made on a combination of the two sorts of crystals which gave a net *optical* rotation of almost zero. All results on right- and left-hand crystals and on the combination gave magnetic rotations of the same sign and essentially the same magnitude.

RESULTS AND DISCUSSION

The results are shown in Figs. 2 and 3. Too much reliance should not be placed on the absolute values of the ordinates as almost the entire emphasis in this work was on the relative values, i.e., the *dispersion* of the rotation (i.e., of the Verdet constant), or *form* of the curves. A striking anomaly, somewhat resembling that found for the optical rotation[6] at λ 1.16μ, is seen to hold also for the magnetic rotation. (There is also a minor anomaly undoubtedly connected with the absorption band at 0.69μ.) There is this important difference, however, that while in the natural or optical rotation the temperature effect is almost independent of wave-length,[7] in the present case the *ratio* of the two rotations is itself an "anomalous" function of the wave-length, as shown in Fig. 3.

In attempting to explain these results we at once find ourselves in difficulty because of a lack of knowledge of the refractive index, or rather indices, of this material in this spectral region. As a matter of fact we have already expended a great deal of effort in trying to clear up this matter but the results to date are not such as will justify their use. It will apparently be necessary to attack the problem from another angle.

In the meantime, however, a fairly satisfactory qualitative explanation can be offered for the form of the curves of Figs. 2 and 3. If the explanation of the Faraday rotation is based on the inverse Zeeman effect and if it is further assumed that the intensities of the absorption bands are unequal, an anomaly[8] of the type of

[6] See reference 1, Ingersoll, Rudnick, Slack, and Underwood, p. 1149.

[7] See reference 2, Rudnick and Ingersoll, p. 624.

[8] See Wilhelm Schütz, Wien-Harms Handbuch **16**, 82 (1936).

Fig. 2 results. To see if it would be possible to explain, on a reasonable basis, the form of the ratio curve as given in Fig. 3, we used the general equation for magnetic rotation,[9] written for a single term in the summation as

$$\alpha = NHL\frac{(n^2+2)^2}{9n}\left[A\frac{\omega^2}{(\omega_0^2-\omega^2)^2} + B\frac{\omega^2}{\omega_0^2-\omega^2} + \frac{C}{T}\frac{\omega^2}{\omega_0^2-\omega^2}\right], \quad (1)$$

ω being the frequency of the light.

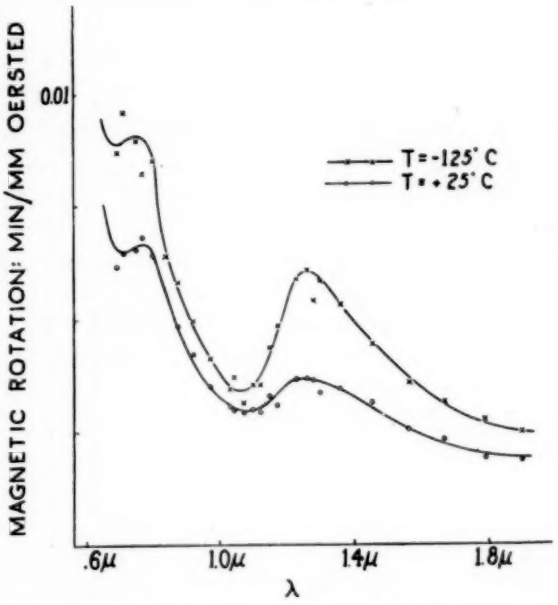

FIG. 2. Dispersion of the magnetic rotation of crystalline nickel sulphate at room temperature and low temperature.

[9] Reference 8, p. 86.

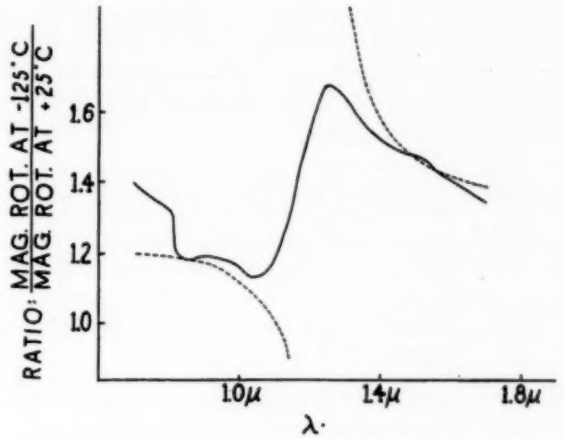

FIG. 3. Solid line, observed ratio of the magnetic rotations of crystalline nickel sulphate at −125°C and 25°C. Dotted line, theoretical ratio calculated from Eq. (1).

Lacking more exact information on the variation of n, the terms preceding the bracket have been treated as constant. We then find that if we assume $B/A = -0.01$ and $C/A = -5.00$ and if we furthermore apply an over-all factor of about $\frac{3}{4}$, there results a curve (see dotted line in Fig. 3) which has some qualitative resemblance to the one found by experiment. This is perhaps as far as it is profitable to go until more can be learned about the dispersion of the refractive index.

We wish to acknowledge our indebtedness to Professor Philip Rudnick and to Messrs. Francis Davis, Edward Strait, W. J. Pearce, and others who have aided in this investigation, and particularly to the Wisconsin Alumni Research Foundation for financial assistance.

PHYSICAL REVIEW VOLUME 64, NUMBERS 3 AND 4 AUGUST 1 AND 15, 1943

Theory of Cosmic-Ray Mesons

J. HAMILTON, W. HEITLER, AND H. W. PENG
Dublin Institute for Advanced Studies, Dublin, Ireland

(Received June 17, 1943)

The quantum theory of damping developed by two of us (Heitler and Peng) is applied to the production of mesons by proton-proton collisions. For this purpose the modification of the meson theory proposed by Møller and Rosenfeld is used. A primary radiation consisting of protons with a suitable energy spectrum is assumed, and it is shown that the rate of meson production is so high that nearly all mesons are produced in a top layer of the atmosphere of thickness 15–30 cm H_2O. The variation of the meson intensity with energy, height, and geomagnetic latitude is found to be in good agreement with the experiments. The transverse mesons, which have a very short lifetime, are seen to give, by decay, a satisfactory account of the soft component in the high atmosphere. A number of other effects (meson showers, transformation into neutretto's) are discussed in Sections VI and VII.

I. INTRODUCTION

UNTIL recently it has not been possible to apply Yukawa's meson theory of the nuclear forces to cosmic-ray mesons and thus to establish the identity of the particles predicted by Yukawa with the cosmic-ray mesons. The reason for this deep-rooted difficulty is the following: The interaction between a meson and a nuclear particle is, in contrast to the electron-light interaction, a strong one, and becomes increasingly stronger at high energies. This makes a proper treatment of the reaction forces exerted by the meson field on the nuclear particles imperative. However, as is well known, a treatment of the radiation reaction is intimately connected with the divergence difficulties occurring in every quantized field theory. To remove this difficulty two distinctly different sets of ideas have been put forward recently. Their difference can best be understood by remembering Lorentz's expansion of the reaction force which a light wave emitted by an electron exerts on the electron. This reaction force can be expanded according to powers of the electronic radius r: The first term is proportional to the acceleration and to r^{-1} thus diverging for a point particle. This term is usually thought to be included in the inertia of the particle. The second term, the usual damping term, is independent of r and proportional to the time derivative of the acceleration. Higher terms are proportional to positive powers of r and are, as a rule, neglected. In the meson case it is the charge-and-spin degrees of freedom of the nuclear particle which are coupled strongly with the meson field. We expect, therefore, that the reaction force will produce a twofold effect: (i) a large inertia to be attributed to these degrees of freedom, (ii) a large damping. In the first set of theories[1] mentioned above attention is concentrated on the first effect. It is clear that in order to make the inertia term finite, a finite particle radius has to be introduced which makes a relativistic treatment of the nuclear particle so far impossible. In the second kind of theory no physical reality is attributed to the first term of the reaction force at all. The particle is strictly considered as a point particle. By suitable subtraction the diverging inertia term of the reaction force is made to vanish (and so are the other diverging integrals occurring in the theory). The only finite part of the reaction force is then the damping term. Along this line Dirac's[2] new quantum-electrodynamics (confined so far to the electromagnetic field) is based. Independently of Dirac but in the same spirit, though less general, two of us (Heitler and Peng)[3] have made an attempt at "guessing" the correct equations of

[1] The so-called "strong coupling theory" put forward by Wentzel [Helv. Phys. Acta. **13**, 269 (1940)], Oppenheimer and Schwinger [Phys. Rev. **60**, 150 (1941)], and recently Pauli and Dancoff [Phys. Rev. **62**, 85 (1942)]. This theory is closely connected with former suggestions made by Bhabha, Ma, and Heitler, in which it was assumed that a proton and neutron can exist in excited charge and spin states.

[2] Dirac, Proc. Roy. Soc. **180**, 1 (1942) and lectures given at the Dublin Institute for Advanced Studies, to appear shortly in the Communication of the Dublin Institute for Advance Studies.

[3] Heitler and Peng, Proc. Camb. Phil. Soc. **38**, 296 (1942).

quantum electrodynamics by omitting consistently and systematically all the diverging features from the quantized field theories. A simple new set of equations has been obtained which, however, can so far only be used for non-static problems (transition probabilities) whilst the static field appears to be a problem of a higher order of difficulty. This paper[3] will, in the following, be referred to as *I*. In contrast to the older expansion method used previously for the calculation of transition probabilities the new theory includes a damping force. In cases where a classical analogue exists it can be shown that the theory is equivalent to a treatment of the second classical damping term. The transition probabilities are to be calculated from a set of simultaneous inhomogeneous integral equations. The application to multiple processes in *I* shows that the results are at least "reasonable." We hope to be able to show that our theory can, at any rate as a good approximation, be derived from Dirac's quantum-electrodynamics.[4]

It should be possible to decide between the two kinds of theories experimentally. The cross section for the scattering of mesons by a proton depends upon the energy in a different way in the two theories. More precise measurements of the scattering cross section especially as a function of the energy are therefore very desirable. An experimental decision would virtually decide whether the elementary particles have a finite radius or are point particles (*cum grano salis*).

Further applications of our theory to the creation of mesons by light quanta and through proton-proton collisions are made in two papers,[5] the results of which are the basis of the present work (referred to as *II* and *III*, respectively). They are summarized as far as they are needed in Section II. The aim of this paper is to show that the theory gives a satisfactory account—as far as we can see—of all the chief cosmic-ray phenomena connected with mesons, including their creation, their diffusion through the atmosphere, meson showers, and the transformation into neutrettos.

We shall assume that mesons are created by a primary radiation consisting of protons, in accordance with the geomagnetic evidence.

It will be seen that the rate of production of mesons is so great that practically all the mesons are produced in a very thin top layer of the atmosphere. This is indeed what recent experiments[6] have shown to be the case.

A certain ambiguity arises from the fact that at present it is not quite known which of the various modifications of the meson theory is to be used. As we endeavor to give a *connected account of cosmic-ray and nuclear phenomena* we choose that form of the meson theory which gives the best account of the nuclear forces: This is undoubtedly the form of the theory proposed by Møller and Rosenfeld.[7] Thus we assume that vector and pseudoscalar mesons exist (with equal coupling constants for transverse and pseudoscalar mesons) and that neutrettos (neutral mesons) also exist, whose coupling constants are half of those of charged mesons.

In accordance with this theory and with the fact that only pseudoscalar mesons are found at sea level we assume that vector mesons have a much smaller lifetime than pseudoscalar mesons. A lifetime of 10^{-8} sec. at rest suffices to explain that all vector mesons decay practically at the point where they are created. The meson producing layer of the atmosphere will be seen to have a thickness of less than 15–30 cm H_2O. Most of the electrons arising from the decay of the transverse mesons are, therefore, also produced in a very thin top layer of the atmosphere. We shall see in Section V that the number of these decay electrons and their energy spectrum is just of the right magnitude and type to produce, by cascade multiplication, the soft component in the high atmosphere. The observed intensity curve is in good agreement with the calculated one. Thus the *soft component can be explained as tertiary products of the incoming primary protons.*

II. PRODUCTION OF MESONS BY PROTON-PROTON COLLISIONS. RANGE OF FAST PROTONS

If a fast proton collides with another nuclear particle it may emit a meson in analogy to the

[4] This does not mean that our results should be regarded as a proof for Dirac's theory, even if our equations should prove to be in quantitative agreement with the experiments. Indeed many of the special features of Dirac's theory only become apparent when static problems are treated.

[5] Hamilton and Peng; Heitler and Peng, to appear shortly in the Proceedings of the Royal Irish Academy.

[6] Schein, Jesse, and Wollan, Phys. Rev. **59**, 615 (1941).

[7] Møller and Rosenfeld, Kgl. Danske Vid. Sels. Math.-Fys. Medd. **17** (1940).

"bremsstrahlung" emitted when a fast charged particle is deflected in a Coulomb field. The rate of production has been calculated in *III* by applying the method of Weizsäcker-Williams which has proved useful in the electromagnetic case: The field of the fast proton is expanded into a Fourier series and is, at sufficiently high energies, equivalent (i) to a beam of light quanta arising from the expansion of the Lorentz-transformed Coulomb field and (ii) to a beam of mesons arising from the Lorentz-transformed nuclear field. Both types of quanta interact with the nuclear particle at rest and can produce a meson, (i) by the process,

$$h\nu + P \rightarrow N + Y^{+} \tag{1}$$

and (ii) by scattering. It has been shown in *III* that the contribution of (i) is entirely negligible compared with that of (ii) except if the proton has an energy $>10^{12}$ ev which is not of great interest in the present work.

Thus the cross section for meson production is obtained by multiplying the number of mesons of a given energy occurring in the spectrum of the transformed nuclear field by the cross section of scattering of mesons by the nuclear particle at rest.

Throughout this paper we shall use "natural meson" units, putting $\hbar = c = \mu$ (meson mass) $= 1$. Energies are then measured in units of $\mu c^2 \sim 90$ Mev and cross sections in units of $(\hbar/\mu c)^2 = 4.3 \times 10^{-26}$ cm^2. Furthermore, we introduce a unit for the thickness of matter traversed, namely, that thickness which a fast particle with unit charge has to traverse in order to lose an energy by ionization equal to $\mu c^2 = 1$. This unit thickness is about 45 cm H_2O. Thicknesses measured in these units are denoted by x. The coupling constants of longitudinal, transverse, and pseudoscalar mesons with a nuclear particle are denoted by g^2, f^2, f'^2 (dimensionless), respectively, and their numerical values taken from the theory of nuclear forces (cf. reference 7):

$$g^2 = 0.054, \quad f^2 = f'^2 = 0.13. \tag{2}$$

The coupling constants for neutrettos are halves of these values ($f_0^2 = f_0'^2 = 0.065$, $g_0^2 = 0.027$). For the meson mass we assume the value $\frac{1}{10}$ of the proton mass.

In the "equivalent spectrum" of the field of the fast proton with energy E, charged and neutral mesons of all polarizations occur. The number of longitudinal mesons, however, is negligible. The number of transverse and pseudoscalar mesons with energy between ϵ and $\epsilon + d\epsilon$ was found in *III* to be

$$q_{tr}^{(\epsilon)d\epsilon} = \frac{d\epsilon}{\pi\epsilon} f^2 D_{tr}, \quad q_{ps}^{(\epsilon)d\epsilon} = \frac{d\epsilon}{\pi\epsilon} f^2 D_{ps}. \tag{3}$$

Here the D's are rather complicated functions of ϵ/E, involving Hankel functions, but when plotted against ϵ/E it turns out that they can quite well be represented by the following simple functions (with errors less than 30 percent):

$$\begin{aligned} &D_{tr} = 165, \qquad D_{ps} = 50(\epsilon/E)^{\frac{1}{2}}, \\ &D_{tr} + D_{ps} = 200, \quad \tfrac{1}{2}D_{tr} + D_{ps} = 115. \end{aligned} \tag{4}$$

Only these combinations of the D's will occur. D_{tr} comprises both transverse polarizations. The number of neutrettos occurring in the spectrum is half of (3).

The above method and therefore the expressions (3) are only accurate if: (i) $\epsilon \gg 1$, (ii) $E \gg M$ (proton mass). For smaller proton energies the Weizsäcker-Williams method fails completely. (For a more detailed discussion of the validity of the method cf. *III*.) In the following we shall only be interested in meson energies $\epsilon > 1/f \backsimeq 3$ for which (i) is fairly well satisfied. We shall use (3) for energies E down to values $\sim M$. This is certainly crude, but cannot involve very large errors because the slower protons are not very effective in producing mesons, on account of their small energy. If $E < M$ a proton may still produce mesons. A guidance as to the order of magnitude of this effect can be obtained in the following way: If the damping is neglected altogether and if $E \ll M$ the rate of meson production can quite easily be calculated directly by the old methods.[8] The result can be compared with that obtained by using the Weizsäcker-Williams method, also, of course, neglecting the damping, which means $\epsilon < 1/f \backsimeq 3$. The result is that the actual rate of meson production is about 10 times smaller than that obtained by using (3). We therefore expect that the *rate of meson production drops rapidly for*

[8] Cf. for example: Nordheim and Nordheim, Phys. Rev. **54**, 254 (1938).

$E<M$, and we shall neglect the contribution from protons with $E<M$.

The cross section for scattering of a meson by a nuclear particle has also been derived in *III*.[9] Since the exact expressions would be very complicated, we use only their asymptotic forms for $\epsilon \gg 1/f$. ϵ may then still be either $<M$ ("non-relativistic case") or $>M$ ("extreme relativistic case"). Since a meson with given charge and polarization may be "scattered" into a meson with different charge (a charged meson may be transformed into a neutretto and vice versa) and different polarization, we write the result in the form of a matrix attributing rows to the primary and columns to the secondary particles. Attributing rows and columns to the various polarizations as indicated in the formulae we found for the scattering cross sections:

$$\Phi=\frac{4\pi}{\epsilon^2}\begin{pmatrix} 1 & \cdot & \cdot & \cdot & \cdot & \cdot \\ \cdot & \frac{1}{3} & \frac{1}{3} & \cdot & \cdot & \cdot \\ \cdot & \frac{1}{3} & \frac{1}{3} & \cdot & \cdot & \cdot \\ \cdot & \cdot & \cdot & \frac{1}{3} & \frac{1}{3} & \cdot \\ \cdot & \cdot & \cdot & \frac{1}{3} & \frac{1}{3} & \cdot \\ \cdot & \cdot & \cdot & \cdot & \cdot & 1 \end{pmatrix} \begin{matrix} \text{long.} \\ \text{transv.} \\ \text{pseud.} \\ \text{pseud.} \\ \text{transv.} \\ \text{long.} \end{matrix} \begin{matrix} \\ \left.\begin{matrix} \\ \\ \end{matrix}\right\}\text{charged} \\ \left.\begin{matrix} \\ \\ \end{matrix}\right\}\text{neutral} \\ \\ \end{matrix} \qquad (\epsilon \ll M) \qquad (5a)$$

$$\Phi=\frac{16\pi}{\epsilon M}\begin{pmatrix} 1 & \cdot & \cdot & \cdot & \cdot & \cdot \\ \cdot & \frac{1}{4} & \cdot & \cdot & \cdot & \cdot \\ \cdot & \cdot & 1 & \cdot & \cdot & \cdot \\ \cdot & \cdot & \cdot & 1 & \cdot & \cdot \\ \cdot & \cdot & \cdot & \cdot & \frac{1}{4} & \cdot \\ \cdot & \cdot & \cdot & \cdot & \cdot & 1 \end{pmatrix} \begin{matrix} \text{long.} \\ \text{transv.} \\ \text{pseud.} \\ \text{pseud.} \\ \text{transv.} \\ \text{long.} \end{matrix} \begin{matrix} \\ \left.\begin{matrix} \\ \\ \end{matrix}\right\}\text{charged} \\ \left.\begin{matrix} \\ \\ \end{matrix}\right\}\text{neutral} \\ \\ \end{matrix} \qquad (\epsilon \gg M) \qquad (5b)$$

The rows and columns marked transv. are to be understood as giving the transition probabilities into *any one* of the two transverse polarizations of the secondary meson and thus have actually to be understood as a submatrix: for instance $\begin{pmatrix} \frac{1}{4} & \frac{1}{4} \\ \frac{1}{4} & \frac{1}{4} \end{pmatrix}$ instead of $\frac{1}{4}$ in (5b). At the places marked by dots in (5) expressions occur which are of a smaller order of magnitude containing high negative powers of ϵ. We shall use (5a) and (5b) for energies $\epsilon \lesssim M$ and $\epsilon \gtrsim M$, respectively.

In the rows and columns marked transv. of (5b) an additional diagonal term has been omitted which increases with ϵ but is multiplied by such a small factor that it becomes only appreciable for $\epsilon \gtrsim 1000$. There are also other processes, not considered in this paper at all, which become important for such extremely high energies. Throughout this paper it must be kept in mind that our formulae are no longer valid whenever such high energies are involved.

The most remarkable feature of (5) is the occurrence of *selection rules*. A meson has the tendency to conserve its charge as well as—to some extent—its polarization, and this becomes a strict law in the limit of high energies. The occurrence of these selection rules is a special feature of our theory and entirely due to the damping. No such selection rules occur if damping is neglected (which is permissible only for $\epsilon \lesssim 1/f$) and our matrices (5) would be filled everywhere with expressions of the same order of magnitude. For the interpretation of cosmic rays it will be of particular importance that charged mesons cannot be transformed into neutrettos in a collision with a nuclear particle, except at very small energies ($\epsilon \sim 1/f$) (cf. Section VII).

Another remarkable fact is that the energy dependence changes from a $1/\epsilon^2$ to a $1/\epsilon$ law for $\epsilon > M$. This fact will be fundamental for our understanding of cosmic rays.

Multiplying (5) by (3) we obtain the cross section for the production of a meson of given energy and polarization. If $\epsilon < M$ it is seen from (5a) that the pseudoscalar and the transverse parts of the equivalent spectrum combine to produce either transverse or pseudoscalar mesons. Thus the cross sections for the production of a meson with energy ϵ become

$$\Phi_{tr}(\epsilon)d\epsilon=\frac{8}{3}f^2\frac{d\epsilon}{\epsilon^3}(D_{tr}+D_{ps}), \qquad (\epsilon<M) \qquad (6a)$$

$$\Phi_{ps}(\epsilon)d\epsilon=\frac{4}{3}f^2\frac{d\epsilon}{\epsilon^3}(D_{tr}+D_{ps}). \qquad (6b)$$

Equation (6a) is already summed over both transverse polarizations. If $\epsilon > M$ the pseudoscalar part of the equivalent spectrum produces

[9] Earlier work assuming charged mesons only: Heitler, Proc. Camb. Phil. Soc. **37**, 291 (1941), and Wilson, *ibid.*, 301. (In these two papers only the non-relativistic case is treated.) Exact relativistic expression (for charged vector mesons only) by S. T. Ma, *ibid.*, in the press. Cf. also Fierz, Helv. Phys. Acta. **14**, 105 (1941); Landau, J. Phys. U. S. S. R. **2**, 483 (1940).

only pseudoscalar mesons and the transverse part only transverse mesons. Thus

$$\Phi_{tr}(\epsilon)d\epsilon=(8/M)f^2\frac{d\epsilon}{\epsilon^2}D_{tr}, \quad (\epsilon>M) \tag{6c}$$

$$\Phi_{ps}(\epsilon)d\epsilon=(16/M)f^2\frac{d\epsilon}{\epsilon^2}D_{ps}. \tag{6d}$$

In (6c, d) ϵ is not the energy of the meson produced but the energy lost by the moving proton, i.e., the energy of the meson produced plus the recoil energy of the nuclear particle originally at rest. The probability for the meson to take up an energy ϵ' leaving the energy $\epsilon-\epsilon'$ to the recoil particle is simply $d\epsilon'/\epsilon$. This is true if, as in fact is the case, the angular distribution of scattering is uniform in a Lorentz system where the meson and nuclear particle are colliding with opposite and equal momenta; thus the cross section for producing a meson of energy ϵ' is in the extreme relativistic case:

$$d\epsilon'\int_{\epsilon'}^{E}\Phi_{tr}(\epsilon)\frac{d\epsilon}{\epsilon}\backsimeq\tfrac{1}{2}\Phi_{tr}(\epsilon')d\epsilon', \tag{6'c}$$

$$d\epsilon'\int_{\epsilon'}^{E}\Phi_{ps}(\epsilon)\frac{d\epsilon}{\epsilon}\backsimeq\tfrac{2}{3}\Phi_{ps}(\epsilon')d\epsilon'. \quad (\text{for } E\ll\epsilon') \tag{6'd}$$

The energy distribution remains the same but the number of mesons is only $\frac{1}{2}$ or $\frac{2}{3}$ of what it would be if all the energy would be taken up by the meson. The rest of the energy is taken up by the recoil particles. Their energy distribution is also given by (6c, d) and their number is (6c, d) multiplied by $\frac{1}{2}$ and $\frac{1}{3}$, respectively. These recoil particles are further capable of producing mesons and recoil particles. The process repeats itself until the energy has degenerated to a sufficiently low value to make further meson production impossible. The process very much resembles the *cascade multiplication* of electrons but is not so pronounced because the energy distribution (6) favors low energies more strongly than in the case of the bremsstrahlung emitted by a fast electron. Thus the energy degenerates more quickly than in the electromagnetic case. A detailed treatment of this cascade process lies outside the scope of this paper which is only intended to give a first orientation. We can take account of it in a crude way by using (6c, d) instead of (6'c, d) also for the number of mesons produced. By doing so we represent the energy loss of the primary proton correctly. Also the total energy content of the charged mesons is correct because the energy given by the recoil particles to neutrettos is compensated by the energy of those charged mesons which are produced by the recoil particles from neutrettos. Using (6c, d), we overrate the number of fast mesons by a factor 2 or $\frac{3}{2}$, respectively, but we also underrate the number of slower mesons. Thus the error committed by using (6c, d) is a slight distortion of the energy spectrum in favor of high energies, whilst the total number of mesons will be somewhat bigger than what we obtain in this way.

We multiply (6) by the number of nuclear particles contained in a cylinder of unit length, measured in our x units, and with cross section equal to our unit cross section. For water or air this figure is 1.18, but is not very different for other materials (for Pb it is about 1.3).

We then obtain the number of mesons with energy ϵ produced by a proton in traveling the distance dx (using (2) and (4)):

$$\left.\begin{aligned}\Phi_{tr}(\epsilon)d\epsilon dx&=82\frac{d\epsilon}{\epsilon^3}dx \qquad (7a)\\ \Phi_{ps}(\epsilon)d\epsilon dx&=41\frac{d\epsilon}{\epsilon^3}dx \qquad (7b)\end{aligned}\right\}\ (\epsilon<M),$$

$$\left.\begin{aligned}\Phi_{tr}(\epsilon)d\epsilon dx&=21\frac{d\epsilon}{\epsilon^2}dx \qquad (7c)\\ \Phi_{ps}(\epsilon)d\epsilon dx&=12.3\left(\frac{\epsilon}{E}\right)^{\frac{1}{2}}\frac{d\epsilon}{\epsilon^2}dx \qquad (7d)\end{aligned}\right\}\ (\epsilon>M).$$

For neutrettos the above figures are to be halved. All these formulae are only valid for $\epsilon>1/f\backsimeq 3$.

From (7) it is seen immediately that a very fast proton produces more mesons with energy between $1/f$ and M than with $\epsilon>M$, but far the greater part of the *energy* is contained in the fast mesons.

The mesons with $\epsilon>M$ are all emitted in the forward direction, within a very small angle. This is not so for the mesons with $\epsilon<M$. The latter play a not very important role, except in

TABLE I. Range of fast proton.

E_0	20	50	100	300	1000	10,000
$x_{E_0,M}$	0.18	0.45	0.83	2.0	4.1	28

the top part of the atmosphere. For the calculation of intensities, the error will not be *very* large if we disregard any angular dependence and assume that *all particles* are always *emitted in the forward direction*. This we shall do throughout this paper. For this reason, and because we use in many places asymptotic laws instead of exact ones, and finally because we have only taken a crude account of the cascade process mentioned above, we must not expect too high an accuracy for our calculations. On the average, errors will be of the order of magnitude of, say, a factor 2.

From (7) the energy loss of a proton can be obtained immediately. Multiplying by $\frac{3}{2}$ to account for the energy lost by producing also neutral particles and summing over-all polarizations we find (for $E>M$, of course)

$$-\frac{dE}{dx}=\sum_{\text{polar.}}\int_{1/\beta}^{E}\epsilon\Phi(\epsilon)d\epsilon=43\log 0.3E. \quad (8)$$

The energy loss is very high. It depends in a similar way on E to the ordinary energy loss by ionization but is roughly a hundred times larger. Per cm Pb (about $\frac{1}{5}$th of our x units) a proton with an energy of 3×10^9 ev loses an energy of 2×10^9 ev.

Accordingly the *range of a fast proton* is very small. Of course, (8) is only valid for $E>M$; therefore, we can calculate only the distance a proton travels until it is slowed down to an energy $\sim M$. We find

$$x_{E_0,M}=\int_M^{E_0}dE\Big/\left(-\frac{dE}{dx}\right)$$
$$=\frac{1}{13}\{\text{li}(0.3E)-\text{li}(0.3M)\} \quad (9)$$

where "*li*" is the integral-logarithm. For practical purposes *lix* can well be replaced by $x/\log x$ (this is exact for large x). For $x_{E_0,M}$ we thus find for the range the values given in Table I. In our units the thickness of the atmosphere is 22. Thus a proton needs an energy of more than 7000, i.e., 7×10^{11} ev in order to penetrate through the whole atmosphere and still retain an energy M. The majority of the protons entering the atmosphere at a latitude of 50° ($E\sim22-50$) lose the effective part of their energy in distances of 0.2–0.5 (9–23 cm H_2O).

The theory does not tell us how quickly a proton loses its energy *after* having been slowed down to an energy M. Although meson production is then negligible compared with its rate at higher energies, the energy loss may still be much greater than that due to ionization. If our above estimate is correct (rate of meson production $\frac{1}{10}$ of that at higher energies), the energy loss would be 10 times greater than that due to ionization and the range of a proton with $E\sim M$ about 2 of our units (1 m H_2O).

Below we shall need the distance a proton travels in order to lose energy from E_0 to E:

$$x_{E_0,E}=\frac{E_0}{43\log 0.3E_0}-\frac{E}{43\log 0.3E} \quad (10)$$

in which we have replaced the $li(x)$ function by $x/\log x$.

III. PRODUCTION AND DIFFUSION OF PSEUDOSCALAR MESONS IN THE ATMOSPHERE

Since the primary protons have an extremely short range the majority of the mesons is produced in a thin top layer of the atmosphere. The transverse mesons are expected to decay almost at once, and only the pseudoscalar mesons will travel through the atmosphere. Their absorption is due to two factors: (i) energy loss by ionization (ii) β-decay. The latter depends upon the distance the meson travels but not on the amount of matter traversed. We assume for simplicity that the density of the atmosphere at a depth x below the top is proportional to x. The probability of a meson at a depth x and with energy ϵ decaying while traveling the distance dx is therefore $dxb/\epsilon x$, where b is inversely proportional to the lifetime τ of a meson at rest. We choose τ from the results of Rossi and Hall,[10] who measured the ratio τ/μ. For $\mu=185$, τ becomes $2\times7\times10^{-6}$ sec. b is then

$$b=\frac{1}{c\tau}\times(\text{distance in cm corresponding to one } x \text{ unit at sea level})\times(\text{height of atmosphere in } x \text{ units})$$

or $b=13$.

[10] Rossi and Hall, Phys. Rev. **59**, 223 (1941).

Let $f(\epsilon, x)d\epsilon$ be the number of mesons with energy ϵ at depth x and $S(\epsilon, x)dx$ the number of mesons produced at depth x in the distance dx. Then f satisfies the diffusion equation

$$\frac{\partial f}{\partial x}=\frac{\partial f}{\partial \epsilon}\frac{b}{\epsilon x}f+S. \tag{11}$$

This differs from the diffusion equation considered and solved previously by Euler and Heisenberg[11] by the inclusion of the source function S (which is determined by our theory). The term $\partial f/\partial\epsilon$ accounts for the energy loss by ionization. Equation (11) can be solved by introducing new variables

$$\eta=\epsilon+x, x$$

instead of ϵ and x. The solution with the boundary condition $f=0$ for $x=0$ is

$$f(\eta, x)=\left(\frac{\eta-x}{x}\right)^{b/\eta}\int_0^x S(\eta, \xi)\left(\frac{\eta-\xi}{\xi}\right)^{-b/\eta}d\xi,$$

$$\eta=\epsilon+x. \tag{12}$$

S is determined by our theory if we know the number of protons of each energy and at each depth x. The latter depends, of course, on the energy spectrum of the protons falling onto the top of the atmosphere. From the measurements at great depths it will be seen below that the primary spectrum is within certain comparatively wide energy regions a simple power law. For our purpose it is convenient to include also the logarithmic term occurring in (8) in the expression for the primary spectrum; thus we assume that the number of primary protons with energy larger than E is of the form $A\{E/43\log 0.3E\}^{-\alpha}$. There is, of course, not the slightest reason why α should be exactly a constant. The experiments only show that α does not vary much if E changes by a factor 10 or so. Indeed, the measurements at extreme depths indicate an increase of α with increasing E. We shall determine α from underground measurements and shall find $\alpha=2.2$ for E between 100 and 1000. For larger E, α is bigger. Consequently we expect α to be smaller for $E<100$. The latter energy region will be of importance for the upper regions of the atmosphere and for the intensity curve of the soft component. α can be determined then from the shape of the Regener-Pfotzer-curve. We found $\alpha=1.3$ satisfactory for $E<100$. Thus the chief phenomena of cosmic radiation will be explained by the following crude but simple primary differential spectrum:

$$dF(E)=\frac{\partial}{\partial E}\frac{A}{(E/43\log 0.3E)^{2.2}}\quad(\text{for } E>100),$$

$$dF(E)=\frac{\partial}{\partial E}\frac{B}{(E/43\log 0.3E)^{1.3}}\quad(\text{for } E<100), \tag{13}$$

$$B=\frac{2.2}{1.3}\left(\frac{43\log 30}{100}\right)^{0.9}A=2.4A,$$

the connection between B and A being determined by the continuity of the primary spectrum. In reality α will change gradually from smaller to larger values as E increases. For any depth x larger than 2 only the high energy part of (13) will be important. The number of protons with energy larger than E at depth x is, according to (10) and (13):

$$F(E, x)=A\left(\frac{E}{43\log 0.3E}+x\right)^{-2.2},$$

$$F(E, x)=B\left(\frac{E}{43\log 0.3E}+x\right)^{-1.3}$$

$$-B\left(\frac{100}{43\log 30}+x\right)^{-1.3}$$

$$+A\left(\frac{100}{43\log 30}+x\right)^{-2.2}, \tag{14}$$

according to whether

$$\frac{E}{43\log 0.3E}+x\gtrless\frac{100}{43\log 30}.$$

The source function $S(\epsilon, x)$ for pseudoscalar mesons is then, by (7b, d),

$$S(\epsilon, x)=41\frac{1}{\epsilon^3}F(M, x)\quad(\epsilon<M), \tag{15a}$$

$$S(\epsilon, x)=12.3\frac{1}{\epsilon^2}\int_\epsilon^\infty\left(\frac{\epsilon}{E}\right)^{\frac{1}{2}}\frac{\partial F(E, x)}{\partial E}dE$$

$$(\epsilon>M). \tag{15b}$$

[11] Euler and Heisenberg, Ergeb. d. exakt. Naturwiss. **17** (1938).

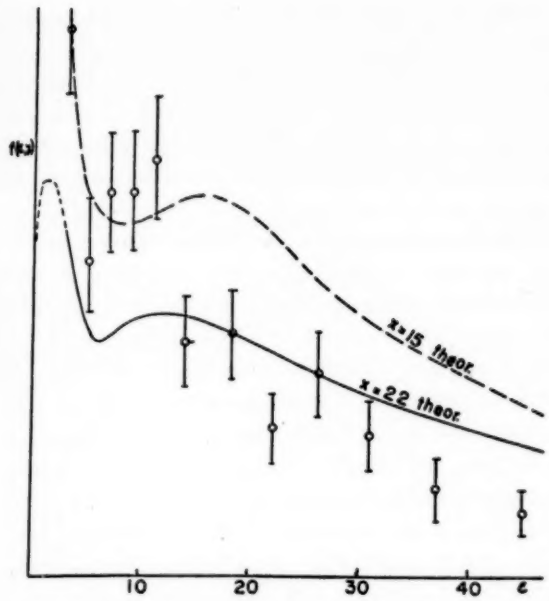

FIG. 1. Energy spectrum of pseudoscalar mesons at sea level, theoretical and experimental. Dotted curve: theoretical spectrum at a height of 4000 m (50 cm Hg).

Thus $f(\epsilon, x)$ becomes:

$$f(\epsilon, x)=41\left(\frac{\eta-x}{x}\right)^{b/\eta}\int_0^x \frac{\xi^{b/\eta}}{(\eta-\xi)^{2+b/\eta}}F(M, \xi)d\xi \qquad (\eta-\xi<M), \quad (16a)$$

$$f(\epsilon, x)=12.3\left(\frac{\eta-x}{x}\right)^{b/\eta}\int_0^x d\xi\int_{\eta-\xi}^{\infty} dE\left[\frac{(\eta-\xi)}{E}\right]^{\frac{1}{2}} \times\frac{\xi^{b/\eta}}{(\eta-\xi)^{2+b/\eta}}\frac{\partial F(E, \xi)}{\partial E} \qquad (\eta-\xi>M), \quad (16b)$$

$$\eta=\epsilon+x.$$

In (16) the limits 0, x have to be replaced: in (16a) by $\eta-M\cdots x$ and in (16b) by $0\cdots\eta-M$ if $\eta-M$ lies between 0 and x. After the integration η is again to be replaced by $\epsilon+x$. In (16) the expression (14) for $F(E, X)$ is to be inserted. Actually each integral (16) consists of two parts with two different values of α. It turns out, however, that for most values of ϵ, x, only one part of (14) is predominant, the other leading only to minor corrections; in particular for any depth $x\geqslant 2$ only that part of F with $\alpha=2.2$ is important.

The integrals (16) cannot be worked out exactly in closed form, but for most values of ϵ, x good approximations can be found. Equation (16a) is needed only for a few values of x and ϵ ($\epsilon<M$) and has been worked out numerically. In (16b) the logarithm occurring in F may be replaced by an average value. The chief contribution arises from small ξ (corresponding to the fact that the protons have extremely small range). For any value of $x>2$, and even with reasonably good approximation for $x=1$, ξ can be neglected against $\eta=\epsilon+x$ and the integration be extended to ∞ instead of x. The exact condition for this to be true is

$$x\gg\frac{\eta}{43\log 0.3\eta} \qquad (17)$$

which is satisfied for all but extremely small x or extremely large ϵ. Equation (16b) then becomes, if only the high energy part of F, ($\alpha=2.2$) is used

$$f(\epsilon, x)=12.3A\frac{\Gamma(1+b/\eta)\Gamma(\alpha-b/\eta)}{\Gamma(\alpha)\Gamma(\alpha-\frac{1}{2}-b/\eta)}\left(\frac{\epsilon}{x}\right)^{b/\eta}\eta^{-1-\alpha} \times(43\log 0.3\eta)^{\alpha-1-b/\eta} \quad \eta=\epsilon+x. \quad (18)$$

For $x<1$ the contribution of (16b) has only been estimated but here (16a) is much more important than (16b).

From (18) the asymptotic laws can immediately be read off:

(i) *Tail end of the energy spectrum.* Consider $\epsilon\gg x$ which for the lower part of the atmosphere also implies $\epsilon\gg b=13$.

$$f(\epsilon, x)d\epsilon\propto d\epsilon\cdot\epsilon^{-1-\alpha}(\log 0.3\epsilon)^{\alpha-1}. \qquad (19)$$

Since $\alpha=2.2$ the energy spectrum falls off a little less rapidly (because of the logarithmic term) than $\epsilon^{-3.2}$.

(ii) *Great depths.* For underground measurements in dense materials the decay constant b should be put equal to zero. $f(\epsilon, x)$ is then a function of $\epsilon+x$ only. Integrating over ϵ we find for the total number of mesons:

$$I(x)=\int_{1/f}^{\infty} f(\epsilon, x)d\epsilon\propto x^{-\alpha}(\log 0.3x)^{\alpha-1}. \qquad (20)$$

Thus the total intensity decreases like $x^{-\alpha}$, again apart from a logarithmic modification, and it is in this way that $\alpha=2.2$ was determined.

In Fig. 1 the theoretical energy spectrum is

compared with the measurements by Blackett[12] for small and medium energies. It is seen that the shape of the theoretical curve is nearly the same as the experimental one. On the whole the theoretical spectrum falls off less rapidly than the experimental one. This was to be expected because of the crude way in which we have accounted for the cascade production of mesons as explained in Section II. The experimental minimum at $\epsilon = 20$ does not appear in the theoretical

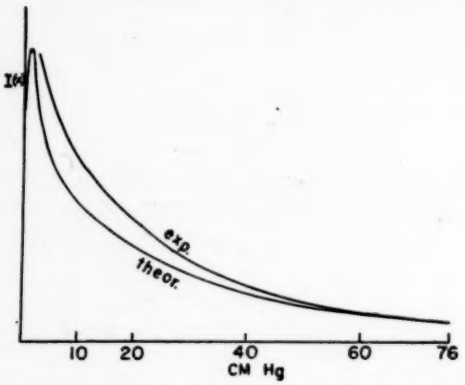

FIG. 2. Theoretical number of pseudoscalar mesons and experimental number of penetrating particles as function of height.

curve and is probably due to a special absorption process as was supposed by Blackett (production of proton pairs?). The maximum at $\epsilon = 10$ is clearly indicated in the experiments as well as in the theoretical curve. It is difficult to trace the origin of this maximum as many factors combine to produce it. This maximum did not appear, however, in the calculations of Heisenberg and Euler, in which the exact source function was not used. For the low energy end ($\epsilon \sim 3$) of $f(\epsilon, x)$ also the contribution from those very few very energetic protons which penetrate to the lower parts of the atmosphere and produce a large number of slow mesons is important. Hence the rise of the spectrum for small ϵ. Actually the curve will bend down to zero for $\epsilon < 3$, as indicated in the figure, but in order to reproduce this part of the curve correctly it would be necessary to use the exact cross section for scattering instead of the asymptotic one (5).

There is another reason why we must expect to find few slow mesons for $\epsilon < 3$, say. It will be seen in Section VII that a meson, once having reached an energy $\epsilon < 4$, has a probability of 79 percent to be transformed into a neutretto before reaching the end of its range. This would remove a large fraction of mesons from the lower end of the spectrum.

The high energy tail end of the spectrum, i.e., the decrease of $f(\epsilon, x) \propto \epsilon^{-3 \cdot 2}$ (modified by the logarithmic term) has already been adequately discussed by Euler and Heisenberg[11] and was found to agree with the measurements. In order to see how the energy spectrum varies with height we have also plotted the theoretical spectrum for $x = 15$ (50 cm Hg). Slow mesons become relatively more predominant.

In Fig. 2 the total number of mesons

$$I(x) = \int_{1/\beta}^{\infty} f(\epsilon, x) d\epsilon$$

is plotted against height and compared with the recent measurements by Schein, Jesse, and Wollan.[13] Here also the agreement is as good as can be expected. The maximum occurs at an extreme height of $x = 0.5$ corresponding to only 22 cm H_2O or 1.8 cm Hg. In the measurements at extreme heights presumably some of the primary protons also are included as "penetrating particles," but it is difficult to say how many protons have to be classed as "penetrating" because we do not know exactly the range of a proton with energy less than M. We estimate the range to be about 2 x units (=9 cm Pb) for $E = M$ and accordingly smaller for $E < M$. The theoretical curve of Fig. 2 refers to pseudoscalar mesons only. The two curves are normalized so as to agree at sea level.

IV. LATITUDE EFFECT

In the calculations of Section III no account has been taken yet of the fact that the primary energy spectrum is cut off for energies smaller than E_ϑ depending on the geomagnetic latitude ϑ. $E_\vartheta = 22$ for $\vartheta = 50°$ and $E_\vartheta = 150$ for $\vartheta = 0°$ (equator). The correction can easily be made. From (16) the contribution from those protons which, at the top of the atmosphere had an

[12] Blackett, Proc. Roy. Soc. **159**, 1 (1937), **165**, 11 (1938). Compare also: Jones, Rev. Mod. Phys. **11**, 235 (1939); Hughes, Phys. Rev. **57**, 592 (1940).

[13] Schein, Jesse, and Wollan, Phys. Rev. **59**, 615 (1941).

energy $<E_\vartheta$ has to be subtracted, i.e., for which

$$\xi+E/43\log 0.3E<E_\vartheta/43\log 0.3E_\vartheta.$$

It has turned out that for "normal latitudes" 50°, say, the correction is negligible throughout the atmosphere. This means that *no increase of intensity is to be expected for more northern latitudes*, not only at sea level but also at any height above sea level, except the very top of the atmosphere, and even there the increase is small. This explains the well known *knee of the latitude effect* at 50°.

The reason is easily to be understood. Protons stop producing mesons for $E<M=10$.

Even the contribution from protons with energy between 10 and 22 is very small on account of their smaller energy (in fact even smaller than assumed in this paper where the asymptotic law for meson production for $E\gg 10$ has been extended to $E=10$). Thus the reason for the knee of the latitude effect is simply the fact that protons of energy less than $E_{50°}$ cease to produce, or produce very few mesons. The same applies to the soft component. We shall see in Section V, that the soft component is probably due to the decay of transverse mesons in the high atmosphere, the former being also produced by the same primary protons. Thus the same knee of the latitude effect is to be expected for electrons, which is also found experimentally.[14] The fact that the soft component shows the same latitude knee as the hard component supports the assumption that both are produced by the same primary radiation, i.e., by protons, as explained by our theory.

TABLE II. Latitude effect. $(I_{50°}-I_{equ})/I_{50°}$.

	mesons				soft component
x	22 (sea level)	15	2	1	$x=2$
theor.	0.13	0.13	0.18	0.33	0.62
exp.	0.1	—	—	—	0.75

For latitudes $<50°$ an appreciable latitude effect is to be expected. We calculate the *latitude defect* $\Delta_\vartheta f(\epsilon,x)$, i.e., the difference of $f(\epsilon,x)$ between the North Pole and the latitude ϑ. As mentioned above $\Delta_\vartheta f(\epsilon,x)$ is negligible for $\vartheta>50°$. From (16) those contributions have to be subtracted for which $\xi+E/43\log 0.3E<E_\vartheta/43\log 0.3E_\vartheta$. Thus $\Delta_\vartheta f(\epsilon,x)$ is given by (for $\eta-\xi>M$):

$$\Delta_\vartheta f(\epsilon,x)=12.3\left(\frac{\eta-x}{x}\right)^{b/\eta}\int_0^{\xi_\vartheta}d\xi\int_{\eta-\xi}^{E_{\vartheta\xi}}dE \times\left[\frac{(\eta-\xi)}{E}\right]^{\frac{1}{2}}\frac{\xi^{b/\eta}}{(\eta-\xi)^{2+b/\eta}}\frac{\partial F(E,\xi)}{\partial E}, \quad (21)$$

with

$$\frac{E_{\vartheta\xi}}{43\log 0.3E_{\vartheta\xi}}+\xi=\frac{E_\vartheta}{43\log 0.3E_\vartheta},$$

$$\xi_\vartheta=\frac{E_\vartheta}{43\log 0.3E_\vartheta}-\frac{\eta}{43\log 0.3\eta}$$

$$\eta=\epsilon+x.$$

(In the condition for ξ_ϑ, ξ has been neglected compared with η). $\Delta_\vartheta f$ is, of course, zero whenever in (21) an upper limit is smaller than the lower limit. A similar integral holds for $\eta-\xi<M$.

We have worked out the integrals numerically. Here the change of α at $E=100$ is important. Integrating over ϵ we find the latitude effect for the total number of mesons:

$$I_{50°}-I_\vartheta=\int_{1/f}^{\infty}\Delta_\vartheta f(\epsilon,x)d\epsilon.$$

The results are given in Table II. The latitude effect is fairly constant for low levels and only increases for $x<2$. The figure for sea level is in good agreement with the experiments, whilst at greater elevations no measurements seem to have been made yet for the hard component. For the figure concerning the soft component see Section V.

V. THE TRANSVERSE MESONS AND THE SOFT COMPONENT

In addition to pseudoscalar mesons the primary protons produce a large number of transverse mesons which we assume to decay at once. If the mesons have energy $\epsilon\gg 1$—which is nearly always the case—the decay electrons are emitted in the forward direction and take up with equal probability, any amount of energy between 0 and ϵ. Thus a large number of slow and fast electrons are produced. The fast ones multiply by cascade multiplication and it will be seen that a satisfactory account of the soft component can be

[14] Carmichael and Dymond, Proc. Roy. Soc. **171**, 321 (1939).

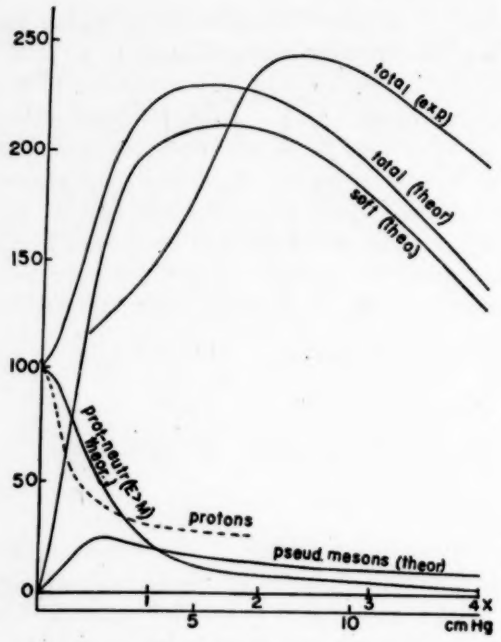

FIG. 3. Cosmic-ray intensities in the top part of the atmosphere for 100 primary protons. Soft component (theor.), pseudoscalar mesons (theor.), primary protons and neutrons (theor.), and total intensity (theor. and exp.).

given in this way. Let $F(\epsilon, x)$ be the number of protons at depth x with energy larger than ϵ. [F is given by (14).] Then the number of electrons produced at x in the energy interval $d\mathfrak{E}$ is

$$d\mathfrak{E}\int_{\mathfrak{E}}^{\infty} F(\epsilon, x)\Phi_{tr}(\epsilon)\frac{d\epsilon}{\epsilon}.$$

Let now $C(\mathfrak{E}, \xi)$ be the cascade multiplication function (i.e., the number of electrons produced in a depth ξ by one primary electron of energy $\mathfrak{E}$), the total number of electrons at depth x is

$$Z_{tr}(x)=\int_0^x d\xi\int_0^{\infty} d\mathfrak{E}\int_{\mathfrak{E}}^{\infty}\frac{d\epsilon}{\epsilon}\Phi_{tr}(\epsilon) \times F(\epsilon, \xi)C(\mathfrak{E}, x-\xi). \quad (22)$$

Equation (22) can be worked out partly by making suitable approximations and partly numerically. For $\Phi_{tr}(\epsilon)$ the expressions (7a, c) and for F (14) are to be used. For the high atmosphere ($x<4$, say) practically only the low energy part of $F(\alpha=1.3)$ is important. For C we have used the figures given by Arley.[15]

[15] Arley, Proc. Roy. Soc. **A168**, 519 (1938). In the cascade theory different units for the thickness of matter traversed are usually used. For air or water one cascade unit is about $\frac{1}{3}$ of our x units.

To obtain an idea of the effect to be expected we consider large values of x. ($x>5$, say.) We can then make the following approximations: $F(\epsilon, \xi)$ decreases rapidly with ξ for any ϵ of importance. $C(\mathfrak{E}, x-\xi)$ can be replaced by $C(\mathfrak{E}, x)$ and the integral over ξ extended to infinity instead of to x. This amounts to assuming that all the mesons produced in the atmosphere are practically produced at the very top and, decaying at once, produce a "primary" electron spectrum $N(\mathfrak{E})d\mathfrak{E}$ say, which later produces cascade effects. $N(\mathfrak{E})$ is given by

$$N(\mathfrak{E})=\int_{\mathfrak{E}}^{\infty}\Phi_{tr}(\epsilon)\frac{d\epsilon}{\epsilon}\int_0^{\infty}F(\epsilon, \xi)d\xi. \quad (23)$$

We divide the range of energy $\mathfrak{E}$ into 4 regions, and find for $N(\mathfrak{E})$ (considering logarithmic terms as constants, and using the low energy part of F only):

$$\begin{aligned} N(\mathfrak{E})d\mathfrak{E} &= 33B\frac{d\mathfrak{E}}{\mathfrak{E}^2}\left(\frac{43\log 0.3\mathfrak{E}}{\mathfrak{E}}\right)^{0.3} && (\mathfrak{E}>E_0=22)\\ &= Bd\mathfrak{E}\left\{\frac{61}{\mathfrak{E}^2}-\frac{99}{\mathfrak{E}43\log 0.3\mathfrak{E}}+0.1\right\} && (E_0>\mathfrak{E}>M=10)\\ &= Bd\mathfrak{E}\left\{\frac{142}{\mathfrak{E}^3}+0.34\right\} && (10>\mathfrak{E}>1/f=3)\\ &= 5.6Bd\mathfrak{E} && (\mathfrak{E}<3). \end{aligned} \quad (24)$$

Equation (24) plays the role of the primary electronic energy spectrum responsible for the soft component. $N(\mathfrak{E})$ decreases approximately like $1/\mathfrak{E}^2$, at any rate in the high energy region. But there are also a large number of soft electrons present. Apart from the latter $N(\mathfrak{E})$ is indeed very similar to the primary electron spectrum deduced first by Nordheim and Heitler[16] from the intensity curve of the soft component on grounds of the cascade theory and later found by Bowen, Millikan, and Neher[17] by latitude measurements. We therefore expect that (24) should give rise to an intensity curve for the soft component very similar to the observed one. The effect of the low energy electrons with small range also present in

[16] Nordheim, Phys. Rev. **51**, 1110 (1937); Heitler, Proc. Roy. Soc. **161**, 261 (1937).

[17] Bowen, Millikan, and Neher, Phys. Rev. **52**, 80 (1937) and **53**, 855 (1938).

(24) will be that the intensity curve does not fall down very steeply near the top but becomes in fact rather flat.

For the most interesting part of the atmosphere ($x=2, 3$, maximum of the Regener-Hotzer-curve) the use of (24) is too crude an approximation. In fact quite a number of low energy mesons are still produced at levels $x>2$. We have therefore used (22) directly and evaluated the integrals. We find that on the average one primary proton produces about 1.5 electrons at $x=2$ or 3 in this way.

In addition to the electrons produced by the decay of transverse mesons there are also electrons produced by the decaying pseudoscalar mesons. Their number is smaller but not negligible compared with the number of electrons due to transverse mesons. We easily find:

$$Z_{ps}=\int_0^x d\xi\int_0^\infty d\beth\int_\beth^\infty \frac{d\epsilon}{\epsilon}\frac{b}{\xi}f(\epsilon,\xi)C(\beth,x-\xi), \quad (25)$$

where $f(\epsilon, \xi)$ is the energy spectrum of pseudoscalar mesons as calculated in Section III. The result is for instance the following for $x=2$ and for one primary proton: $Z_{tr}=1.5$, $Z_{ps}=0.6$, $Z_{tr}+Z_{ps}=2.1$. Thus one primary proton produces in the average altogether about 2 electrons at the Regener-maximum, roughly $\frac{1}{3}$ of which are due to pseudoscalar and $\frac{2}{3}$ to transverse mesons. This is in very good agreement with the experiments. In Fig. 3 we have plotted the intensities of all the cosmic-ray components for the top part of the atmosphere (normalized for 100 incident protons). The agreement with the Regener-Hotzer-curve for the total intensity is as good as can be expected. The position of the maximum is, however, slightly shifted towards greater heights, than is found experimentally. The reason is probably that we have been overrating the production of slow mesons (and therefore slow electrons) by protons of energy just above M.

The latitude effect of the soft component is very large. We have calculated it for $x=2$ and included the result in Table III. The agreement with the measurements by Bowen, Millikan, and Neher[17] is good. The latter measurements refer to the total intensities, of which, however, the soft component is far the strongest.

There is one experiment which is apparently in contradiction to our assumption that the soft component originates from primary protons. Whilst the mesons in the lower atmosphere show an east-west asymmetry as big as the latitude effect proving that they originate from positive primaries no such east-west asymmetry has been found for the soft component in the high atmosphere although the latter is also—and very strongly—latitude sensitive.[18] If this result is taken at its face value it would mean that the soft component originates from equal numbers of positive and negative primary particles. We must remember, however, that the soft component is, if our picture is correct, created by the primary protons in a rather indirect way: The protons first produce mesons which decay into electrons, which then multiply by means of the cascade process. An east-west asymmetry can only be expected if in each of these three processes the particles are always strictly emitted in the forward direction with no appreciable angular straggling. This is surely the case if the secondary mesons have energies large compared with M, and if these mesons then decay while still having an energy large compared with one.

In the high atmosphere, however, low energy particles are predominant. Indeed, as it appears from the calculations of this section, most of the electrons in the high atmosphere originate from mesons with energy less or not much greater than M. These mesons are bound to be emitted in all directions with only a slight favoring of forward directions. Even for the more energetic particles the predominance of forward directions will be impaired to some extent by the many processes which have to take place to produce the soft component. It might, therefore, well be that the east-west effect is completely masked by the large angular straggling of the soft component.

TABLE III. Cosmic-ray intensities (100 primary particles).*

	soft comp. $x=2$	soft+hard $x=2$	mesons sea level	energetic protons and neutrons sea level
theor.	208	220	1.7	1/500
exp.	—	225	4	1/2000

* The column soft+hard ($x=2$) does not include the primary protons at this depth. Their number should be added to the theoretical figure 220 but is probably less than 20 (cf. Section VI).

[18] Johnson, Phys. Rev. **56**, 219 (1939).

For a judgment of this theory it must be remarked that, once the number of primary protons is normalized, and their energy spectrum given, the theory allows one to calculate the *absolute intensities* of all cosmic-ray components at each depth without further adjusting our intensities to those of the experiments. It is clear that the values of the intensities depend entirely on the constants occurring in the theory, especially on the nuclear coupling constants g, f. All these constants are either determined from nuclear facts (g, f) or by direct experiments (meson mass, decay constants). It is interesting to compare the intensities obtained by our theory with the experimental ones. Table III gives a selection of data. The absolute number of mesons at sea level is about twice of that calculated. This is quite what we had to expect as was remarked in Section II. (The last column refers to measurements by Jannossy, discussed in Section VI.)

VI. PROTONS, NEUTRONS, MESON-SHOWERS

The primary protons entering the atmosphere are very quickly slowed down to energy ~ 10. Since their energy loss is mainly due to producing charged mesons we must expect that half of these "protons" have in fact become neutrons after having travelled only a very small distance. In Fig. 3 we have plotted the number of these protons or neutrons with energy $>M$ as a function of depth for the primary energy spectrum (13), the number simply being given by the relation (14). It is seen that their intensity decreases very rapidly. For a discussion of the experiments, however, we would rather like to know the number of protons (not neutrons) with all energies, including $E<M$. This number can only be guessed at present, since we do not know at what rate protons lose their energy once E is less than M. All we can say is that the number of protons drops very quickly to half the initial value (the other half have become neutrons). We might estimate that the energy loss of a proton becomes say 10 times smaller as E becomes less than M (cf. Section II)—a figure which can only be a very crude guess. The intensity curve thus obtained is dotted in Fig. 3. The recoil protons and neutrons are not included in these curves. The curve marked "total" does not include these protons except those at the very top of the atmosphere.

After having reached an energy $E<M$ the protons and neutrons have a much larger range than the distance that a proton or neutron can travel while having an energy $>M$. It is therefore not surprising that a large number of slow protons and neutrons are found in the upper atmosphere. Fluctuations of the range are large, since energy is lost in large portions, thus a small but appreciable fraction of them may even manage to travel through a considerable part of the atmosphere. In addition there are numerous fast and slow recoil protons. The experiments show a rapid increase of slow protons and neutrons with height, though their number is still very small at a height of 4000 m compared for instance with the number of mesons. A quantitative discussion is not yet possible. A certain fraction of these slow protons and neutrons are recoil products or are produced by photoelectric nuclear disintegrations, etc.

In addition to these slow particles we must expect, in any part of the lower atmosphere, a very small number of very energetic protons and neutrons, namely, the primaries themselves which have sufficient energy to travel such large distances. Let us estimate their number, at sea level. The energy necessary to penetrate through the atmosphere is at least 7×10^{11} ev. The primary energy spectrum (13) is valid for E up to 1000 (10^{11} ev). For higher energies we know from the measurements at great depths that α increases with increasing energy. Thus for the energies in question we may assume $\alpha=3$, for $E>1000$, say. The number of primary protons at sea level is then given by $A'x^{-3}$, $x=22$ where A' is determined by A [Eq. (13)] and the condition that the spectrum is continuous at $E=1000$, thus $A'=23$ if A, B, A' are normalized for 100 incident protons. Thus we find 1/500 energetic protons or neutrons at sea level for 100 primary protons at the top of the atmosphere.

This figure may in fact be still too large, for the following reason: As was mentioned in Section II, our formula for the energy loss of a fast proton is no longer valid for energies $>5\times 10^{11}$ ev, because then other modes of energy

TABLE IV. Number of mesons (with $\epsilon>10$) produced by energetic proton or neutron.

E_0	100	300	1000
$x_{E_0, M}$	0.9	2.1	4.3
$N_{ps}+N_{tr}$	3.3	6.3	11.0

loss become appreciable.[19] Thus still higher energies may be required for a proton to penetrate to sea level making their number still smaller. From measurements discussed below Janossy found that the number of protons or neutrons at sea level is about 1/12,000 of the total number of cosmic-ray particles at sea level. Putting the latter value to be about 6 (for 100 incident protons) the experiments would give the number of these energetic protons and neutrons as 1/2000 which may be considered to be in reasonable agreement with our theoretical estimate 1/500.

When these energetic particles travel through matter they will produce a number of mesons in succession thus producing a *meson-shower*. Showers consisting of penetrating particles have been observed by several authors.[20] The most extensive measurements are due to Janossy: A radiation whose intensity was found to be 1/12,000th of the total cosmic-ray intensity at sea level was found to produce showers consisting of penetrating particles which are certainly mesons with energy $\epsilon>10$. The transition curve of these showers in lead reaches saturation at about 5 cm Pb (about 1 x unit). About a third of the primary radiation producing these showers consists of neutral particles. Janossy found, however, that for showers produced by the neutral primaries saturation is only reached after 10 cm of Pb. Each shower consists of an average number of 2–6 *recorded* penetrating particles. The actual number of particles in each shower may be larger.

We can only give a very preliminary discussion of these experiments. The most obvious explanation is that the very energetic protons and neutrons expected from our theory are responsible for these showers. There should be about equal numbers of protons and neutrons. Janossy found about a third to be neutral particles. Let $E\gg M$ be the average energy of the protons and neutrons and $x_{E,M}$ their range as given in Table I (i.e., the distance travelled until the energy is M).

The number of mesons with energy >10 produced is then according to (7):

$$N_{tr}=21\int_M^{E_0}\frac{dE}{-dE/dx}\int_{10}^{E}\frac{d\epsilon}{\epsilon^2}\sim 2.1x_{E_0,\ M},$$

$$N_{ps}\sim 15.5E_0^{-\frac{1}{2}}x_{E_0,\ M}.$$

Thus the total number of mesons produced is for various energies E_0 (from Table I) given by Table IV.

These values cannot, however, be compared directly with the experiments. It has kindly been pointed out to us by Janossy, that the saturation point of the transition curve is not at all identical with the range of the primary radiation but marks the point where enough mesons are produced to be recorded as a shower. This figure is about 2–3. A further increase of the lead thickness will only increase the size of the showers but not the number of the showers. Experimentally, we find, therefore, that 2 or 3 mesons are produced in the first 5 cm Pb or in the first x unit. This is in very good agreement with Eq. (26), the theoretical number of mesons produced in $x=1$ being $2.1+15.5E_0^{-\frac{1}{2}}$. We do not know E_0 exactly, but it certainly is rather large (>100). For greater thickness of Pb, Table IV shows that the size of the showers increases very much and even large showers are quite possible. On the other hand it is difficult to understand why neutrons should give rise to showers with a larger saturation thickness, than that for showers produced by protons. The processes considered in this paper lead to no explanation of this asymmetry.

There are, however, a number of points, omitted so far in the present theory, which will have to be considered before a final discussion of the penetrating showers can be given:

(i) As was mentioned in Section I, there are further modes of energy loss by a fast proton, expected from the present theory, including also a higher rate of production of transverse mesons,

[19] The limit of validity for the energy loss formula is higher than that for the scattering cross section because the former is an integral of the latter.

[20] Wataghin, de Souza Santos, and Pompeia, Phys. Rev. **57**, 61 and 339 (1940). Janossy, Proc. Roy. Soc. **179**, 361 (1942); Janossy, McCusker, and Rochester, Nature **148**, 660 (1941).

which become important if the energy exceeds the value 5000, say. The primary protons would then hardly have a chance at all to reach sea level. The protons and neutrons responsible for the penetrating showers must be the fast recoil particles mentioned above which naturally have also smaller energies than the primaries. (If this argument holds the last column in Table III has no meaning.) Some of the processes taking place at extremely high energies depend on the Coulomb field of the proton which might perhaps indirectly account for the difference of the behavior of the protons and neutrons.

(ii) Throughout this paper we have neglected the occurrence of multiple processes. It is indeed possible that a fast proton creates mesons, not only one by one in succession, but several mesons in one elementary act. We obtain the rate of occurrence of this event by multiplying the equivalent meson spectrum of a fast proton by the cross section for the splitting up of a meson into several mesons instead of by the scattering cross section (5). The splitting up processes have been calculated in *I* for the case when all energies concerned are smaller than M. In this case it has been found, indeed, that the splitting-up cross section for such multiple processes is always at least 10 times smaller than that for ordinary scattering (which is the reason why multiple processes were neglected in this paper). It may well be—but this could only be decided by further, rather difficult, calculations—that the ratio is more in favor of multiple processes if the energy of the proton is $>M$. If this should turn out to be true, the range of the fast protons would be diminished and the number of mesons increased.

(iii) We have always assumed that the particles in the nuclei of the matter traversed act independently. It might very well be that the nuclear fields of the nuclear particles overlap and interfere (as their Coulomb field does) producing an effect which increases with a different power of the atomic weight than the first power. This might lead to some changes of our theoretical results for heavy materials but hardly for air.

(iv) So far we have considered only protons and neutrons as primary agents. It is to be expected that mesons also could create penetrating showers themselves, by the very splitting up process mentioned in (ii). Again no quantitative discussion is possible unless the calculations are performed for energies $>M$. A crude estimate on grounds of the non-relativistic calculations shows indeed that the rate of occurrence of this process is of the observed order of magnitude.

Mesons have also been found to occur in very large cascade showers. This is easily understood. According to our theory, a large cascade shower owes its origin to a very energetic primary proton emitting an energetic transverse meson which, by decaying, produces the very energetic electron responsible for the cascade. Naturally, the primary proton will also produce numerous other mesons, including pseudoscalar ones, during its path through the atmosphere. These mesons will, of course, occur together with the cascade shower. In addition, energetic light quanta, have a small chance of creating mesons themselves by process (1) instead of producing an electron pair. The cross section for (1) was found in *II* to be $\sqrt{2}\pi^2 ef/\epsilon^2$ for pseudoscalar mesons, if $\epsilon < M$. Comparing this with the cross section for pair production $\sim 15Z^2/137$ we find that the chance for a light quantum producing a meson with $\epsilon = 10$, say, is in air 1/200. Since in a big cascade shower at the point of its maximum several thousand light quanta may occur, quite a number mesons are to be expected. The mesons accompany the cascade shower but are much more slowly absorbed; the ratio of the number of mesons to that of soft particles may therefore be quite appreciable at sea level.

VII. NEUTRETTOS

According to our theory neutrettos should be very frequent particles in cosmic radiation. The total number produced is half the total number of charged mesons produced. We know nothing, however, about their absorption and possible β-decay nor does it seem that they could produce any noticeable secondary effects. It is true, though, that in colliding with a nuclear particle a neutretto can be transformed into a charged meson. But, as mentioned in Section II, the cross section is very small at high energies decreasing like ϵ^{-6} and it is unlikely that this effect will ever be observed. Slow neutrettos must be

very rare because there is nothing that would slow down a once fast neutretto.

There is, however, one observable effect, by which the existence of neutrettos could be established experimentally, namely, the transformation of a charged meson into a neutretto. At high energies $\epsilon \gg 1/f \sim 3$ again the cross section Φ^0 for this transformation is negligible ($\Phi^0 \propto \epsilon^{-6}$) compared with the cross section for scattering ($\propto \epsilon^{-2}$). This is, indeed, an important result of our theory because it explains why all attempts at detecting this transformation[21] have failed whereas the anomalous scattering of mesons has been observed. This is no longer true for energies of the order of magnitude $\epsilon \sim 3$. The cross section becomes then appreciable and, as we shall see, big enough to lead to observable effects.

The method for calculating Φ^0 as a function of ϵ is described in detail in *III* and the calculations are carried out up to a point where numerical evaluation is possible. The exact formula would be a rather lengthy and complicated expression because no approximation can be made in this case except that we can assume ϵ to be small compared with M. We shall not give the formula here. Φ^0 is, for very small energies, proportional to $p^2=\epsilon^2-1$, rises to a maximum at $\epsilon=2$ and decreases rapidly for higher values. The value of Φ^0 at the maximum ($\epsilon=2$) is in our units $\Phi^0_{max}=0.56$. This refers to the transformation of a pseudoscalar charged meson into neutrettos of all polarizations (longitudinal, transverse, or pseudoscalar).

We shall calculate the total probability for a meson to be transformed into a neutretto while traveling through matter, starting with a high initial energy $\epsilon \gg 1/f$ until it is stopped. If $-\partial\epsilon/\partial x$ is the energy loss by ionization this probability is

$$w=\frac{NA}{2}\int_1^\infty \frac{\Phi^0(\epsilon)}{-\partial\epsilon/\partial x}d\epsilon, \qquad (27)$$

where N is the number of nuclei per cm^3, A the atomic weight. The factor $\frac{1}{2}$ is due to the fact that a positive meson can only be transformed into a neutretto if it collides with a neutron and a negative meson only if it collides with a proton. The average number of "active" nuclear particles is therefore $A/2$. We have worked out (27) by numerical integration for Pb and found[22]

$$w=0.79. \qquad (28)$$

For any other materials w will not be very different because $\partial\epsilon/\partial x$ is nearly proportional to NZ which differs only slightly from $NA/2$. Practically the whole contribution to the integral (27) arises from energies between $\epsilon=\frac{3}{2}$ and $\epsilon=4$.

We see that, once a meson has reached an energy as small as 4, the chance is so great that it will be transformed into a neutretto. Only 21 percent of the mesons reach the end of their range as charged mesons. It may very well be that this is one of the reasons why so very few slow mesons with $\epsilon<2$ occur in cosmic radiation.

The length of path a meson has to travel in order to lose energy from $\epsilon=4$ to $\epsilon=\frac{3}{2}$ is about 1 km of normal air or 18 cm of Pb. While traveling through the gas of a cloud chamber the chance is so negligible that the effect could be observed. But, if mesons are stopped in a thick block of lead an appreciable fraction of the mesons should not reach the end of their range but should be transformed *earlier* into neutrettos. This is important for the type of experiments carried out by Rassetti.[23] Rassetti found that if mesons are stopped in 10 cm of aluminum (equivalent to 2.8 cm of Pb) only a certain fraction (42 ± 15 percent) give rise to decay-electrons. The effect was interpreted by Rassetti in the following way: Once a meson is stopped entirely and retains only an energy of a few electron volts it may either decay or else be captured by a nucleus giving its rest energy to the nucleus. Only negative mesons, however, can be captured in this way, since a positive meson with such a small energy could not come in contact with the nucleus. Calculations referred to by Rassetti indicate indeed, that for such slow negative mesons the capture-probability is larger than the decay probability. It may very well be, that transformation into neutrettos as well as nuclear capture is responsible for the fact that only a fraction of the mesons are really

[21] Cf., for instance, Nishina and Birus, Sci. Pap. Inst. Phys. Chem. Res. Tokyo **38**, 360 (1941).

[22] For this result the numerical values (2) for the coupling constants have been used.

[23] Rassetti, Phys. Rev. **60**, 198 (1941).

decaying. In the above experiment 12 percent of the mesons should be transformed into neutrettos before being stopped. Of the remaining 88 percent half should be captured leaving 44 percent decaying into electrons.

The experiments are not accurate enough to decide whether the number of decay electrons is actually appreciably less than 50 percent. The actual percentage should depend on the thickness of the absorber.

VIII. CONCLUSIONS

On the whole the theory was seen to give a satisfactory account of all the chief cosmic-ray phenomena. Although a number of points, especially the cascade production of mesons (cf. Section II), the east-west effect of the soft component and the penetrating showers, must await further investigation, it is probable that this theory is fundamentally correct. The conclusions that can be drawn from our results are twofold: (i) The theory of damping used as a basis for all our calculations will be a correct part of future quantum electrodynamics or at least a good approximation. (ii) Cosmic-ray mesons are in fact identical with the quanta predicted by Yukawa which are responsible for the nuclear fields. It may perhaps be too early to say that the special form of the meson theory used in this paper (the one suggested by Møller and Rosenfeld) is the correct form of the meson theory. We have carried out all the calculations also with a different form of the theory (assuming that only charged mesons exist) and found the agreement with cosmic-ray experiments less good, though this form of the theory cannot be wholly excluded. (The energy loss of fast protons would be three times smaller.) It is satisfactory that the form of the meson theory which gives the best account of the nuclear forces also agrees best with cosmic-ray facts. Especially, the assumption of both pseudoscalar and transverse mesons is strongly supported by the fact that all components of cosmic radiation can be explained as owing their origin to one kind of primary particles, i.e., protons.

We are very much indebted to Dr. L. Janossy for a most useful comment on this paper and also for communicating some of his experimental results to us before publication.

PHYSICAL REVIEW VOLUME 64, NUMBERS 3 AND 4 AUGUST 1 AND 15, 1943

On the Adiabatic Demagnetization of Iron Alum

J. A. SAUER*
Harvard University, Cambridge, Massachusetts
(Received April 26, 1943)

The behavior of iron alum during adiabatic demagnetization to temperatures near the absolute zero is of particular theoretical interest because of the deviations from Curie's law that arise from the perturbing actions of crystalline field and magnetic dipole-dipole coupling. The effect of these perturbations on the magnetic moment and the entropy is calculated exactly to second-order terms in the magnetic coupling and to third-order terms in the crystalline potential. The calculations are presented for crystalline fields of either cubic or axial symmetry and are valid for the case of large applied fields in which saturation effects become important. Theoretical values of the adiabatic moment are found to be in satisfactory agreement with the experimental values determined by Casimir and de Haas. A true thermodynamic scale is established that enables the temperature to be calculated at any value of the magnetic field during demagnetization. The relationship of this scale to the temperatures determined by the magnetic method of de Haas and Wiersma is discussed.

PART I: DESCRIPTIVE ANALYSIS

I. Introduction

ONE of the greatest difficulties encountered in the production of low temperatures by the method of adiabatic demagnetization is the determination of the thermodynamic temperature. Until recently, it has been the general practice of experimenters to set up a "magnetic" temperature scale based on the validity of Curie's law. Deviations from this law, however, will be

* Now at Mellon Institute of Industrial Research, University of Pittsburgh, Pittsburgh, Pennsylvania.

produced both by the magnetic interaction between the paramagnetic ions of the alum and by the Stark splitting due to the crystalline electric field. These effects become progressively more important as the temperature is lowered so that there may exist an appreciable difference between the "magnetic" or "reciprocal susceptibility" temperature T^* and the true Kelvin temperature T.

To overcome this uncertainty in temperature measurement, various procedures have been proposed, most of which base their determination of the true thermodynamic temperature on calorimetric measurements. De Haas and Wiersma,[1] however, have proposed a method of determining the Kelvin temperature entirely from magnetic measurements. Their procedure is based essentially on the experimental fact that when certain alums are subject to an adiabatic demagnetization process, the magnetic moment is found to remain constant, within the limits of experimental error, as the field is decreased from its initial high value to some much lower value. When this is the case, one can show purely from the laws of thermodynamics that the true temperature T is a function of the field strength H and is given by an expression of the form

$$T-T_0=c(H-H_0), \tag{1}$$

where c is a parameter depending on the value of the initial magnetization, and T_0 and H_0 denote values of temperature and field, respectively, at the beginning of demagnetization. This equation was applied by de Haas and Wiersma to the particular case of caesium titanium alum as this material experimentally showed no change in the value of the magnetic moment in the range from 24,000 gauss to 100 gauss.

Similar experiments on a powdered specimen of iron alum by Casimir and de Haas[2] indicate that the magnetic moment during adiabatic demagnetization does not remain constant over any appreciable interval, but varies with the applied field strength H_a in the following manner:

$$M=M_0(1-b/H_a^2). \tag{2}$$

Here M_0 is the original magnetic moment due to an initial magnetic field H_0 of 18,100 gauss, and b is a constant whose experimental value is 1.7×10^5. From this value of b it is readily seen from Eq. (2) that for sufficiently large values of the field strength ($H_a>10{,}000$) the term in $1/H_a^2$ is negligible compared to unity. Hence for values of the field strength above this magnitude the method of de Haas and Wiersma for determining the true Kelvin temperature is clearly applicable. For fields between 10,000 gauss and 5000 gauss, the existence of the second term in Eq. (2) above will cause a small error to be made in the temperature determination, while for fields less than 5000 gauss the error becomes appreciable.

It is not surprising that the magnetic moment of iron alum fails to remain constant during the process of adiabatic demagnetization. Rather the reverse would be the case as even a simple theoretical treatment shows the existence of a $1/H^2$ term in the expression for the adiabatic moment. Such a treatment has been given by Casimir and de Haas[2] who show that for low values of the initial field, the coefficient of the $1/H^2$ term [i.e., b in Eq. (2)] is some function of the original magnetization and hence of the original field strength, but does not depend on the value of the final field. They were unable to evaluate this function for the general case, but for the special case of low initial fields that do not produce saturation, they found b to be 1.3×10^5 as compared to the experimental value of 1.7×10^5. The discrepancy between the computed and the experimental value is probably due to neglect of saturation effects. The magnetic fields used in their experiment were quite large (18,000 gauss) and for fields of this order of magnitude one would normally expect saturation effects—neglected in their treatment of the problem—to be very important. That such is the case will be demonstrated in this article for, contrary to the opinion of Casimir and de Haas, it *is* possible to make an exact theoretical determination of the adiabatic moment for high fields. The method of solution is described in Part I of this paper but the mathematical details associated with the determination are placed in Part II.

Once the necessary theoretical treatment has been developed, it can be used not only for the determination of the adiabatic magnetic moment

[1] W. J. de Haas and E. C. Wiersma, Physica **3**, 491 (1936).

[2] H. B. G. Casimir and W. J. de Haas, Physica **7**, 72 (1940). The symbol capital B in this paper is the same as our small b.

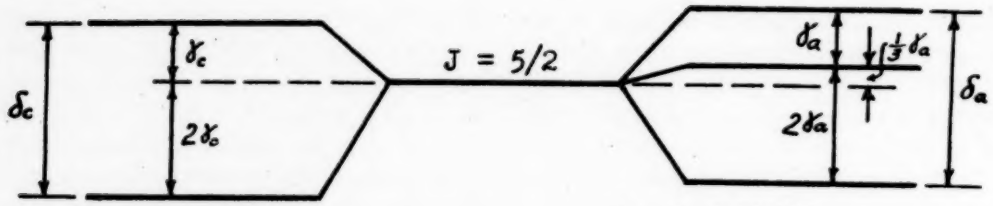

a. Cubic field b. Axial field

FIG. 1. Splitting of $J=5/2$ level by a crystalline field. In notation of Penney and Schlapp (reference 7) $\delta_c=3\gamma_c=72Dq$, $\delta_a=3\gamma_a=18Aa$.

but also becomes immediately available for use in two other connections. First, it enables us to calculate the true thermodynamic temperature and to estimate the error that will arise if the temperature is determined by the simple magnetic method of de Haas and Wiersma, i.e., by use of Eq. (1). Secondly, by comparing the theoretical expression of M with the experimental, we obtain information in regard to the nature of the crystalline field that acts on the paramagnetic ions of the alum.

II. Method of Approach

The procedure adopted is based upon a method of attack originally developed by Van Vleck[3] and used by him to study theoretically the adiabatic demagnetization of caesium titanium alum ($CsTi(SO_4)_2\cdot 12H_2O$). The indicated mathematical treatment is applicable for the case of iron alum ($NH_4Fe(SO_4)_2\cdot 12H_2O$) as well, but there are some significant differences in treatment due to basic differences in the structure of the two materials. In caesium alum the Ti^{+++} ion has a spin $S=\frac{1}{2}$ and lies in a doubly degenerate ground state and hence, according to a fundamental theorem of Kramers,[4] is unaffected by a surrounding crystalline field of any type of symmetry. The free orientation of the paramagnetic ions is thereby hindered only through the agency of the magnetic coupling, and possibly a little exchange coupling, between spins. In iron alum, on the other hand, the paramagnetic Fe^{+++} ion has a spin $S=5/2$ and lies in a sixfold degenerate ground state. This sixfold level is subject to Stark splitting by the electric fields of the crystal as has been shown by Bethe,[5] Kramers,[4] and Van Vleck and Penney.[6] A field of axial symmetry splits the sixfold degenerate level of the ground state into three separate doubly degenerate levels, while a crystalline field of cubic symmetry separates the sixfold level into a fourfold and a twofold one. This is illustrated in Fig. 1 (see Penney and Schlapp[7]).

Hamiltonian Function

The first step in our theoretical treatment must be to set up an expression for the Hamiltonian that will correctly represent the conditions to which the paramagnetic alum is subject during the adiabatic demagnetization process. In addition to the applied magnetic field acting on the paramagnetic ions of the alum, there is a magnetic coupling of the three-dimensional array of dipoles and an electrostatic interaction between the various paramagnetic ions and their surrounding crystalline fields. The Hamiltonian may therefore be written

$$\mathcal{H}=-g\beta H\sum_i S_{z_i}+\sum_{j>i} w_{ij}+\sum_i V_i, \quad (3)$$

where g is the Lande splitting factor, β the Bohr magneton, and S the spin of the Fe^{+++} ion. The first term thus represents the Zeeman energy due to a field H supposedly directed along the z axis. The second and third terms respectively represent the magnetic dipole-dipole coupling and the crystalline field interaction. The exchange interaction between the paramagnetic ions has been neglected in Eq. (3) because, in iron alum, the ions are known to be spaced relatively far apart.[8]

[3] J. H. Van Vleck, J. Chem. Phys. **6**, 81 (1938). One typographical error should be noted. In the expression for G_s on p. 83 the sign before the $(g\beta H/kT)$ term should be reversed.

[4] H. A. Kramers, Proc. Kon. Akad. Amst. **33**, 953 (1930); **34**, 965 (1931).

[5] H. A. Bethe, Ann. d. Physik **3**, 133 (1929).

[6] J. H. Van Vleck and W. G. Penney, Phil. Mag. **17**, 961 (1934).

[7] W. G. Penney and R. Schlapp, Phys. Rev. **41**, 194 (1932); **42**, 666 (1932).

[8] C. A. Beevers and H. Lipson, Proc. Roy. Soc. **148**, 664 (1935).

In the mathematical treatment that follows, the Zeeman term of Eq. (3) is taken as the unperturbed part of the Hamiltonian, and the other two terms are considered as small perturbations causing slight shifts in the unperturbed energy levels.

The first of the perturbing influences, namely the magnetic dipole-dipole coupling, is explicitly introduced into the analysis by writing for w_{ij} the expression[9]

$$w_{ij}=g^2\beta^2 r_{ij}^{-3}\{(\mathbf{s}_i\cdot\mathbf{s}_j)-3(\mathbf{s}_i\cdot\mathbf{r}_{ij})(\mathbf{s}_j\cdot\mathbf{r}_{ij})r_{ij}^{-2}\}$$

where $\mathbf{s}_i$ is the spin angular momentum vector in units of $h/2\pi$ of atom i, $\mathbf{r}_{ij}$ is the radius vector connecting atoms i and j, and r_{ij} is its modulus. As the lattice spacing is known, there are no unknown constants in this expression, and hence the computation of the influence of this term, though lengthy, is straightforward.

On the other hand, when the crystalline field potential is considered, either one or more unknown constants are introduced depending on the nature of the crystalline field assumed. From x-ray analysis by Beevers and Lipson,[8] it is known that the field surrounding the paramagnetic ion possesses trigonal symmetry. The most general potential of this type is[10]

$$V_t=F_2(r)T_2^0+F_4(r)T_4^0+F_4'(r)(T_4^3+T_4^{-3}), \quad (4)$$

where the F's are coefficients depending only on r, the T_l^m's are spherical harmonics of the form $T_l^m=P_l^m(\cos\theta)\exp(im\varphi)$, and the P_l^m's are Legendre polynomials. In these expressions $\theta=0$ corresponds to the trigonal axis, which coincides with one of the four-body diagonals of the cubic lattice. If the fourth-order terms of Eq. (4) are neglected then the crystalline field is one of axial symmetry and that part independent of r can be expressed by

$$V_a=A(x'^2+y'^2-2z'^2), \quad (4a)$$

where A is an arbitrary constant associated with the strength of the field, and the primed coordinates are rectangular coordinates in which the trigonal axis coincides with the z' axis. This is the only type of second-order term compatible with trigonal symmetry. Probably the most important fourth-order terms in (4) are those having cubic symmetry. In terms of rectangular coordinates referred to the cubic axes, these terms are given by

$$V_c=D(x^4+y^4+z^4-\tfrac{3}{5}r^4), \quad (4b)$$

where D is an arbitrary constant measuring the strength of the field, and the $\frac{3}{5}r^4$ term is included in order to have V_c satisfy La Place's equation.

The Hamiltonian of Eq. (3) is used as the basis for a rigorous calculation of the partition function Z. Once this is established, the magnetic moment and the entropy, both of which are required in order to get the adiabatic moment, are obtained by simple differentiation. In the calculation of Z, we assume the dipole-dipole coupling and the crystalline field potential are both small compared to the energy of thermal agitation. As the partition function is expanded in powers of the ratio of the perturbing influences to kT, the convergence of this expansion will be rapid as long as our original assumption is valid. Fortunately, the ratio is small except at sufficiently low temperatures where the interactions become comparable to kT. The unperturbed energies arising from the first term in the Hamiltonian are not assumed small compared to kT as it is the form of M for *large* values of H that is desired.

The perturbing influences are taken explicitly into account by using the well-known quantum-mechanical expressions from perturbation theory,[11] and then calculating the matrix elements of the perturbing part of the Hamiltonian. The calculation of the matrix elements and also of the partition function is greatly facilitated by use of the methods of group theory. These methods are particularly applicable to our problem where the experimental use of a powdered specimen instead of a single crystal necessitates the writing of the crystalline field and dipole-dipole contribution to the partition function in terms of generalized coordinates over which an average must be taken before the final expressions for the magnetic moment and the entropy can be obtained. It is precisely in the carrying out of this averaging process—otherwise a long-winded and tedious job—that the group theory method affords such a great saving.

[9] J. H. Van Vleck, J. Chem. Phys. **5**, 320 (1937).
[10] A. Siegert, Physica **3**, 85 (1936).
[11] E. C. Kemble, *Fundamental Principles of Quantum Mechanics* (McGraw-Hill, New York, 1938).

III. Adiabatic Moment to Second Order in Perturbing Influences

The development of the partition function is carried out in Sections 6 and 8 of Part II. The expressions for the magnetic moment and the entropy, given by Eqs. (21) and (22) of Section 9, are functions of both T and H. To find the adiabatic magnetic moment, the procedure is to eliminate T between the two equations, and then since S is constant during the course of an adiabatic demagnetization experiment, one has an equation for the adiabatic magnetic moment that depends only on the field strength. In Section 10, this expression is shown to be

$$M=M_0(1-b/H^2), \qquad (5)$$

where b represents a function of the initial field and initial magnetization given by Eq. (29) of Section 10. Equation (5) is of the same form as the experimental relation as regards dependence of M upon H. It should be noted, however, that in the theoretical expression H is to be interpreted as the true field acting on the paramagnetic ions and not as the experimentally applied field.

To find the numerical value of the theoretically derived expression for b the unknown parameter or parameters that entered into the crystalline field potentials must be evaluated. This evaluation is made by comparing the theoretical expression for the specific heat in zero applied field with the experimental. Both are of the form $C_v=A'/T^2$, where the coefficient A' includes the contribution of both the dipole-dipole coupling and the crystalline field interaction. If the trigonal field acting on the paramagnetic ion is taken as purely cubic or purely axial in character, then only a single unknown parameter enters into the expression for A' and the constant is directly evaluated by comparison with the known experimental value of this constant for iron alum. This evaluation is made in Section 10 of Part II. The experimental value of A' has been determined by several investigators, some of whom used entirely different methods of attack. Considering this, it is remarkable how well they agree.[12]

After these unknown crystalline field constants have been evaluated, one can calculate the numerical value of the coefficient of $1/H^2$ and thereby obtain the final expression for M correct to the second order in the two perturbing influences. In Section 10, this expression is shown to be

$$M=M_0(1-9.4\times10^4/H^2). \qquad (5a)$$

The numerical value of 9.4 is calculated on the assumption that the trigonal field acting on the paramagnetic ion is predominantly cubic. This value should be changed to 11.5 if an axial field is assumed. In either case, however, a comparison with the experimental values of Casimir and de Haas shows that the theoretical values of M obtained from (5a) are too high. Part of this discrepancy is accounted for by the fact that, because of demagnetization corrections, the true field H appearing in Eq. (5a) is somewhat less than the applied field H_a entering into Eq. (2). It is shown in Section 10 of Part II that this accounts for only a minor part of the difference between the theoretical values for M and the experimental and leaves the major part of the discrepancy still to be explained.

Two possible reasons for the existence of the discrepancy present themselves. The first of these is the neglect of third and higher order terms in the expansion of the partition function and the second is the restriction that the crystalline field acting on the paramagnetic Fe^{+++} ion is trigonal in character. Of these two, the former seems to be the more likely as the trigonal nature of the field is attested by the experimental x-ray methods of Beevers and Lipson.[8] Still, from a theoretical standpoint, the possibility of the existence of a more general field should not be excluded and hence we shall first consider how the removal of the trigonal restriction would affect the results.

[12] H. B. G. Casimir, W. J. de Haas, and D. de Klerk, Physica **6**, 241 (1939); F. K. du Pre, Physica **7**, 79 (1940); P. Teunissen and C. J. Gorter, Physica **7**, 33 (1940); C. Starr, Phys. Rev. **60**, 241 (1941); F. Simon, private correspondence to J. H. Van Vleck (1940). Casimir, de Haas, and de Klerk determined the specific heat constant by direct magnetic measurements on pure crystals. They find A' to be 2200 ± 40. Du Pre records a value of 2300 ± 50 determined by experiments on paramagnetic relaxation. Indirect measurements by Teunissen and Gorter, from experiments on paramagnetic dispersion, tend to lower this value slightly while similar indirect measurements by Starr tend to raise it by about the same amount. Private correspondence from Simon indicates a value of the splitting distance of 0.193 determined from direct magnetic measurements. This corresponds to a specific heat constant of 2350. All values whether determined by direct or indirect measurements thus approximate 2300 and this we take as the correct magnitude.

TABLE I. Comparison of theoretical and experimental values of adiabatic moment of iron alum.

H_a	H	M(exp.)	M(calc.) Cubic field 2nd ord.	M(calc.) Cubic field 3rd ord.	M(calc.) Axial field 2nd ord.
18,100	18,000	—	4.70	4.70	4.70
11,170	11,040	4.77	4.70	4.70	4.70
5,550	5,420	4.66	4.69	4.68	4.68
3,130	3,000	4.61	4.65	4.64	4.64
1,352	1,230	4.25	4.41	4.33	4.34
912	807	3.7	4.02	3.75	3.87
494	412	2.9	2.10	0.10	1.53

Note: Values of M expressed in units of $N\beta$.

Failure of Arbitrary Crystalline Field to Improve Agreement

Let us replace the trigonal expression for the crystalline field given by Eq. (4) by the more general expression

$$V_c = \sum_{s=-4}^{4} a_{4s} T_4^s + \sum_{r=-2}^{2} b_{2r} T_2^r, \qquad (6)$$

where the a's and b's are arbitrary coefficients. If the coefficients of this general field are so selected as to retain unrestricted trigonal symmetry, it should be noted that (6) still represents an increase in generality over the cubic and axial fields thus far considered. It would be useless to include terms in T_3 and T_1 as matrix elements for odd order potentials must vanish in virtue of the LaPorte rule. The matrix elements have already been computed for the T_4 and T_2 term and hence it is an easy matter to set up the partition function for any combination of these terms with arbitrary coefficients. The contribution of this type of field to the specific heat and to the adiabatic magnetic moment is given by Eqs. (33) and (32), respectively, of Part II. Examination of these two equations discloses that, at least as far as the second-order terms are concerned, *no assigned values of the arbitrary parameters can bring the theoretical and experimental results in closer agreement than already found under the assumption of a trigonal field of axial symmetry*. Hence the failure of the theoretical results to give closer agreement with the experimental data is definitely not due to any restriction on the nature of the crystalline field.

IV. Beneficial Effect of Higher Order Terms

The most likely reason for the discrepancy between the theoretical values of M and the experimental values is the neglect of third and higher order terms in the expansion process employed in the calculation of the partition function. Fortunately, it is possible to save much of the labor associated with the calculation of higher order terms by making use of some previous theoretical work on iron alum by Kronig and Bouwkamp.[13] For large fields and for arbitrary direction of the magnetic field relative to the crystal axes—just the required conditions necessarily imposed on us by experiment—they have calculated the energy levels of iron alum to the third order in the crystalline field parameter. Their calculations were made for a crystalline field of cubic symmetry and do not take into account the effect of the magnetic dipole-dipole coupling. This is not a serious drawback, however, as the neglect of the third-order term in the dipole-dipole coupling will not appreciably change the final result. This is so because the contribution of the crystalline field terms to the magnetic moment is about eight times as large as the dipole-dipole contribution.

Once the energy levels are known, it is a straightforward process to determine the partition function, the entropy, and the magnetic moment. The details of this treatment are given in Section 11. The effect of inclusion of the third-order crystalline field terms is to add a new term in $1/H^3$ to the adiabatic moment. The complete expression for the magnetization then becomes

$$M = M_0(1 - bH^{-2} - b'H^{-3}), \qquad (7)$$

where b' is independent of the final field but depends upon the initial conditions. For the experimental conditions of de Haas and Wiersma b' takes the numerical value of 30×10^6 while b itself has the value previously stated, *vis.*, 9.4×10^4. If M is expressed in the form of Eq. (2), the correction to b due to introduction of the third-order term in the cubic crystalline field interaction is a factor $(1+320/H)$. This factor becomes increasingly important as the field is lowered. The effect of the additional term in the expansion has thus been to increase the value of the coefficient of the H^{-2} term and hence its inclusion has tended to lower the value of the adiabatic magnetic moment in the proper direc-

[13] R. de L. Kronig and C. J. Bouwkamp, Physica **6**, 290 (1939).

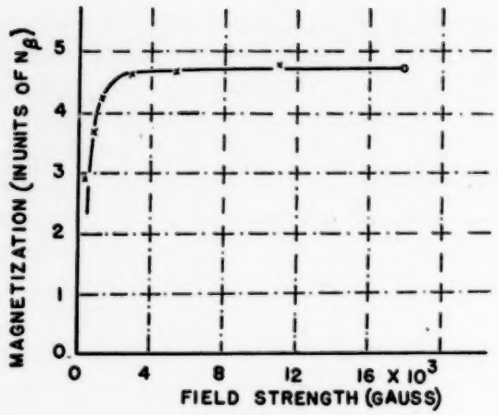

FIG. 2.

tion in order to give better agreement with experimental data.

The theoretical values of M based on Eq. (7) and Eq. (5) are compared with the experimental data in Table I. From this table it is readily seen that the agreement between the third-order theoretical and the experimental values of M is now quite satisfactory. One exception is the last row in the table, but here the true field strength is less than 500 gauss and for a field as low as that, the temperature obtained by assuming the law of de Haas and Wiersma to apply is already below the characteristic magnetic coupling temperature. When this is the case, the convergence of the expansion breaks down completely.

The relation between the magnetic moment and the final field strength is graphically shown by Fig. 2, where the actual experimental points are indicated by the small crosses. No experimental value of M is recorded by de Haas and Wiersma in the neighborhood of the original field, and no mention is made of the order of accuracy of their experimental data. We are no doubt safe in assuming that the experimental error is of the order of 3 percent. For all values of the field above 900 gauss the greatest difference between the theoretical and the experimental value of M is less than this amount. Hence it does not appear worth while at present to carry out any further calculations on the effect of still higher order terms.

Nature of Crystalline Field Present in Iron Alum

It was thought likely when the theoretical calculations were first started that a comparison between the experimental values of the adiabatic moment and the theoretical values, as computed on the assumption of crystalline fields of varying types, would enable us to determine the proper symmetry characteristics of the crystalline field present in iron alum. On the basis of second-order calculations alone, it would appear from Table I that a trigonal field of axial symmetry leads to slightly better agreement with experiment than a crystalline field of predominantly cubic symmetry. However, when third-order terms in the cubic field are taken explicitly into account in the calculations, the agreement between theory and experiment is found to be much improved.

Further examination of Table I might lead one to suspect that had third-order terms also been calculated for the crystalline field of axial symmetry, the theoretical values of M might be drawn still closer to the experimental values. To take this statement as evidence in support of a trigonal field of axial symmetry in preference to one of cubic symmetry would, however, be definitely misleading since the difference between the two cases is probably less than the experimental error involved in making the measurements. Furthermore, it is now quite possible that a more general trigonal field consisting of a combination of the axial and cubic terms would also fit the facts, but as long as the agreement is so close as indicated in Table I there is no means of deciding on the exact form this arbitrary field should take. The one definite conclusion that can be drawn from the evidence presented is that values of M calculated to the third order in the cubic field perturbation are in somewhat closer agreement with experiment than values based

TABLE II. Temperatures and corresponding field strengths.

H_0	H	T(calc.)	T [From Eq. (1)]	% difference
18,100	18,000	1.18	1.18	—
15,330	15,200	1.00	1.00	—
12,330	12,200	.800	.803	0.37
9,270	9,140	.600	.604	0.67
6,210	6,080	.400	.405	1.25
3,170	3,040	.200	.206	3.00
2,400	2,275	.150	.156	4.00
1,630	1,510	.100	.106	6.00
1,305	1,190	.080	.085	6.25
1,140	1,030	.070	.074	6.25

only on second-order calculations with an axial field assumption.

Determination of True Temperature

To find the true temperature appropriate to any value of the field strength after the beginning of adiabatic demagnetization, the procedure is to solve the entropy equation [(22) plus (40) of Part II] for T in terms of H. Since the entropy retains a constant value during the process of demagnetization, the resulting equation immediately enables us to find T for any H or H for any T, provided only that the temperatures are not so low that the expansion process employed in the calculation of the adiabatic moment breaks down. In Table II are shown the values of the temperatures appropriate to a number of different fields.[14]

In column 4 of Table II appear the temperature values one would obtain by using the simple de Haas-Wiersma procedure discussed in the Introduction of this paper. In principle their procedure is never applicable to iron alum, but it is clear from inspection of the table that the temperature estimated by use of the de Haas-Wiersma equation [Eq. (1)] differs very little from the exact temperature for all values of the field down to about 7000 gauss. Between 7000 and 1000 gauss, the percentage error incurred by use of Eq. (1) rises from about 1 percent to about 6 percent. For fields less than 1000 g the expansion process employed in the determination of the entropy, and hence of the exact relation between T and H, is no longer valid.

On the basis purely of the experimental relation between the adiabatic moment and the field strength, Casimir and de Haas[2] have noted that for fields down to 2500 gauss the error in temperature measurement caused by use of Eq. (1) is probably less than 0.01°K. Our calculations show an error in temperature measurement at 2500 g of 0.006°K. This appears to be the maximum absolute error involved at all values of the field for which Table II and our method of calculation are valid.

PART II: MATHEMATICAL ANALYSIS

V. Preliminary Details

We require expressions for the magnetic moment and the entropy of an assembly of atomic magnets subject both to an applied magnetic field and a crystalline electrical field and coupled together magnetically. These are most easily obtained from the partition function by means of the equations

$$M = kT\frac{\partial}{\partial H}(\log Z), \quad S = \frac{\partial}{\partial T}(kT \log Z). \tag{8}$$

The partition function is given by

$$Z = \sum_\lambda \exp\,(-W_\lambda/kT), \tag{9}$$

where the summation is over all states of the entire crystal considering the crystal as a giant molecule. Since we are dealing with the partition function instead of the individual energy levels of each atom, we are concerned only with the energy W_λ of the crystal as a whole.

The Hamiltonian function has already been described in Section II. We choose a system of representation which diagonalizes the first (or Zeeman) term of $\mathfrak{H}$ and then consider the spin-spin coupling and the crystalline field potential as small perturbations. The unperturbed energies are given by

$$W_\lambda^0 = -g\beta H \sum_i M_i, \tag{10}$$

where the M_i are the characteristic values of S_{z_i} and the letter λ is used to represent the totality of quantum numbers for a given state of the entire crystal. The crystalline energies W_λ are given in

[14] Values of H in Table II are not whole numbers, as it was found simpler to assume values of T and then determine corresponding values of H.

terms of the unperturbed energies by the expression

$$W_\lambda = W_\lambda^0 + W_1 + W_2, \tag{11}$$

where W_1 and W_2 are the first- and second-order energy corrections corresponding to the perturbing potentials. If now we replace these latter two terms by the well-known quantum mechanical expressions from perturbation theory, substitute Eq. (10) into Eq. (11), and Eq. (11) into Eq. (9), expand the perturbing terms of the partition function in powers of kT, and retain terms to the second order in the perturbing potentials, we find the partition function to be

$$Z = Z_0(1 + A + B + \cdots), \tag{12}$$

with

$$A = -(1/kTZ_0) \sum_\lambda \mathcal{H}^{(1)}(\lambda;\lambda) \exp(-W_\lambda^0/kT), \tag{12a}$$

$$B = (1/2k^2T^2Z_0) \sum\nolimits^{=}_{\lambda\lambda'} \mathcal{H}^{(1)}(\lambda;\lambda')\mathcal{H}^{(1)}(\lambda';\lambda) \exp(-W_\lambda^0/kT)$$
$$+ (1/kTZ_0) \sum\nolimits'_{\lambda\lambda'} \{\mathcal{H}^{(1)}(\lambda;\lambda')\mathcal{H}^{(1)}(\lambda';\lambda)/(W_{\lambda'} - W_\lambda)\} \exp(-W_\lambda^0/kT), \tag{12b}$$

and

$$Z_0 = \sum_\lambda \exp(-W_\lambda^0/kT) = [\sum_{M_i} \exp\{-W_i(M_i)/kT\}]^N. \tag{12c}$$

In these expressions Z_0 represents the partition function in the absence of the perturbing potentials and $\mathcal{H}^{(1)}(\lambda;\lambda)$, which represents the perturbing part of the Hamiltonian, includes both the dipole-dipole coupling $\sum_{j>i} w_{ij}(\lambda;\lambda)$ and the crystalline field potential $\sum_i V_i(\lambda;\lambda)$. The equality and prime signs on the summations are in accordance with the notation of Van Vleck.[9] The equality sign indicates that only those values of λ' for which $W_{\lambda'} = W_\lambda$, or in the later Eq. (13b) those $M_i'M_j'$ for which $W_i(M_i) + W_j(M_j) = W_i(M_i') + W_j(M_j')$, are to be included in the summation; the prime sign means that just these values are to be excluded.

Now let

$$\sum_{j>i}(w_{ij})_{Av} = \sum_{j>i} d_i d_j \sum_{M_iM_j} w_{ij}(M_iM_j; M_iM_j) \exp[-(W_i(M_i) + W_j(M_j))/kT],$$
$$\sum_i (V_i)_{Av} = \sum_i d_i \sum_{M_i} V_i(M_i; M_i) \exp[-W_i(M_i)/kT],$$

where

$$d_i = (\sum_{M_i} \exp[-W_i(M_i)/kT])^{-1}.$$

Then the A part of the partition function becomes

$$A = -(1/kT)\mathcal{H}_{Av}^{(1)} = -(1/kT)\{\sum_{j>i} (w_{ij})_{Av} + \sum_i (V_i)_{Av}\}, \tag{13a}$$

while the B part is

$$B = \tfrac{1}{2}k^{-2}T^{-2}\{\sum_{ijkl} (w_{ij})_{Av}(w_{kl})_{Av} + \sum_{ijk} (w_{ij}w_{jk})_{Av} + \sum_{ik} (V_i)_{Av}(V_k)_{Av}\}_{j>i,\ l>k,\ (i,\ j\neq k,\ l)} + \alpha, \tag{13b}$$

where

$$(w_{ij}w_{jk})_{Av} = d_i d_j d_k \sum_{M_iM_jM_k} \{2kT \sum\nolimits'_{M_j'} w_{ij}(M_iM_j; M_iM_j')w_{jk}(M_j'M_k; M_jM_k)/[W_i(M_i) - W_j(M_j)]$$
$$+ w_{ij}(M_iM_j; M_iM_j)w_{jk}(M_jM_k; M_jM_k)\} \exp[-(W_i(M_i) + W_j(M_j) + W_k(M_k))/kT]$$

and

$$\alpha = \tfrac{1}{2}k^{-2}T^{-2}\{\sum_{j>i} d_i d_j \sum\nolimits^{=}_{M_iM_jM_i'M_j'} |w_{ij}(M_iM_j; M_i'M_j')|^2 \exp[-(W_i(M_i) + W_j(M_j))/kT]$$
$$+ \sum_i d_i \sum\nolimits^{=}_{M_iM_i'} |V_i(M_i; M_i')|^2 \exp[-W_i(M_i)/kT]\}$$
$$+ k^{-1}T^{-1}\{\{\sum_{j>i} d_i d_j \sum\nolimits'_{M_iM_jM_i'M_j'} \{|W_{ij}(M_iM_j; M_i'M_j')|^2/(W_i(M_i') + W_j(M_j')$$
$$- W_i(M_i) - W_j(M_j))\} \exp[-(W_i(M_i) + W_j(M_j))/kT]$$
$$+ \sum_i d_i \sum\nolimits'_{M_iM_i'} \{|V_i(M_i; M_i')|^2/(W_i(M_i') - W_i(M_i))\} \exp[-W_i(M_i)/kT]\}\}.$$

Equations (13a) and (13b) are more general than the corresponding equations given by Van Vleck[9] as provision is here made to take account of a cystalline field contribution to the partition function

as well as of a contribution from the magnetic dipole-dipole coupling. It may be noticed that only terms linear or quadratic in each interaction appear in these last equations whereas one would expect the operations of Eq. (12) to lead also to cross terms, i.e., terms containing a product of the two perturbing potentials. Such terms do arise but have been omitted from Eqs. (13) as it can be shown[15] that for our application their contribution to the magnetic moment vanishes. This being so, the complete contributions of the two perturbing potentials to the partition function are directly additive and may be considered separately.

VI. Partition Function to Second Order in Dipole-Dipole Coupling

In order to determine the contribution of the dipole-dipole parts of Eqs. (13a) and (13b) to the partition function, the matrix elements of this coupling must first be evaluated. This evaluation has already been carried out in a paper by Van Vleck,[16] henceforth called l.c., in which the partition function is calculated to the second order in the magnetic coupling for the case of arbitrarily large applied fields and for arbitrary direction of field relative to cubic axes. We have[17]

$$Z/Z_0=1-\tfrac{1}{2}Nk^{-1}T^{-1}B_1^2\Omega_0+\tfrac{1}{8}Nk^{-2}T^{-2}\Omega_0^2[B_1^4(N-4)+4B_1^2B_2]$$
$$+\tfrac{1}{5}Nk^{-2}T^{-2}\Omega_1[\tfrac{1}{4}B_1^4-\tfrac{1}{2}B_1^2B_2+\tfrac{1}{4}B_2^2+\tfrac{1}{16}(S^2+S-B_2)^2-\tfrac{1}{16}B_1^2+\tfrac{1}{8}B_1(S^2+S-B_2)(kT/g\beta H)]$$
$$+\tfrac{1}{5}Nk^{-2}T^{-2}\Omega_2[\tfrac{1}{4}B_1(S^2+S-B_2)-B_1^3+B_1B_2](kT/g\beta H)$$
$$+\tfrac{1}{5}Nk^{-2}T^{-2}\Omega_3[\tfrac{1}{16}(S^2+S-B_2)^2-\tfrac{1}{16}B_1^2-\tfrac{1}{8}(S^2+S-B_2)B_1(kT/g\beta H)], \quad (14)$$

where the Ω's are functions of the coefficients of the product terms $S_{qi}S_{qj}(q=xyz)$ that appear in the expression for the dipole-dipole coupling referred to a set of axes fixed relative to the crystal instead of to the magnetic field direction. It has been shown in l.c. that the Ω's can be expressed as[18]

$$\Omega_0=-Ng^2\beta^2\Phi, \quad \Omega_1=2N^2g^4\beta^4Q_0, \quad \Omega_2=\tfrac{3}{2}N^2g^4\beta^4Q_0, \quad \Omega_3=-N^2g^4\beta^4Q_0, \quad (14a)$$

where $Q_0=2N^{-2}\sum r_{ij}^{-6}$. This summation, varying as the inverse sixth power of the atomic distance, converges rapidly. The value of Q_0 for a face-centered lattice such as that occupied by the paramagnetic ions in iron alum is 14.4. The quantity Φ is defined as the sum of the Lorentz local field factor $(4\pi/3)$ and the demagnetization factor (η). It takes account of the fact that the H of Eq. (14) which represents the applied field, differs from the true field acting on the paramagnetic ions.

The B functions of Eq. (14) are Brillouin functions defined by

$$B_n=(1/Q)(\partial^nQ/\partial\theta^n), \quad (15)$$

where

$$Q=\sum_{M=-S}^{S}\exp(M\theta) \quad \text{and} \quad \theta=(g\beta H/kT).$$

VII. Matrix Elements of Crystalline Field

For simplicity we consider first the matrix elements for a trigonal field containing only second-order terms, i.e., a crystalline field of axial symmetry. Such a field is represented by Eq. (4a) of

---

[15] J. A. Sauer, Doctoral Dissertation, University of Cambridge (1941). The cross terms are found to drop out regardless of the shape of the specimen. Essentially the reason is that these terms are linear in the representation coefficient and hence vanish when the spatial averaging is performed.

[16] J. H. Van Vleck, Phys. Rev. **52**, 1178 (1937), henceforth l.c.

[17] Our Eq. (14) differs from Eq. (21) of l.c. only in the absence of a term in Ω_4. This term was needed in the study of anisotropy but for our application to demagnetization experiments performed on a powdered specimen this term can be omitted as it vanishes when averages over all directions are included.

[18] In the Ω's as defined by Eq. (27) of l.c., there also appear terms in the exchange integral. These have been omitted from our Eq. (14a) as exchange effects can be neglected in our treatment because of the known magnetic diluteness of iron alum.

TABLE III. Matrix elements of crystalline field of axial symmetry.

M_J	5/2	3/2	1/2	−1/2	−3/2	−5/2
5/2	$D_2^{00}/\sqrt{6}$	$-D_2^{10}/\sqrt{5}$	$D_2^{20}/\sqrt{10}$	0	0	0
3/2	$D_2^{-10}/\sqrt{5}$	$-\frac{1}{2}D_2^{00}/\sqrt{6}$	$-\frac{3}{2}D_2^{10}/\sqrt{2}$	$\frac{3}{2}D_2^{20}/\sqrt{2}$	0	0
1/2	$D_2^{-20}/\sqrt{10}$	$\frac{3}{2}D_2^{-10}/\sqrt{2}$	$-\frac{1}{2}D_2^{00}/\sqrt{6}$	0	$\frac{3}{2}D_2^{20}/\sqrt{2}$	0
−1/2	0	$\frac{3}{2}D_2^{-20}/\sqrt{2}$	0	$-\frac{1}{2}D_2^{00}/\sqrt{6}$	$\frac{3}{2}D_2^{10}/\sqrt{2}$	$D_2^{20}/\sqrt{10}$
−3/2	0	0	$\frac{3}{2}D_2^{-20}/\sqrt{2}$	$-\frac{3}{2}D_2^{-10}/\sqrt{2}$	$-\frac{1}{2}D_2^{00}/\sqrt{6}$	$D_2^{10}/\sqrt{5}$
−5/2	0	0	0	$D_2^{-20}/\sqrt{10}$	$-D_2^{-10}/\sqrt{5}$	$D_2^{00}/\sqrt{6}$

Note: All matrix elements to be multiplied by $\frac{2}{5}I_2A\sqrt{10}$ or, in the notation of Penney and Schlapp, by $10Aa\sqrt{6}$.

Section II or by the equivalent expressions

$$V_a = Ar^2(1-3\cos^2\theta) = -Ar^2\frac{2\sqrt{10}}{5}T_2^0, \tag{16}$$

where T_2^0 is a spherical harmonic of the second order normalized to unity. Since the experiments of Casimir and de Haas were performed on a powdered specimen in which all directions of magnetic field relative to the cubic axes are equally probable, it is necessary to transform from the x, y, z system relative to fixed axes over to a new coordinate X, Y, Z system relative to the arbitrary magnetic field direction. Under this transformation the Tesseral harmonic of order two will transform into a sum of other Tesseral harmonics of the same order. In particular, $T_2^0 = \sum_{m'} D_2^{m',0} T_2^{m'}$ where the $D_l^{mm'}$'s are the so-called representation coefficients of order l. The desired matrix elements are now found by use of the Kramers symbolic method[4,19] or by direct computation from the fundamental quadrature. The matrix representing V_a in the "M" system of representation is given in Table III. The symbol I_2 multiplying the matrix elements is given by $I_2 = c_J \int r^2 R^2 dr$, where c_J is an undetermined parameter that enters in the Kramers group-theory method of calculation of the matrix elements and R is the radial wave function. The value of I_2 may be determined by comparing the diagonal element for $M=5/2$ with the corresponding matrix element determined by Penney and Schlapp.[7] Their value is applicable only for a pure crystal in which the magnetic field is directed along the z axis. Taking this restriction into account and comparing, we find that our expression $\frac{2}{5}I_2A\sqrt{10}$ is the same as $10Aa\sqrt{6}$ in the notation of Penney and Schlapp.

If the second-degree terms of the trigonal crystalline field are omitted and only the fourth-degree cubic terms considered, that part of the crystalline potential independent of r can be written

$$V_c = \frac{2}{15}\sqrt{2}T_4^0 + \frac{2}{105}(35)^{\frac{1}{2}}T_4^4 + \frac{2}{105}(35)^{\frac{1}{2}}T_4^{-4}, \tag{17}$$

where the T_4^m's are fourth-order harmonics normalized to unity. In this expression $\theta=0$ refers to a direction along one of the cubic axes. In transforming over to a new coordinate system with polar axis in direction of magnetic field, the T_l^m's transform like representation coefficients of the rotation group of dimensionality $2l+1$ so that

$$T_4^m = \sum_{m'} D_4^{m'm} T_4^{m'}.$$

The matrix table for any one of the fourth-order Tesseral harmonics is now obtained by use of the Kramers symbolic method. The matrix elements for that combination of spherical harmonics given by the cubic crystalline field of Eq. (17) are given in Table IV. In this table, the symbol D_4^m stands

[19] H. C. Brinkman, Doctoral Dissertation, University of Utrecht (1932).

TABLE IV. Matrix elements of crystalline field of cubic symmetry.

M_J	5/2	3/2	1/2	−1/2	−3/2	−5/2
5/2	$D_4^0/\sqrt{70}$	$-2D_4^1/\sqrt{70}$	$3D_4^2/\sqrt{70}$	$-D_4^3/\sqrt{5}$	$D_4^4/\sqrt{5}$	0
3/2	$2D_4^{-1}/\sqrt{70}$	$-3D_4^0/\sqrt{70}$	$D_4^1/\sqrt{7}$	$-D_4^2/\sqrt{14}$	0	$D_4^4/\sqrt{5}$
1/2	$3D_4^{-2}/\sqrt{70}$	$-D_4^{-1}/\sqrt{7}$	$2D_4^0/\sqrt{70}$	0	$-D_4^2/\sqrt{14}$	$D_4^3/\sqrt{5}$
−1/2	$D_4^{-3}/\sqrt{5}$	$-D_4^{-2}/\sqrt{14}$	0	$2D_4^0/\sqrt{70}$	$-D_4^1/\sqrt{7}$	$3D_4^2/\sqrt{70}$
−3/2	$D_4^{-4}/\sqrt{5}$	0	$-D_4^{-2}/\sqrt{14}$	$D_4^{-1}/\sqrt{7}$	$-3D_4^0/\sqrt{70}$	$2D_4^1/\sqrt{70}$
−5/2	0	$D_4^{-4}/\sqrt{5}$	$-D_4^{-3}/\sqrt{5}$	$3D_4^{-2}/\sqrt{70}$	$-2D_4^{-1}/\sqrt{70}$	$D_4^0/\sqrt{70}$

Note: All matrix elements to be multiplied by $\frac{2}{105}(35)^{\frac{1}{2}}DI_4$ or, in the notation of Penney and Schlapp, by $60Dq$.

for the following combination of representation coefficients:

$$D_4^m=(14/5)^{\frac{1}{2}}D_4^{m0}+D_4^{m4}+D_4^{m,-4} \quad \text{and} \quad I_4=c_J\int r^4R^2dr.$$

The switch to the Penney and Schlapp notation is carried out in the same manner as indicated above.

Numerical Checks: One check on the numerical accuracy of both matrix tables that we have verified is that those elements which arise due only to even values of m in T_2^m or T_4^m must agree with values previously calculated by Van Vleck and Hebb[20] in connection with a different problem.

Secondly, since the diagonal terms of the cubic field matrix were used to change from our notation to that of Penney and Schlapp, a comparison of the off-diagonal terms in the two cases can be used as a check. All that is necessary is to give the representation coefficients their specific numerical value for the special case considered by Penney and Schlapp, and when this is done and the comparison made, the two expressions are found to be alike.

VIII. Partition Function to Second Order in Crystalline Field Interaction

The partition function for the crystalline field terms is now obtained by substituting the matrix elements from Table III or IV into Eqs. (13a) and (13b). The resultant expressions are functions of the $D_l^{mm'}$'s that appear in the matrix elements. These representation coefficients, however, can be eliminated by performing the spatial averaging required in virtue of the powdered form of the test samples.[21] The averaging is easily carried out by using the group theory relationship

$$\int\int\int D_l^{mn}D_{l'}^{pq}d\Omega\Big/\int\int\int d\Omega=\delta_{mp}\delta_{nq}\delta_{ll'}/\nu. \tag{18}$$

Here δ is the Dirac delta function and ν is the dimensionality of the representation given by $2l+1$.

After carrying out the indicated procedure, we find the contribution of the axial crystalline field to log Z to be

$$(N/45)\gamma_a^2T^{-2}\{-2Q^{-2}(5\cosh 5x-\cosh 3x-4\cosh x)^2+Q^{-1}(25\cosh 5x+\cosh 3x+16\cosh x)$$
$$+3Q^{-1}(kT/g\beta H)(25\sinh 5x-3\sinh 3x-4\sinh x)\}. \tag{19}$$

For the crystalline field of cubic symmetry, the contribution to log Z is

$$(N\gamma_c^2/21T^2)\{-2Q^{-2}(\cosh 5x-3\cosh 3x+2\cosh x)^2+Q^{-1}(\cosh 5x+9\cosh 3x+4\cosh x)$$
$$+4Q^{-1}(kT/3g\beta H)(25\sinh 5x+18\sinh 3x-11\sinh x)\}. \tag{20}$$

[20] J. H. Van Vleck and M. H. Hebb, Phys. Rev. **46**, 17 (1934).

[21] The averaging should be carried out not on Z itself but on log Z. The reason why Z can't be used is clear when we recall that log $(1+x)$ where x is small compared to unity is equal to $x-\frac{1}{2}x^2$ to the second order. Hence, if average was taken on Z itself instead of log Z, we would be dealing with $\langle x\rangle_{Av}^2$ instead of with $\langle x^2\rangle_{Av}$ and these are by no means equivalent.

In these expressions $x=(g\beta H/2kT)$ and γ_a and γ_c have taken the place, respectively, of the crystalline field constants $6Aa$ and $24D_q$. The γ symbols may be considered as characteristic temperatures associated with the crystalline field splitting pattern. If we set up and solve the secular equation for the one atom problem, we find that the γ's of Eqs. (19) and (20) are exactly $\frac{1}{3}$ the δ's of Fig. 1.

IX. Magnetic Moment and Entropy to Second Order in Perturbing Potentials

Expressions for the magnetic moment and entropy correct to the second order in the perturbing potentials are now found by substituting Eqs. (12c), (14), and either (19) or (20) into Eq. (12) and using Eq. (8). We obtain:

$$(M/Ng\beta)=B_1+(\tau/T)f_{M'}+(\tau/T)^2(f_{M''}+G_M)+(\gamma/T)^2v, \tag{21}$$

$$S/Nk=\log Q-(g\beta H/kT)B_1+(\tau/T)f_{s'}+(\tau/T)^2(f_{s''}+G_s)+(\gamma/T)^2u. \tag{22}$$

Here τ is a characteristic temperature associated with the dipole-dipole coupling and for iron alum with $S=5/2$ it takes the value

$$\tau=Ng^2\beta^2S(S+1)/k=0.0472°.$$

The f' and f'' terms of Eqs. (21) and (22) are the first- and second-order effects of the local field plus demagnetization corrections while the G terms, entering only in the second order, represent the perturbations due to the dipole-dipole interaction that are not included in the Φ terms. They are defined by

$$f_{M'}=\Phi S^{-1}(S+1)^{-1}B_1(B_2-B_1^2), \tag{21a}$$

$$f_{M''}=\Phi^2S^{-2}(S+1)^{-2}\{B_1(B_2-2B_1^2)(B_2-B_1^2)+\tfrac{1}{2}B_1^2(B_3-B_1B_2)\}, \tag{21b}$$

$$\begin{aligned}G_M=\tfrac{1}{8}Q_0S^{-2}(S+1)^{-2}\{&(B_3-B_1B_2)[-B_1^2+B_2-\tfrac{1}{8}(S^2+S-B_2)+\tfrac{3}{4}(kT/g\beta H)B_1]\\&+(B_2-B_1^2)[2B_1^3-2B_1B_2-\tfrac{1}{8}B_1+\tfrac{3}{4}(kT/g\beta H)(S^2+S+B_2-6B_1^2)]\\&+(kT/g\beta H)^2[-\tfrac{3}{4}B_1(S^2+S-B_2)-\tfrac{3}{2}B_1B_2+\tfrac{3}{2}B_1^3]\}.\end{aligned} \tag{21c}$$

$$f_{s'}=-\Phi S^{-1}(S+1)^{-1}(g\beta H/kT)B_1(B_2-B_1^2), \tag{22a}$$

$$\begin{aligned}f_{s''}=\tfrac{1}{2}\Phi^2S^{-2}(S+1)^{-2}\{&B_1^4-B_1^2B_2-(g\beta H/kT)B_1^2(B_3-B_1B_2)\\&-(g\beta H/kT)2B_1(B_2-2B_1^2)(B_2-B_1^2)\},\end{aligned} \tag{22b}$$

$$\begin{aligned}G_s=-(Q_0/10)S^{-2}(S+1)^{-2}\{&B_1^4-2B_1^2B_2+B_2^2+\tfrac{1}{8}(S^2+S-B_2)^2-\tfrac{1}{8}B_1^2+\tfrac{3}{2}B_1(B_3-B_1B_2)\\&+\tfrac{3}{2}(B_2-B_1^2)[(S^2+S-B_2)-6B_1^2+2B_2]+(g\beta H/kT)[(B_2-B_1^2)(4B_1^3-4B_1B_2-\tfrac{1}{4}B_1)\\&+(B_3-B_1B_2)(2B_2-2B_1^2-\tfrac{1}{4}(S^2+S-B_2))]\}.\end{aligned} \tag{22c}$$

These equations are true for any value of the spin S, but a convenient check on the correctness of the algebraic manipulations involved in the derivation of the above equations can be had by restricting the atomic spin to the value $\frac{1}{2}$ and then comparing these expressions with the corresponding ones given by Van Vleck.[3] After making the required restriction, we find complete agreement.

The v and u terms of Eqs. (21) and (22) represent the perturbations due to the crystalline field. Consider first the field of axial symmetry and let

$$\mathbf{C}^n(a,b,c)=Q^{-n}(a\cosh 5x+b\cosh 3x+c\cosh x)^n,$$

$$\mathbf{S}^n(a,b,c)=Q^{-n}(a\sinh 5x+b\sinh 3x+c\sinh x)^n$$

with

$$Q=2(\cosh 5x+\cosh 3x+\cosh x).$$

Then

$$45v_a=4B_1\mathbf{C}^2(5,-1,-4)-2\mathbf{C}(5,-1,-4)\mathbf{S}(25,-3,-4)-B_1\mathbf{C}(25,1,16)+\tfrac{1}{2}\mathbf{S}(125,3,16)$$
$$+\tfrac{3}{2}(kT/g\beta H)[\mathbf{C}(125,-9,-4)-2B_1\mathbf{S}(25,-3,-4)-2(kT/g\beta H)\mathbf{S}(25,-3,-4)], \quad (21d)$$

$$45u_a=2\mathbf{C}^2(5,-1,-4)-\mathbf{C}(25,1,16)-\tfrac{3}{2}\mathbf{C}(125,-9,-4)+3B_1\mathbf{S}(25,-3,-4)$$
$$+(g\beta H/kT)[-4B_1\mathbf{C}^2(5,-1,-4)+B_1\mathbf{C}(25,1,16)-\tfrac{1}{2}\mathbf{S}(125,3,16)$$
$$+2\mathbf{C}(5,-1,-4)\mathbf{S}(25,-3,-4)]. \quad (22d)$$

For a trigonal field of cubic symmetry, the v and u symbols are given by[22]

$$21v_c=4B_1\mathbf{C}^2(1,-3,2)-2\mathbf{C}(1,-3,2)\mathbf{S}(5,-9,2)-B_1\mathbf{C}(1,9,4)+\tfrac{1}{2}\mathbf{S}(5,27,4)$$
$$+\tfrac{2}{3}(kT/g\beta H)[\mathbf{C}(125,54,-11)-2B_1\mathbf{S}(25,18,-11)-2(kT/g\beta H)\mathbf{S}(25,18,-11)], \quad (21e)$$

$$21u_c=2\mathbf{C}^2(1,-3,2)-\mathbf{C}(1,9,4)+\tfrac{4}{3}B_1\mathbf{S}(25,18,-11)-\tfrac{2}{3}\mathbf{C}(125,54,-11)$$
$$-(g\beta H/kT)[4B_1\mathbf{C}^2(1,-3,2)+\tfrac{1}{2}\mathbf{S}(5,27,4)-B_1\mathbf{C}(1,9,4)-2\mathbf{C}(1,-3,2)\mathbf{S}(5,-9,2)]. \quad (22e)$$

If one neglects the correction terms in Eqs. (21) and (22) arising from the dipole-dipole and crystalline field interactions, the expressions for M and S reduce to

$$M=Ng\beta B_1, \quad (23)$$

$$S=Nk(\log Q-\theta B_1). \quad (24)$$

Since S remains constant during an adiabatic demagnetization process, it can readily be seen from the above equations, remembering that $\theta=(g\beta H/kT)$, that the temperature is a linear function of the field of the form $T=C_1H+C_2$ with C_2 zero. The procedure of de Haas and Wiersma for determining the true thermodynamic temperature now clearly applies. It has been shown by Van Vleck[3] that even if the correction terms in f' and f'' are retained Eqs. (23) and (24) are still valid provided only that the magnetic field H be no longer interpreted as the applied field but as the true local field $H+\Phi M$. The linear equation between T and H still holds, but the coefficients now satisfy the relation $C_2/C_1=\Phi M$.

Thus, even for specimens of non-spherical shape—for spherical specimens the Φ terms are always zero—the f terms may now be omitted from Eqs. (21) and (22) though care must be taken when comparing the results of theory with experiment first to convert the applied field over into the true local field by introducing the proper demagnetization corrections for the shape in question.

X. Determination of Adiabatic Magnetic Moment

To derive an expression for the magnetic moment valid throughout the entire demagnetization process, one needs only to solve Eq. (22) for T in terms of H and then substitute this function in Eq. (21). In this manner one obtains an equation involving only M, M_0, and H. We are primarily interested in the form of M for large initial fields and therefore assume, as a comparable approximation to those previously made, that the primary terms in M and S in Eqs. (21) and (22) can be expanded as a Taylor's series in $\theta-\theta^0$ and only first-order terms retained. Furthermore, it is assumed that the argument of the v, u, and G terms, which are all small perturbations, has the same value as at the initial helium temperatures. This means that θ can be everywhere replaced in these terms by θ^0.

---

[22] One helpful check on the algebraic accuracy of Eqs. (21) and (22) which has been useful is:
$$(\partial S/\partial H)_T=(\partial M/\partial T)_H.$$

After expanding the leading terms in M and S, we find

$$(S-S_0)/Nk=0=-\theta^0[B_2{}^0-(B_1{}^2)^0](\theta-\theta^0)+(\tau/T)^2G_s{}^0+(\gamma/T)^2u^0, \tag{25}$$

$$(M-M_0)/Ng\beta=[B_2{}^0-(B_1{}^2)^0](\theta-\theta^0)+(\tau/T)^2G_M{}^0+(\gamma/T)^2v^0, \tag{26}$$

where the superscript zero in the B_n, G, u, and v terms means that these are to be evaluated at $\theta=\theta^0=g\beta H_0/kT_0$. From Eqs. (25) and (26) we get

$$M-M_0=Ng\beta\left\{\left(\frac{\tau}{T_0}\right)^2\left(\frac{G_s{}^0}{\theta^0}+G_M{}^0\right)+\left(\frac{\gamma}{T_0}\right)^2\left(\frac{u^0}{\theta^0}+v^0\right)\right\}\left(\frac{H_0}{H}\right)^2. \tag{27}$$

In order that this equation apply for both axial and cubic crystalline fields, μ^0 and v^0 should be taken, respectively, as $u_a{}^0$, $v_a{}^0$ and $u_c{}^0$, $v_c{}^0$.

Equation (27) is the theoretical expression for the adiabatic magnetic moment correct to the second order in the perturbing potentials. For purposes of comparison with the experimental relation between M and H found by de Haas and Casimir, it can be put in the form

$$M=M_0(1-b/H^2), \tag{28}$$

where[23]

$$b=-\left(\frac{H_0{}^2}{B_1{}^0}\right)\left\{\left(\frac{\tau}{T_0}\right)^2\left(\frac{G_s{}^0}{\theta^0}+G_M{}^0\right)+\left(\frac{\gamma}{T_0}\right)^2\left(\frac{u^0}{\theta^0}+v^0\right)\right\}. \tag{29}$$

Another convenient check on our calculations is now available. De Haas and Casimir[2] have given a theoretical derivation for b that is accurate only for the case of low initial fields. Our analysis is valid for fields of any nature and hence our expression should reduce to theirs if we restrict H to low values only. The procedure is to expand the various correction terms G_s, u_a, etc., that appear in Eq. (29) in powers of θ and then retain only the lowest terms in the expansion. When this is done we find $b=3A'/2\tau$ and this is equivalent to the expression given by de Haas and Casimir.[24] The numerical value of $3A'/2\tau$ is 1.3×10^5. This should not be expected to agree with the experimental value of b of 1.7×10^5 since the demagnetization experiments were carried out at such high values of the initial field that saturation effects cannot be neglected.

For the more important case of high fields, the numerical value of b must be taken directly from Eq. (29). The characteristic magnetic coupling temperature τ has already been evaluated and numerical values of $G_s{}^0$ and $G_M{}^0$,[25] representing the effect of the magnetic coupling on the adiabatic moment, can be calculated directly from Eqs. (21c) and (22c) as these equations depend only on θ^0, Q_0, and S, whose respective numerical values are 2.04, 14.4, and 5/2. The v and u terms of Eq. (29) can also be directly evaluated[25] from their defining equations, but the complete crystalline field contribution to the adiabatic moment cannot yet be found as this contribution contains an unknown crystalline field parameter, *vis.*, γ_a or γ_c. Hence, it is first necessary to evaluate these parameters and this is done by calculating the theoretical expression for the specific heat in zero applied field and comparing it with the known experimental value.

Crystalline Field Constants for Specific Heat Data

The theoretical expression for the specific heat is obtained directly from the partition function by means of the equation

$$C_v=\frac{\partial}{\partial T}\left(kT^2\frac{\partial}{\partial T}\log Z\right). \tag{30}$$

[23] The bracketed part of Eq. (29) is always found to be negative; hence b itself is essentially positive.

[24] The expression actually given by de Haas and Casimir is $A/2a$ where small a is the coefficient of H/T in the ordinary formula for M when saturation is neglected. However, since in our notation this coefficient is $\tau/3$ and since our A' is identical with their A, the two expressions are equivalent.

[25] The calculated values of these various quantities are stated explicitly in reference 15.

We desire the specific heat in the absence of an applied field. Taking into account this condition and substituting Eqs. (14) and (19) into Eq. (30) we find

$$C_v = Nk\{2.4(\tau/T)^2 + 1.55(\gamma_a/T)^2\}, \tag{31}$$

where the first term represents the contribution of the dipole-dipole coupling and the second term that of an axial crystalline field. If the partition function derived for the case of a cubic crystalline field be substituted in Eq. (30), then $1.55\gamma_a^2$ should be replaced by $2.00\gamma_c^2$.

Equation (31) is of the form $A'T^{-2}$ as found experimentally by various observers.[12] Since the value of τ is known, this equation may be used for determining γ_a or γ_c by substituting for C_v on the left-hand side of the equation the accepted experimental value of $2300T^{-2}$. The crystalline field parameters now become $\gamma_c = 0.063$ and $\gamma_a = 0.072$ corresponding to splitting distances (see Fig. 1) of $\delta_c = 0.190$ and $\delta_a = 0.215$. Substituting these values and those of the other parameters into Eq. (29), we find $b = 9.4 \times 10^4$ for a field of cubic symmetry and $b = 11.5 \times 10^4$ for a field of axial symmetry.

Effect of Demagnetization Corrections on Adiabatic Moment

For either type of crystalline field, the calculated values of the coefficient b are found to be too low and hence the theoretical values of M are higher than the experimental. As mentioned in Part I, some of the discrepancy between the theoretical and the experimental values is due to the fact that the H of Eq. (28) is no longer the same as the applied field H_a of Eq. (2). To find the true local field H when H_a is known, it is first necessary to determine the proper demagnetization factor η for the shape of specimen used in the experiments. De Haas and Casimir used a powdered specimen of iron alum pressed in the form of a cylinder 90 mm long by 30 mm wide. Since the true demagnetization factor is calculable only for an ellipsoid, all one can do is to estimate this factor by assuming that the specimen can be adequately represented by an ellipsoid of revolution with an axes ratio of 3 : 1. The magnetic field was applied at right angles to the longitudinal axis of the ellipsoid. For this case $\Phi = (4/3)\pi - \eta$ becomes negative and hence the local field $H(=H_a + \Phi M)$ is less than the applied field H_a. This has a tendency to lower the theoretical values of M, thereby bringing them in somewhat closer relation to the experimental data. However, a direct evaluation shows that while a minor improvement has been made the major part of the discrepancy between the theoretical values of M and the experimental still exists.

Effect of a More General Crystalline Field

In Section III of Part I, the thought was raised that possibly a crystalline field of a more general nature than one of cubic or axial symmetry would lead to better agreement between theory and experiment. To examine this question more thoroughly, we calculate the contribution to the partition function and the magnetic moment of the arbitrary crystalline potential specified by Eq. (6) of Section III. We need the matrix elements of this potential and can easily obtain them from the calculations already made. The matrix elements of the T_2 terms of Eq. (6) can be obtained directly from the numerical values listed in Table II, and each of the T_4 terms of Eq. (6) leads to a matrix table similar to that of Table III. The only change that must be made in these tables is the replacement of the original coefficients of the T_l's that appear in Eqs. (16) and (17) by the new coefficients from Eq. (6). On substitution of the matrix elements into Eqs. (13) the contribution of the arbitrary crystalline potential to the log of the partition function is found to be the sum of Eqs. (19) and (20) with $\gamma_a^2/45$ replaced by

$$(\sum_{-2}^{2}{}_r (a_{2r})^2/750) \text{ and } \gamma_c^2/21 \text{ replaced by } (\sum_{-4}^{4}{}_s (a_{4s})^2/630).$$

The expressions for the magnetic moment and entropy previously given by Eqs. (21) and (22) can be made to apply to the general crystalline field, by replacing, respectively, the $\gamma^2 v$ and $\gamma^2 u$ terms of

these equations by the following expressions:

$$(v_c/30)\sum_{-4}^{4}{}_s a_{4s}^2+(3v_a/50)\sum_{-2}^{2}{}_r a_{2r}^2 \quad \text{and} \quad (u_c/30)\sum_{-4}^{4}{}_s a_{4s}^2+(3u_a/50)\sum_{-2}^{2}{}_r a_{2r}^2.$$

The adiabatic moment and the specific heat found in the same manner as previously indicated, are

$$M=M_0(1-b_g/H^2)$$

with

$$b_g=-(H_0^2/B_1^0)\left\{\left(\frac{\tau}{T_0}\right)^2\left(\frac{G_s^0}{\theta^0}+G_M{}^0\right)+\frac{\sum_s a_{4s}^2}{30T_0^2}\left(\frac{u_c^0}{\theta^0}+v_c^0\right)+\frac{3}{50}\frac{\sum_r a_{2r}^2}{T_0^2}\left(\frac{u_a^0}{\theta^0}+v_a^0\right)\right\} \tag{32}$$

and

$$C_v=NkT^{-2}\left\{2.4\tau^2+\frac{1}{15}\sum_s a_{4s}^2+\frac{7}{75}\sum_r a_{2r}^2\right\}. \tag{33}$$

These are the exact expressions correct to the second order in the perturbing influences which include both the magnetic dipole-dipole coupling and the arbitrary crystalline potential of Eq. (6). All the coefficients of this potential are at our disposal and the problem now is to give b_g and C_v their experimental values for iron alum and then determine whether a suitable choice of coefficients can be found that will lead to agreement in both equations. The results of this procedure have already been discussed in Section III of Part I.

XI. Adiabatic Moment to Third Order in Crystalline Field Potential

The problem of the determination of the energy levels of iron alum supposed subject to a large applied magnetic field of arbitrary direction and to a crystalline electric field of cubic symmetry has been considered by Kronig and Bouwkamp.[13] They were able to calculate, correct to the third order in the cubic field splitting parameter, all six energy levels of the normally degenerate ground state. The six expressions are:[26]

$$\left.\begin{matrix}W_1\\W_2\end{matrix}\right\}=\pm\tfrac{1}{2}g\beta H+p\gamma\pm\frac{2q_1\gamma^2}{g\beta H}+\frac{4r_1\gamma^3}{g^2\beta^2H^2}\pm\cdots,$$

$$\left.\begin{matrix}W_3\\W_4\end{matrix}\right\}=\pm\tfrac{3}{2}g\beta H-\tfrac{3}{2}p\gamma\pm\frac{2q_2\gamma^2}{g\beta H}+\frac{4r_2\gamma^3}{g^2\beta^2H^2}\pm\cdots, \tag{34}$$

$$\left.\begin{matrix}W_5\\W_6\end{matrix}\right\}=\pm\frac{5}{2}g\beta H+\tfrac{1}{2}p\gamma\pm\frac{2q_3\gamma^2}{g\beta H}+\frac{4r_3\gamma^3}{g^2\beta^2H^2}\pm\cdots,$$

where

$$p=1-5\varphi,\quad q_1=-\frac{5\varphi}{6}(7-25\varphi),\quad q_2=\frac{5}{32}+\frac{5}{32}\varphi(22-75\varphi),\quad q_3=\frac{5}{32}+\frac{5}{96}\varphi(50-113\varphi),$$

$$r_1=\frac{-5}{144}\varphi(196-1635\varphi+3125\varphi^2),\quad r_2=\frac{5}{128}+\frac{15}{128}\varphi(79-615\varphi+1125\varphi^2), \tag{35}$$

$$r_3=\frac{-5}{128}-\frac{25}{1152}\varphi(113-705\varphi+1075\varphi^2).$$

In these equations φ is a specific function of the direction cosines α_1, α_2, α_3 of H with respect to the

[26] Our symbol γ is the same quantity as that indicated by a in the Kronig-Bouwkamp paper.

cubic axes given by

$$\varphi=\alpha_2^2\alpha_3^2+\alpha_3^2\alpha_1^2+\alpha_1^2\alpha_2^2. \tag{36}$$

Let the six energy levels of Eq. (34) be substituted into the partition function

$$Z=[\textstyle\sum_M \exp(-W_M/kT)]^N.$$

Expanding the exponential and retaining terms only to the third order in the cubic field potential, we find

$$Z/Z_0=\left\{1-(\gamma/T)p\mathbf{C}(1,-3,2)+(\gamma/T)^2\left[\frac{1}{4}p^2\mathbf{C}(1,9,4)+4(kT/g\beta H)\mathbf{S}(q_3,q_2,q_1)\right]\right.$$
$$\left.-(\gamma/T)^3\left[\frac{1}{24}p^3\mathbf{C}(1,-27,8)+8(kT/g\beta H)^2\mathbf{C}(r_3,r_2,r_1)+2(kT/g\beta H)\mathbf{S}(pq_3,-3pq_2,2pq_1)\right]\right\}^N. \tag{37}$$

In order that our final results be applicable to a powdered specimen, it is necessary to calculate the average value of the various quantities p_1, r_2, q_3, etc., that depend on the direction cosines. Performing this averaging,[25] expanding log Z, and retaining terms only to the second power in γ, we obtain an expression for the log of Z that is identical with our previous Eq. (20) and thereby provides another check on the algebraic manipulation involved in its derivation. Since the effect on the magnetic moment and entropy of that part of the partition function given by Eq. (20) has already been considered, it is only necessary for us to consider now the third-order terms of Eq. (37). The contribution of these terms to the average value of $(1/N)$ log (Z/Z_0) is found to be

$$(1/3003)(\gamma/T)^3\{-6\mathbf{C}(1,-27,8)-48\mathbf{C}^2(1,-3,2)+36\mathbf{C}(1,-3,2)\mathbf{C}(1,9,4)$$
$$+(kT/g\beta H)[\mathbf{S}(125,453,-664)+2\mathbf{C}(1,-3,2)\mathbf{S}(-125,151,-332)]$$
$$+\tfrac{1}{6}(kT/g\beta H)^2\mathbf{C}(12295,9441,-2854)\}. \tag{38}$$

The additional term in the magnetic moment, due to inclusion of the above third-order term in the partition function, is found by differentiating Eq. (38) with respect to H and multiplying by kT. This term is

$$Ng\beta(\gamma/T)^3 w_M, \tag{39}$$

where

$$w_M=(1/7)w_M'+(1/3003)w_M''$$

with

$$w_M'=-(kT/g\beta H)\{(kT/g\beta H)\mathbf{S}(.268,1.05,1.55)+2(kT/g\beta H)^2\mathbf{C}(4.78,-3.67,1.04)$$
$$+B_1\mathbf{S}(.268,1.05,1.55)-\tfrac{1}{2}\mathbf{C}(1.34,3.15,1.55)$$
$$+B_1\mathbf{C}(4.78,-3.67,1.04)-\tfrac{1}{2}\mathbf{S}(23.9,-10.0,1.04)$$

and

$$w_M''=+6B_1\mathbf{C}(1,-27,8)-3\mathbf{S}(5,-81,8)-72\mathbf{C}^2(1,-3,2)\mathbf{S}(5,-9,2)+144B_1\mathbf{C}^3(1,-3,2)$$
$$-72B_1\mathbf{C}(1,-3,2)\mathbf{C}(1,9,4)+18\mathbf{S}(5,-9,2)\mathbf{C}(1,9,4)+18\mathbf{C}(1,-3,2)\mathbf{S}(5,27,4)$$
$$+(kT/g\beta H)\{-2(kT/g\beta H)\mathbf{C}(1,-3,2)\mathbf{S}(-125,151,-332)$$
$$-4B_1\mathbf{C}(1,-3,2)\mathbf{S}(-125,151,-332)+\mathbf{S}(5,-9,2)\mathbf{S}(-125,151,-332)$$
$$+\mathbf{C}(1,-3,2)\mathbf{C}(-625,453,-332)\}.$$

The contribution to the entropy of the third-order terms in the partition function is found to be

$$Nk(\gamma/T)^3 w_s, \tag{40}$$

where

$$w_s = (1/7)w_s' + (1/3003)w_s''$$

with

$$w_s' = +(kT/g\beta H)[-\mathbf{S}(.268, 1.05, 1.55) + \mathbf{C}(4.78, -3.67, 1.04) + \tfrac{1}{2}\mathbf{S}(23.9, -10.0, 1.04)] + B_1\mathbf{S}(.268, 1.05, 1.55) - \tfrac{1}{2}\mathbf{C}(1.34, 3.15, 1.55)$$

and

$$\begin{aligned} w_s'' = (g\beta H/kT)[&-6B_1\mathbf{C}(1, -27, 8) + 3\mathbf{S}(5, -81, 8) - 144B_1\mathbf{C}^3(1, -3, 2) \\ &+ 72\mathbf{C}^2(1, -3, 2)\mathbf{S}(5, -9, 2) + 72B_1\mathbf{C}(1, -3, 2)\mathbf{C}(1, 9, 4) - 18\mathbf{S}(5, -9, 2)\mathbf{C}(1, 9, 4) \\ &- 18\mathbf{C}(1, -3, 2)\mathbf{S}(5, 27, 4)] + 96\mathbf{C}^3(1, -3, 2) + 12\mathbf{C}(1, -27, 8) - 72\mathbf{C}(1, -3, 2)\mathbf{C}(1, 9, 4) \\ &+ 4B_1\mathbf{C}(1, -3, 2)\mathbf{S}(-125, 151, -332) - \mathbf{S}(5, -9, 2)\mathbf{S}(-125, 151, -332) \\ &- \mathbf{C}(1, -3, 2)\mathbf{C}(-625, 453, -332) - 2(kT/g\beta H)\mathbf{C}(1, -3, 2)\mathbf{S}(-125, 151, -332). \end{aligned}$$

Complete expressions for the magnetic moment and entropy to the third order in the crystalline field interaction and second order in the dipole-dipole coupling are obtained by adding Eqs. (39) and (40) to the previous Eqs. (21) and (22) developed in Section X. The adiabatic magnetization, found by solving the entropy equation for T as a function of H and substituting into the expression for the magnetic moment, is

$$M = M_0\left\{1 + \frac{H_0^2}{B_1^0 H^2}\left[\left(\frac{\tau}{T_0}\right)^2\left(\frac{G_s^0}{\theta^0} + G_M^0\right) + \left(\frac{\gamma}{T_0}\right)^2\left(\frac{u^0}{\theta^0} + v^0\right)\right] + \frac{H_0^3}{B_1^0 H^3}\left[\left(\frac{\gamma}{T_0}\right)^3\left(\frac{w_s^0}{\theta^0} + w_M^0\right)\right]\right\}, \tag{41}$$

where the sub- (or super-) script indicates that the quantities are to be evaluated at $\theta = \theta^0 = g\beta H_0/kT_0 = 2.04$. Placing numerical values of third-order correction terms—obtained directly from their defining equations—into Eq. (41) along with the proper values of the second-order correction terms and of the characteristic temperatures τ and γ, we finally obtain

$$M = M_0(1 - 9.4\times10^4 H^{-2} - 30\times10^6 H^{-3}). \tag{42}$$

This expression is exact to the second order in the dipole-dipole coupling and to the third order in the cubic crystalline field interaction. The agreement between it and experiment is discussed thoroughly in Section IV of Part I.

The writer wishes to thank Professor Van Vleck for suggesting this problem and for freely offering his assistance on many occasions

PHYSICAL REVIEW VOLUME 64, NUMBERS 3 AND 4 AUGUST 1 AND 15, 1943

The Electrical Conductivity and Isothermal Hall Effect in Cuprous Oxide

WILLIAM FELDMAN
University of Pennsylvania, Philadelphia, Pennsylvania
(Received December 7, 1942)

The electrical conductivity of cuprous oxide is studied from room temperature to 700°C. It is observed that whereas the conductivity may be represented by the formula $\sigma = A_e^{-\epsilon/kT}$ at the higher temperatures, below 300°C the exponential law is not obeyed. The maxima and minima of the conductivity curves observed in the latter region are presumed to result from a combination of a saturation of clusters and a rapid decrease of mobility with temperature. Hall effect measurements up to 450°C show that the number of current carriers does not obey the exponential law of temperature dependence. An anomaly in the mobility is observed around 150°C where the mobility changes from a T^{-5} to a T^{-7} dependence.

INTRODUCTION

THE semi-conductor, cuprous oxide, has been the object of many investigations in the past decade because of its peculiar electrical properties which are of theoretical and technical importance. However, the results and interpretations of these investigations have differed so markedly as to prevent the formulation of a unique theory of conduction in cuprous oxide. Englehard[1] and Angello[2] have studied the dependence of the conductivity and Hall coefficient on the impurity content and past history of various specimens. Their results indicate that the conductivity increases rapidly with rise in temperature and with an increase in the concentration of excess oxygen in the lattice. The Hall coefficient is positive, indicating that the current carriers are positively charged. Vogt[3] reached the same conclusion as a result of measurements of the thermoelectric effect. Between 100°C and 1000°C Jusé and Kourtschatow[4] and Dünwald and Wagner[5] have investigated the electrical conductivity. Jusé and Kourtschatow determined the excess oxygen content of their specimens at room temperature and attempted to correlate this with the conductivity. They concluded that at the high temperatures the electrical conductivity was an intrinsic property of the cuprous oxide and depended solely on the temperature. Dünwald and Wagner, on the other hand, investigating the effect of varying the external oxygen pressure on the specimen at constant temperature observed that the conductivity varied as the 1/7 power of the oxygen pressure. This indicates that the conductivity is a function of the amount of absorbed oxygen. The only data on the Hall effect at high temperatures are those of Schottky and Waibel,[6] who interpreted their data initially as indicating a change in the sign of the Hall coefficient. In a later paper Schottky concluded that this interpretation was erroneous. Thermoelectric measurements made at high temperatures by Dünwald and Wagner showed that the sign of the current carriers was positive.

The evidence of the above works indicates that cuprous oxide fits into the band theory of solids in the following manner: Pure cuprous oxide is an insulator which possesses a gap of at least one ev between the top of the highest filled band and the bottom of the lowest unfilled band. When cuprous oxide is in equilibrium with oxygen gas it absorbs oxygen so that the composition is no longer stoichiometric. The absorbed oxygen produces empty discrete energy levels which lie within the forbidden region but close to the top of the filled band. Thermal excitation of electrons to these levels results in electron "holes" in the lower band. The resulting conductivity is then apparently due to positively charged particles. In addition, it is strongly dependent upon the concentration of the ab-

[1] E. Englehard, Ann. d. Physik **17**, 501 (1933).
[2] S. J. Angello, Phys. Rev. **62**, 371 (1942).
[3] W. Vogt, Ann. d. Physik **7**, 183 (1930).
[4] W. Jusé and B. W. Kourtschatow, Physik. Zeits. Sowjetunion **2**, 453 (1932).
[5] H. Dünwald and C. Wagner, Zeits. f. physik. Chemie **22B**, 212 (1933).
[6] W. Schottky and F. Waibel, Physik. Zeits. **34**, 858 (1933); **36**, 912 (1935).

sorbed oxygen. At low temperatures (less than 300°C) the rate at which equilibrium is established between the absorbed oxygen in the solid phase and the gas phase is so low that it is impossible to control the concentration of absorbed oxygen by varying the pressure of the oxygen gas. Thus, the electrical properties at low temperatures depend upon the past history of the sample, such as the manner in which it was cooled from elevated temperatures. At high temperatures, where equilibrium may be assumed, the following mechanism is postulated for the absorption of the oxygen.[7] Oxygen molecules are absorbed on the surface of the cuprous oxide, and copper ions and electrons diffuse to the surface to form additional cuprous oxide with the oxygen molecules. This diffusion process leaves copper ion vacancies in the lattice. The process may be summarized by the reaction

$$2Cu^{+}+\tfrac{1}{2}O_2(\text{gas})\rightarrow 2Cu_A^{++}+O^{=}+2Cu^{+},$$

where Cu_A^{++} represents a copper ion vacancy in the lattice with an electron "hole" bound to a neighboring Cu^{+} ion. This copper ion vacancy is the source of a discrete energy level which lies in the forbidden region. By minimizing the free energy of the above system one obtains the relation for the number of copper ion vacancies

$$n_b=N_0T^{-5/8}p_4^{\frac{1}{4}}\exp(-W/kT),$$

where n_b is the number of copper ion vacancies, p is the pressure of the oxygen gas, $2W$ is the energy needed to place an oxygen atom in the lattice and produce two copper ion vacancies, N_0 is a constant, and k is Boltzmann's constant. It is assumed that n_b is small compared with the number of particles in the solid and also in the surrounding gas.

Using this expression for n_b we may now determine the number of free electron holes to be expected at a given temperature. It is assumed that the ionization of a hole may be treated as if equivalent to the reaction

$$Cu_A^{++}\rightleftarrows Cu_A^{+}+h.$$

Minimizing the free energy of the reaction with respect to a change in the number of free holes, h, we obtain

$$h=h_0n_b^{\frac{1}{2}}T^{\frac{3}{4}}\exp(-E/kT),$$

where E is the energy necessary to free a hole. Using the expression for n_b we have

$$h=\text{const. }p^{1/8}T^{7/16}\exp(-\epsilon/kT),$$

where $\epsilon=W+E$.

With the assumption that the free electron holes may be treated as a perfect gas, their contribution to the electrical conductivity may be calculated by simple classical theory.[8] The conductivity under these conditions is given by $\sigma=ne\mu$, where n is the number of free holes per unit volume, e is the charge of a hole, and μ the mobility of the carriers obtained from the relation $\mu=4el_0/3(2\pi m^*kT)^{\frac{1}{2}}$, where l_0 is the average mean free path and m^* the effective mass of the holes. Using the equation above for the number of free holes we obtain for the conductivity

$$\sigma=\text{const. }p^{1/8}T^{-1/16}l_0\exp(-\epsilon/2kT).$$

This equation can be expected to be valid only when the temperature is sufficiently high so that equilibrium conditions are established at all times. At low temperatures when equilibrium is not established the number of oxygen atoms absorbed will be independent of the temperature and one would expect the conductivity to show an exponential dependence on temperature with an activation energy E. Of course, the assumption is made that the copper ion vacancies in the lattice do not interact with each other. If, however, the density of copper ion vacancies is large enough for this to happen, one might expect a decrease in the activation energy.[9] In the preceding discussion it has been assumed that the mean free path is either constant or is a slowly varying function of the temperature and impurity content. This should be true at the higher temperatures, since the theory assumes that the mean free path is determined by the interaction of electrons with lattice vibrations.

In any case, a measurement of the Hall coefficient in conjunction with conductivity measurements allows one to determine both the

[7] C. Wagner, Trans. Faraday Soc. **34**, 851 (1938).

[8] F. Seitz, *Modern Theory of Solids* (McGraw-Hill, New York, 1940), p. 190.

[9] P. H. Miller, Jr., Phys. Rev. **60**, 890 (1941).

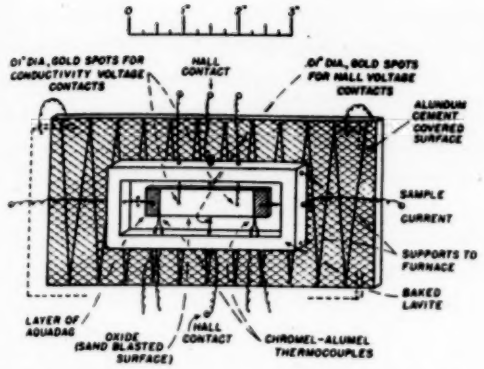

FIG. 1. Schematic diagram of furnace, specimen holder, and specimen in position for measurements.

number of carriers and the mobility independently. The Hall coefficient R is given by the relation $R=-3\pi/8nec$ and the product of the Hall constant and the conductivity gives the mobility

$$\mu=-8R\sigma/3\pi c.$$

If one compares the simple theory with the results of the investigations on cuprous oxide the following conclusions are reached: At high temperatures the conductivity can be expressed rather well by an equation of the form

$$\sigma=\sigma_0 \exp(-U/kT),$$

where U is apparently the same for all samples. Therefore, Jusé and Kourtschatow[4] conclude that this high temperature conductivity is intrinsic. On the other hand, the results of Dünwald and Wagner[5] indicate that the conductivity depends upon the excess oxygen concentration. Furthermore, the work of Waibel and Schottky[6] on the Hall effect at high temperatures indicates that the number of current carriers is not a simple exponential function of the temperature, and that the mobility is a very rapidly varying function of the temperature.

EXPERIMENTAL PROCEDURE

The specimen holder as shown in Fig. 1 is a lavite block which is milled to accommodate the specimen. The Hall and conductivity contacts, as indicated, are made of Nichrome wire which offers the advantage of being able to retain its spring at the higher temperatures. Enclosing the specimen holder is a rectangular transite furnace in which are embedded Nichrome heating elements. These are covered with a mixture of Alundum cement and sodium silicate. Narrow strips of transite separate the two furnace walls and the entire unit is clamped together with screws.

The furnace and holder are mounted between the pole faces of an electromagnet which is made of two cylinders of Armco iron. With 12 amperes through the windings and an air gap of $\frac{3}{4}''$ the field is 7150 gauss at room temperature, as calibrated with a bismuth spiral. All electrical measurements are made with a Leeds and Northrup type K potentiometer. The temperature of the furnace was controlled manually, and temperature measurements of the specimen were made with two Chromel-Alumel thermocouples placed at opposite ends of the sample.

The cuprous oxide was prepared from strips of Chilean copper, $2\frac{1}{4}''\times\frac{1}{2}''\times\frac{1}{16}''$ which were suspended in a furnace at 1000°C for 16 hours.[10] This time was sufficient to effect a complete oxidation of the specimen. After oxidation the sample was placed in an annealing furnace for two hours at a predetermined temperature and then quenched in cold tap water.

Gold contacts, about 0.01" in diameter, evaporated on the specimen, were used for most measurements although it was observed that aluminum gold combinations responded as well. A schematic diagram of the specimen is given in Fig. 1 which also indicates the position of the probes for measurements.

For the Hall measurements two B batteries were used to supply the sample current. It was found advisable to keep the current below one milliampere while fresh samples were being used, since the use of larger currents caused aging,[2] or a decrease in the number of carriers. The e.m.f.'s which are determined initially with the potentiometer must be corrected for the contribution due to electrode misalignment and temperature gradients. Both of these effects are eliminated by taking two readings, one with the magnetic field in a fixed direction, and the other with the field reversed. From the theory of the

[10] The samples of cuprous oxide were kindly furnished by Mr. C. C. Hein of the Westinghouse Research Laboratories, East Pittsburgh, Pennsylvania. A typical analysis of the copper and also the processing technique are given in reference 2.

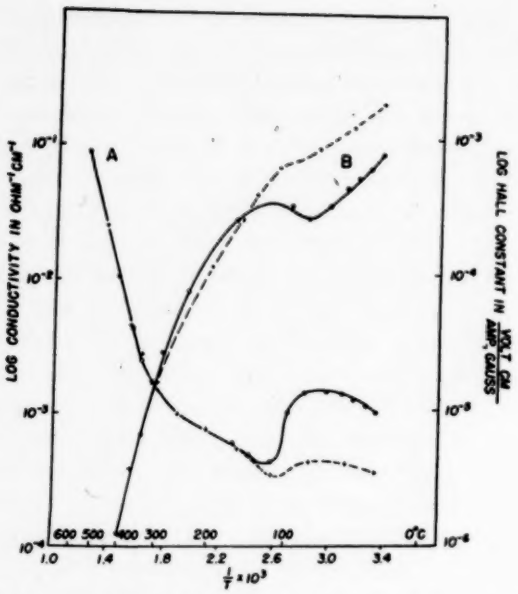

FIG. 2. Conductivity (curve *A*) and Hall constant (curve *B*) as a function of temperature for a fresh sample of CuO_2 quenched from 450°C.

Hall effect the Hall coefficient is given by the equation

$$R = E_H d / IH,$$

where d is the thickness of the specimen, H is the magnetic field in gauss, and I is the specimen current in amperes.

Immediately following the Hall measurements point-probe conductivity determinations are made. The method consists of measuring the potential drop across a fixed portion of the specimen while a known current is flowing in the specimen. The advantage of the technique is that no current is drawn by the probes. The potential drop measured across the probes must be corrected for the contribution due to the thermal e.m.f. Around 100°C the latter represents about a 2 percent correction, and continues to increase till at 900°C the thermal e.m.f. becomes comparable with the true potential drop across the probes. This, of course, depends upon the current flowing through the specimen. For currents of 10 milliamperes the correction at the higher temperatures is about 8 percent, while for one milliampere it approaches 20 percent.

RESULTS AND INTERPRETATION

In Fig. 2 are shown two curves (*A*) giving the variation with temperature of the logarithm of the specific conductivity for a specimen of cuprous oxide quenched from 450°C. The upper curve was obtained with rising temperature and the lower curve with decreasing temperature. The various points were taken at time intervals of twenty minutes. It may be noted that on the lower curve corresponding values of the conductivity at a given temperature have decreased considerably. This is indicative of a definite aging process in which an appreciable number of the current carriers is depleted. Attempts were made to obtain a reversible curve for a fresh sample by making the measurements rapidly. However, the rapidity with which aging set in above 60°C made this impossible. Also, the temperature to which the sample was raised during the run, and the speed of cooling may have influenced the amount of absorbed oxygen and removed all significance from the results.

In curves (*B*) of Fig. 2 are given the Hall constant curves for the same specimen. These curves bear a one to one correspondence relative to the conductivity curves. The regions at which the conductivity shows a hump are those at which the Hall coefficient has a plateau, and the regions at which the conductivity rises rapidly the Hall coefficient decreases rapidly. It might be remarked that the curves of Fig. 2 are representative of the initial behavior of specimens that were quenched from different temperatures. The only distinction is in the magnitude of the Hall constant and the specific conductivity. Since the Hall constant decreases and the conductivity increases with an increase in the number of carriers, we should expect that at a given temperature the latter will be large if the former is small, and vice versa.

In Fig. 3 (curve *A*) are given the conductivity curves for a well-aged specimen run in air. The specimen had previously been quenched from 250°C. The curves exhibit the same sort of characteristics as those in Fig. 2; however, we shall consider them in more detail. At the higher temperatures the conductivity increases in a manner described by a Boltzmann relationship, but below 300°C a marked deviation occurs. Part of the deviation can be explained by assuming that true equilibrium is not attained at the lower temperatures, that is, that oxygen is

frozen in the lattice. It was possible to quench a given sample with a blast of cold air from a given temperature to room temperature and obtain conductivities which varied by a factor of 20. The higher the quench temperature the higher was the room temperature conductivity. This feature accounts for the many branches in the low-temperature region of the curve. These differences in the conductivity disappear around 300°C for above this temperature all curves follow the same pattern. Presumably, the rate of diffusion of oxygen is sufficiently large in the neighborhood of 300°C to bring about equilibrium in the time allotted between measurements. The slope of the curves in the high temperature region turns out to be 0.78 ev and remains the same for all specimens regardless of past history. This slope agrees quite well with that obtained by Jusé and Kourtschatow[4] who found an activation energy for the high temperature part of their curves of 0.72 ev.

An experiment similar to that of Dünwald and Wagner[5] was performed in order to test for the pressure dependence of the resistance of cuprous oxide. A small slab of cuprous oxide was placed between two platinum contacts which were forced together by a spring, and the specimen was then placed in a furnace at 850°C. Resistance measurements were made for various oxygen pressures, and the resistance was found to vary markedly in the range of 10^{-2} to 150 mm oxygen pressure. In Fig. 4 is shown the variation of the logarithm of the resistance with the logarithm of the oxygen pressure for two specimens. The results of several samples give slopes ranging from 1/6.8 to 1/7.2 which agree quite well with Wagner's value of 1/7. However, the departure from a 1/8 law as evidenced in all specimens appears to be a real property of cuprous oxide. Wagner suggests that an incomplete dissociation of the ions and electrons might be the cause of the disagreement.

Figure 3 (curves B) show the variation of the Hall constant with temperature for a well-aged sample. The surprising result obtained from these curves is that n, the number of carriers, cannot be represented by the relation

$$n = n_0 \exp(-\epsilon/kT),$$

where n_0 and ϵ are constant. Data taken from the curves show that ϵ varies from about 1.0 ev at 450°C to about 0.1 ev at room temperature. This agrees qualitatively with the Hall effect data of Waibel and Schottky;[6] however, no evidence was found for a change in sign of the Hall coefficient.

Figure 5 shows the behavior of the mobility as a function of temperature. Again, qualitative agreement is obtained with the data of Waibel and Schottky. The mobility varies approximately as T^{-5} from room temperature to 150°C, and it varies approximately as T^{-7} from 150°C to 450°C. This means that the conductivity, alone, cannot give accurate information concerning the variation of the number of carriers with temperature. Furthermore, it seems difficult to explain this rapid variation of the mobility by assuming that the electrons are scattered only by lattice vibrations. One wonders whether some scattering or trapping process involving the number of impurity centers is not responsible for the observed behavior. It is difficult to reach any definite conclusions at present because little is known about the interaction of slow electrons with lattice vibrations.

In conclusion the results may be summarized as follows:

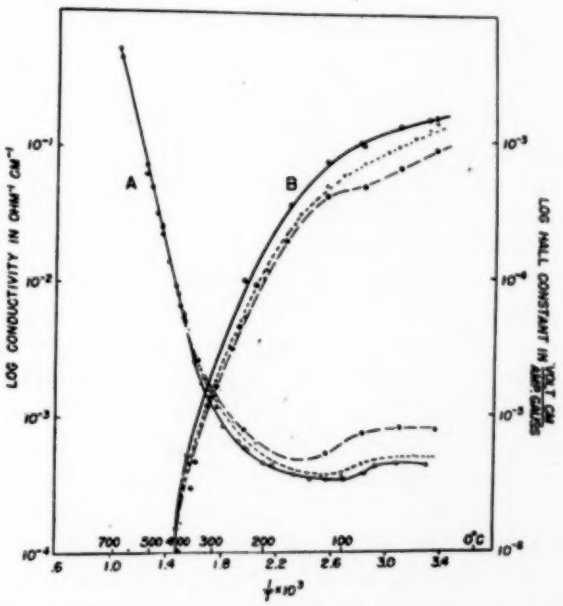

FIG. 3. Conductivity (curves A) and variation of the Hall constant (curves B) of a well-aged sample of cuprous oxide as a function of temperature. The slope of the curve A at the higher temperatures is 0.78 ev.

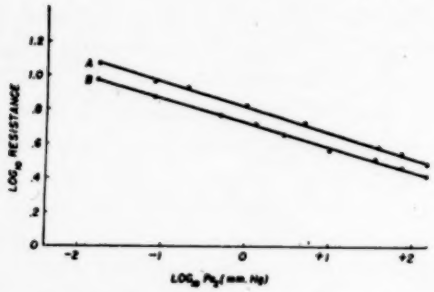

FIG. 4. Resistance as a function of oxygen pressure for two specimens of cuprous oxide measured at 850°C. Slope of curve A is 1/6.8; curve B, 1/7.1.

(1) There is no evidence that an intrinsic conductivity exists in cuprous oxide.

(2) There is no evidence for a change in sign of the Hall coefficient.

(3) The simple theory of semi-conduction needs considerable extension before it can fully explain the data. However, the following general interpretation is suggested. At low temperatures a frozen equilibrium exists in cuprous oxide, and the number of absorbed oxygen atoms is independent of the temperature. The extremely low activation energy observed in this range of temperature is to be associated with the formation of clusters of centers, in the sense suggested by Miller[9] for the case of zinc oxide. The maxima and minima of the conductivity curves observed in the low temperature region result from a combination of a saturation of the clusters and the rapid decrease of the mobility with temperature. Above 300°C an equilibrium exists between the absorbed oxygen and the external oxygen gas. As a result, the number of oxygen atoms absorbed and the fraction of holes ionized depend exponentially upon the temperature. Apparently, we must believe that one or both of the activation energies, E and W (E is the energy to free an electron hole and W is the energy to place an oxygen atom in the lattice as an ion and produce two copper ion vacancies), are functions of the temperature, or the concentration of absorbed oxygen.

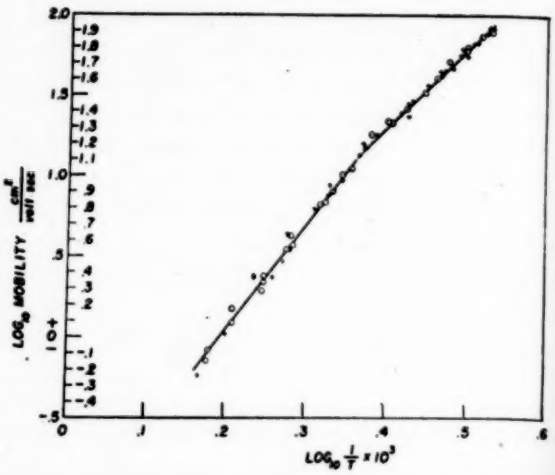

FIG. 5. Mobility as a function of temperature for a well-aged specimen of cuprous oxide. The data are taken from Fig. 3. The low temperature part of the curve shows a T^{-4} dependence, and changes to a T^{-7} dependence beyond 150°C.

Finally, the author wishes to express his sincere appreciation to Professor F. Seitz for his helpful advice and criticism, and to Drs. A. W. Lawson, R. J. Maurer, and S. Pasternack for many stimulating discussions on the interpretation of the data.

The Effect of High Electrostatic Fields on the Conductivity of Tungsten

PETER LOUISA VISSAT
University of Pittsburgh, Pittsburgh, Pennsylvania
(Received June 15, 1942)

A grounded tungsten wire (0.0078-mm diameter) was mounted coaxially with a cylinder which was made negative relative to the wire, and a difference of potential was applied between the cylinder and the wire. The procedure consisted of measuring the resistance of the tungsten wire first without an electric field and then with a field. With a vacuum of about 10^{-6} mm Hg and with fields of about 10^{6} v/cm, measurements showed that: (1) An increase in resistance always resulted with the application of the field; (2) the change was different for different temperatures of the filament and for different vacuum conditions; (3) no measurable change occurred unless the field exceeded a certain value; (4) a small leakage or ionization current was associated with the changes in resistance. The observed changes might have been caused by: (1) leakage current, (2) ionization current, (3) radial stress in the wire resulting from the high field, or (4) other reasons. Calculations showed that reasons (1) and (3) produce changes much smaller than those observed and that the results are explainable wholly by reason (2) if it is assumed that most of the ionization occurs near the surface of the wire.

I. INTRODUCTION

PERKINS[1] in 1921 and again in 1925[2] observed that gold and bismuth exhibited an increase in resistance in the presence of an electrostatic field. M. Pierucci,[3] M. Perucca,[4] and R. Deaglio[5] have observed changes in resistance of thin, metallic films deposited on quartz or glass upon application of a field. Their results indicate that there is a decrease in resistance upon applying a field. In work on the effect of high electrostatic fields upon the vaporization rate of metals A. G. Worthing[6] and G. B. Estabrook[7] observed changes in resistance upon applying high fields. Worthing observed that there was a sudden decrease in the resistance of a tungsten wire upon applying a field and a sudden increase upon removing the field. Estabrook also observed this effect for the case of platinum and molybdenum, but the effect was opposite to that found by Worthing.

The present research was undertaken to obtain quantitative results on the effect of high electrostatic fields on the electrical resistance of small tungsten wires.

[1] H. A. Perkins, Phys. Rev. **18**, 131 (1921).
[2] H. A. Perkins, Phys. Rev. **25**, 584 (1925).
[3] M. Pierucci, Nuevo Cimento **9**, 33–42 (1932).
[4] M. Perucca, Comptes rendus **198**, 456 (1934).
[5] R. Deaglio, Nuevo Cimento **11**, 288 (1934).
[6] A. G. Worthing, Phys. Rev. **17**, 418 (1921).
[7] G. B. Estabrook, Ph.D. Thesis, University of Pittsburgh (1932).

II. APPARATUS

The tungsten[8] used was in the form of a wire 0.00078 cm in diameter. This value measured by a microscope checked well with that obtained with the value 0.18 mg per 200-mm length furnished by the manufacturer. Figure 1 shows a cross-sectional view of the apparatus used. Approximately a 10-cm length of this wire was mounted coaxially with respect to a cylinder. The two springs S made of 5-mil Kovar were used to keep the wire under slight tension. To facilitate centering, holes (0.29-mm diameter) were drilled along two diameters approximately at right angles to each other at the ends and also at the center of the cylinder. The wire was centered by means of the adjusting screws A at each end. The rings N, holding the adjusting screws, were grounded and served as guard rings. The ends of springs S were threaded through short glass capillaries encased in the plates at each end, and the tungsten wire was soldered onto the ends of the Kovar springs. Although solder does not adhere to tungsten, it made a good mechanical and electrical joint as long as the filament was not heated to a very high temperature. The cylinder and the rings were supported by glass rods and the entire assembly introduced into a glass tube connected

[8] Furnished by the General Electric Company, Lamp Development Division, Nela Park, Cleveland, Ohio.

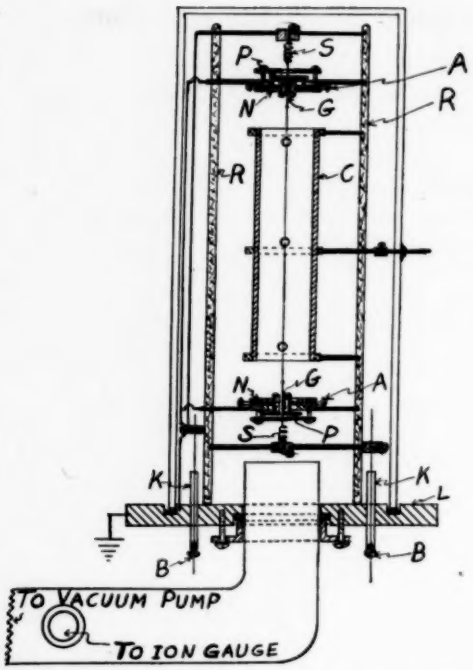

FIG. 1. Cross-sectional view of apparatus. *A*, adjusting screws; *B*, glass beads; *C*, cylinder; *G*, glass capillary; *K*, Kovar tubes; *N*, guard rings; *P*, adjustment plate; *R*, glass rods; *S*, springs; *L*, brass plate ($\frac{1}{3}$ normal size).

to a mercury diffusion pump.[9] For ease in replacing filaments, the glass tube rested on a rubber gasket in a groove of the brass plate *L*. The electrical connections were brought to the outside through two Kovar tubes *K* soldered onto the brass plate. The ends of the tubes were sealed with glass beads *B* which made vacuum seals and insulated the wires from the plate. A No. 46 radio tube served as an ion pressure gauge. A Kohlrausch bridge was used for measuring resistances. Changes in resistance were measured by the galvanometer deflection from the balanced position, galvanometer deflections being previously calibrated in terms of resistance changes. All lead wires and instruments were shielded and grounded. The galvanometer of the Kohlrausch bridge circuit was introduced into the ground circuit in order to detect and measure any "leakage" current.

High voltages for obtaining the fields between the cylinder and wire were produced by an x-ray transformer and a Kenotron KR-3 rectifier. The negative side of the line was connected to the cylinder in the tube and the positive side was grounded at the transformer. The tungsten wire was also grounded.

[9] Built by R. Nestler at the Bartol Foundation.

III. PROCEDURE AND RESULTS

The tungsten wire was well centered along the axis of the cylinder, and the entire assembly (see Fig. 1) was then inserted in the tube connected to the vacuum pump. The tube was outgassed by heating it locally with a gas flame, and all measurements were taken with a vacuum of about 10^{-6} mm Hg. Previous to making measurements with the wire in the electrostatic field, the variation of resistance with current through the wire was measured with increasing and decreasing currents (Fig. 2). This was necessary in order to calculate changes in resistance resulting from a change in current in the circuit in which only the resistance of the tungsten wire would vary as occurred in the course of measurement. The relation is practically linear. Measurements were made after the filament had been heated for about 10 minutes at the highest temperature always below incandescence. The wire was not "well aged;" nevertheless, it behaved in a reproducible and consistent manner. Throughout, the current was measured to the nearest 0.0001 ma by means of a carefully adjusted potentiometer. The temperature of the wire was calculated from a temperature-resistivity calibration.

The deflections of the galvanometer in the Kohlrausch bridge from a balanced position were calibrated in terms of changes in resistance. For the most sensitive conditions, a deflection

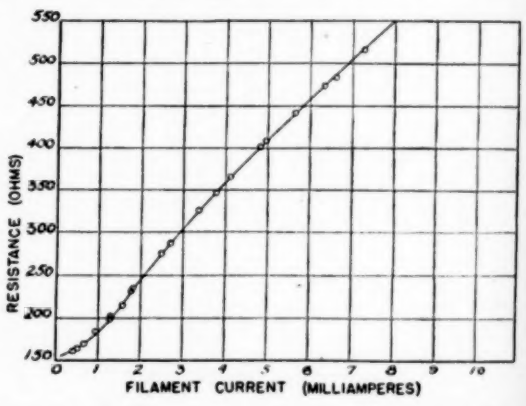

FIG. 2. Variation of resistance with current for an unaged tungsten filament. Diameter 0.00078 cm, length 10.38 cm.

of one division represented a change in resistance of 0.0015 ohm in 500 ohms. A deflection of 0.1 division could be estimated so that it was possible to detect a change of 3 parts in 10,000,000.

The negative side of the high voltage source was then connected to the cylinder, and the tungsten wire was grounded at the galvanometer connection of the bridge. Because of the smallness of the wire, a relatively small difference of potential gave rise to a high field strength at the surface of the wire. For example, a difference in potential of 10,000 volts between the wire and cylinder gave rise to a surface field strength of 3.35×10^6 v/cm. Measurements of changes in resistance with applied fields were made on numerous tungsten wires. The results for one particular wire are shown in Fig. 3. It shows that there was always an increase in resistance with the application of an electric field provided the field exceeded a certain value below which no change could be detected. The magnitude of the change for a particular field strength depended on the temperature of the filament and upon vacuum conditions. The results on the other tungsten filaments were similar. The maximum observed changes are shown in Table I.

No change of resistance was observed until a surface field strength of 0.75×10^6 v/cm was reached for the filament at 20°C and the value at which any change was observed increased as the temperature of the filament increased. The field strengths at which a change was first observed for the various temperatures and vacuum conditions are shown in Table II.

When the galvanometer of the bridge was moved to the ground circuit, it measured any

TABLE I. Maximum observed change in resistance of tungsten wire at various temperatures with field strength at surface of wire.

Temp. of wire °C	Max. observed change, ohms	Percent change	Field strengths 10^6 v/cm
	Vacuum 3×10^{-6} mm Hg		
20	13.8	8.8	2.90
280	2.3	0.71	3.97
580	0.37	0.072	4.77
	Vacuum 8×10^{-7} mm Hg		
20	13.5	8.7	3.18
280	2.5	0.77	4.77
580	0.34	0.066	5.31

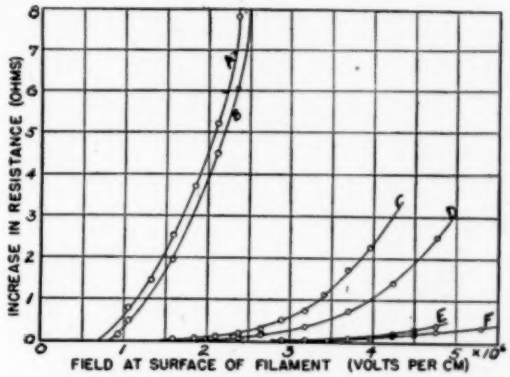

FIG. 3. Change in resistance with applied field of unaged tungsten. Curves A, C, E for pressure 3×10^{-6} mm Hg. Curves B, D, F for pressure 8×10^{-7} mm Hg. Curves A and B—$R=157.3$ ohms, $T=20$°C. Curves C and D—$R=323.9$ ohms, $T=280$°C. Curves E and F—$R=514.7$ ohms, $T=580$°C.

leakage current passing to ground. The measured results are shown in Fig. 4. The maximum deflection was never more than 2 divisions at 100 cm and represented a current of approximately 3×10^{-8} amp. The deflection appeared immediately as soon as the field was applied. As Fig. 4 shows, the current varied with the temperature of the filament and also with the vacuum much in the same way as did the changes in resistance. If the field was kept constant and the temperature was changed from one value to another, there was a change in the leakage current. There was an increase if the change was one from a high temperature to one of a low temperature, and a decrease if the reverse change was made, the increase and decrease always being the same. Also the final leakage current was the same as that found by suddenly applying the field. However, when the temperature of the wire was changed suddenly from a low temperature to a high, there was a sudden decrease in leakage current, but when the temperature was changed from a high to a low value, the current increased very slowly, possibly in consequence of the very slow adjustment to a new temperature equilibrium.

IV. DISCUSSION

Measurements with high electrostatic fields at the surface of the tungsten wire showed that the wire exhibited increases in resistance with applied fields. The magnitude of the changes

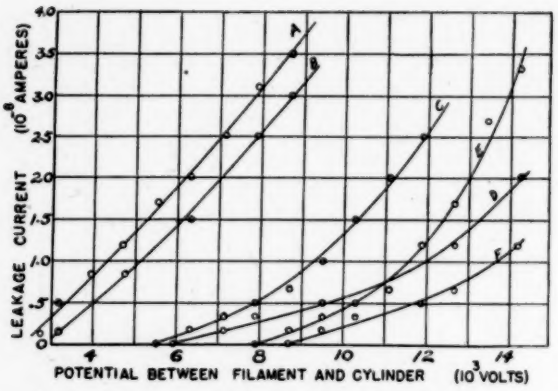

FIG. 4. Variation of leakage current with potential. Curve designations same as for Fig. 3.

depended on the temperature of the wire and on the vacuum conditions. Associated with these changes was a leakage current which varied with the temperature of the wire and vacuum conditions much in the same manner as did the changes in resistance.

The changes in resistance that resulted with the application of high fields might have been due to several reasons:

1. Leakage current passing through the filament, thus heating it and increasing its resistance.
2. Ionization current in the space between the wire and the cylinder passing to the filament, thus heating it and increasing the resistance.
3. Radial stress in the wire resulting from the high electrostatic field.
4. Others.

Simple calculations show that changes due to reasons 1 and 3 are much too small to account for the measured changes in resistance. The fact that the leakage current measured varied with the temperature of the wire and with vacuum conditions suggests that it might be an ionization current. That this is possible at pressures of 10^{-6} mm Hg or better is the basis of all ionization pressure gauges.

If an electron is generated in the gas in the cylinder by photons, γ-rays, or cosmic rays, it will move toward the wire and at some appropriate distance will start to ionize by collision. The negative ions formed will move in toward the wire and the positive ions will move outward to the cylinder. It has been shown by Dempster,[10] Loeb,[11] and Druyvesteyn and Penning[12] that positive ions of sufficient energy striking the cylinder would liberate electrons from it. These electrons would then move toward the wire and produce more ions by collision. Regarding electron emission from the cathode by positive ions, Loeb quotes: "Concerning this process much information is at hand, though none is satisfactory owing to the impossibility of producing or studying reproducible surfaces."[13] A steady current will occur (neglecting ionization by outside sources) when the total number of positive ions produced by a primary electron will eject one electron from the cylinder. The number of extra electrons liberated from the cathode per ion formed between the electrodes is not known for different electrodes[14] at such high ratios of field strength to pressure as used in the course of these measurements, so that a quantitative discussion of this is not possible here. A complete and detailed discussion of what occurs between concentric cylinders at low pressures and high field strengths is complicated by impurities and general conditions in the tube.[15] Quoting from Loeb: "In tubes at very low pressures, 0.01 mm, the character of the gas becomes somewhat doubtful, for adsorbed gases coming from the walls and electrodes, whose nature is unknown, begin to play an important role. Below 10^{-5} mm the gas present is completely indeterminate."[16]

An ionization current would therefore consist of a migration of electrons or negative ions toward the wire and positive ions toward the cylinder. The energy of the electrons in passing through a potential difference in the cylinder

TABLE II. Field strengths at surface of tungsten wire at which a change in resistance was first observed.

Temp. °C	Field strength 10^6 v/cm (Vac. 3×10^{-6} mm Hg)	(Vac. 8×10^{-7} mm Hg)
20	0.75	0.80
280	1.3	1.7
580	2.5	3.3

[10] A. J. Dempster, Phys. Rev. **46**, 728 (1934).

[11] Leonard B. Loeb, *Fundamental Processes of Electrical Discharges in Gases* (John Wiley and Sons, New York, 1939), pp. 377, 480.

[12] M. J. Druyvesteyn and E. M. Penning, Rev. Mod. Phys. **12**, 98, 107 ff. (1940).

[13] Leonard B. Loeb, reference 11, p. 378.

[14] M. J. Druyvesteyn and F. M. Penning, reference 12, p. 106 ff.

[15] Leonard B. Loeb, reference 11, p. 451.

[16] Leonard B. Loeb, reference 11, p. 480.

would be transferred to the wire, heating it and therefore increasing its resistance. To calculate what changes in resistance such assumed ionization current would produce, Fig. 5 was drawn showing the variation of resistance of the wire with power (I^2R) input. The slope of this curve was taken at the experimental values of resistance. The product of this slope and a power determined as dissipated because of ionization currents and transferred to the filament would give the expected change of resistance for the filament on the application of the high electrostatic field. Since the ionization current consists of a stream of negative ions in one direction and an equal number of positive ions in the opposite direction, depending on their place of origin, one might expect something on the order of one-half of the calculated ionization power to be transferred to the wire. The changes that would result if exactly half of the power were transferred to the wire are shown as ΔR_p in Tables III and IV.

TABLE III. Comparison of measured changes in resistance with computed changes assumed to be due to ionization power. Vacuum 3×10^{-6} mm Hg.

R_s ohms	Temp. °C	E 10^6 v/cm	ΔR_s ohms	ΔR_p ohms	$\frac{\Delta R_p}{\Delta R_s}$
514.7	580	2.9	0.0068	0.043	6.3
		3.18	0.013	0.090	6.9
		3.44	0.026	0.15	5.8
		3.71	0.069	0.22	3.7
		3.97	0.14	0.41	2.9
		4.24	0.18	0.63	3.5
		4.50	0.28	1.05	3.7
		4.77	0.37	1.37	3.7
323.9	280	1.59	0.024	0	0
		1.85	0.045	0	0
		2.12	0.10	0.11	1.1
		2.38	0.17	0.23	1.4
		2.65	0.29	0.39	1.3
		2.91	0.48	0.57	1.2
		3.18	0.72	0.93	1.3
		3.44	1.11	1.51	1.4
		3.71	1.71	2.18	1.3
		3.97	2.26	2.92	1.3
157.3	20	0.93	0.13	0.56	4.3
		1.06	0.76	1.9	2.5
		1.33	1.44	4.0	2.8
		1.59	2.51	6.8	2.7
		1.85	3.7	11.3	3.0
		2.12	5.2	15.2	2.9
		2.38	7.8	21.5	2.8
		2.65	10.8	30.5	2.8
		2.91	13.8	36.6	2.7

R_s = Resistance of wire; E = Field strength at surface of wire; ΔR_s = Measured change in resistance due to field; ΔR_p = Calculated change in resistance from ionization power; $(\Delta R_p/\Delta R_s)$ = Ratio of measured change to calculated change in resistance.

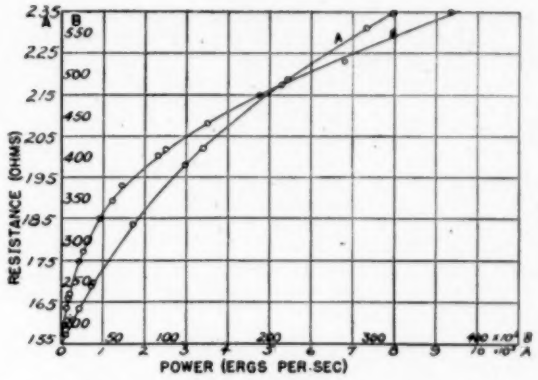

FIG. 5. Variation with power input of resistance of an unaged tungsten filament. Diameter—0.00078 cm, length—10.38 cm.

Comparing the calculated with the observed changes in resistance, it is seen that the computed effects for the observed ionization currents account for more than the observed changes in resistance. The ratios of the calculated changes to the observed are shown also in Tables III and IV.

The ratios of calculated changes to the observed changes for a particular temperature of the filament remain practically constant at different field strengths. The ratios, however, are different for different temperatures of the filament. These results are compatible if the assumption is made that there exists a region of greater density of gas molecules near the surface of the wire than anywhere else inside the cylinder and that the density of the gas near the surface of the wire is decreased when the temperature of the filament is increased. This could well be in the form of adsorbed gas on the surface of the tungsten. This assumption is reasonable because of the high field strength and the large gradient of the radial field existing there. Because of this greater density near the surface of the wire, a large part of the ionization by collision is assumed to occur in this region. Hence, the electrons or negative ions would not pass through the potential difference applied, but would pass through a smaller potential difference, and the energy transferred to the wire per second would be smaller.

By taking the requisite potential difference to give the measured changes in resistance, the distance from the surface of the wire giving this

TABLE IV. Comparison of measured changes in resistance with computed changes assumed to be due to ionization power. Vacuum 8×10^{-7} mm Hg.

R_s ohms	Temp. °C	E 10^6 v/cm	ΔR_s ohms	ΔR_p ohms	$\frac{\Delta R_p}{\Delta R_s}$
513.4	580	3.18	0.011	0.046	4.2
		3.44	0.034	0.10	2.9
		3.97	0.093	0.17	1.8
		4.24	0.130	0.25	1.9
		4.50	0.162	0.26	1.6
		4.77	0.246	0.49	2.0
		5.31	0.339	0.69	2.0
322.6	280	1.99	0.018	0	0
		2.38	0.067	0.12	1.8
		2.65	0.14	0.26	1.9
		3.18	0.35	0.47	1.3
		3.71	0.71	0.73	1.0
		4.24	1.40	1.5	1.1
		4.77	2.50	2.8	1.1
156.1	20	0.93	0.14	0	0
		1.06	0.47	0.4	1.4
		1.59	1.94	4.8	2.5
		2.12	4.48	11.4	2.6
		2.65	9.13	23.7	2.6
		2.91	13.5	31.2	2.3

R_s = Resistance of wire; E = Field strength at surface of wire; ΔR_s = Measured change in resistance due to field; ΔR_p = Calculated change in resistance from ionization power; $(\Delta R_p/\Delta R_s)$ = Ratio of measured change to calculated change in resistance.

potential difference can now be calculated. The potential at a distance r from a grounded cylinder of radius a having a charge q per unit length inside another cylinder of radius b is given by the relation

$$V_r = -2q \ln (r/a). \tag{1}$$

If the potential is to be a fraction of the applied potential, say ${}_fV_b$, then

$$\frac{V_b}{{}_fV_b} = \frac{-2q \ln (b/a)}{-2q \ln (r/a)} = \frac{1}{f} = \frac{\ln (b/a)}{\ln (r/a)}, \tag{2}$$

from which is obtained

$$r = a(b/a)^f. \tag{3}$$

Substituting the values for a and b one obtains

$$r = 0.0039 \text{ mm} \left(\frac{8.2}{0.0039}\right)^f.$$

The average value for f when the wire was at 20°C, pressure 3×10^{-6} mm Hg, is (1/2.8) and leads to 0.06 mm for the value of r. This distance is 7.3×10^{-3} of the radius of the cylinder or a distance 15 times as great as the radius of the wire. This value of r would indicate that most of the ionization occurs in a volume of 1.1×10^{-2} mm³ per unit length of the wire or 5.4×10^{-5} of the total volume. The value of r when the filament was operated at 280°C, vacuum 3×10^{-6} mm Hg, was 1.4 mm or 0.17 of the radius of the cylinder. The ionization occurred inside a volume 6.2 mm³ per unit length of wire, or 0.029 of the total volume. This value for r at 280°C was larger than the value at 20°C. This is in agreement with the assumption made, namely, that as the temperature of the filament is increased, the density of the molecular cloud around the filament decreases. The ionization would be expected to occur, therefore, at the higher temperature throughout a larger volume and to be smaller for a given voltage applied between wire and cylinder. The value for r at 580°C should be larger than at 280°C, and the ionization should be less for any given voltage applied. However, the ionization current at the highest temperature was found, as expected, to be smaller than at the lower temperatures, but the value of r, contrary to expectations, was smaller than the value for r at 280°C. To check with what was expected, the leakage current should have been very much smaller. A larger ionization current than expected might have resulted from several reasons: (1) The filament might have liberated adsorbed gases at the higher temperature; (2) A noticeably greater part of the ionization current at the high temperatures was leakage surface current because of the higher voltages at which the data for the high temperatures were taken (see Fig. 3 and Tables III and IV).

The values of r calculated for various conditions are shown in Table V. As has been mentioned, the results depend considerably on the impurities present and the nature of the cathode surfaces.

TABLE V. Values of radii inside which most of the ionization occurs.

R_s ohms	Temp. °C	r mm	r mm
		(Press. 3×10^{-6} mm Hg)	(Press. 8×10^{-7} mm Hg)
514	580	0.04	0.22
323	280	1.4	2.3
156	20	0.06	0.08

There are reasons to suspect[17] that the ionization may not occur in such large volumes as indicated in Table V. The results can be explained then if it is assumed that only a fraction of the measured ionization current passes through the potential difference applied between cylinder and filament. The mechanism can be viewed in this fashion. It is assumed that there exists adsorbed gases and/or adsorbed tungsten oxide at the surface of the tungsten filament. Suppose that by some means or other an electron is liberated at the inner surface of the cylinder, the cathode. The electron will be accelerated towards the filament and will ionize only when it strikes the adsorbed layer. There equal number of electrons and positive ions will be produced; the electrons passing through a very small potential difference to the filament while the positive ions are accelerated towards the cylinder by passing through the entire potential difference. The positive ions arriving at the cylinder will liberate more electrons and the same process repeated again. A steady current will result when the number of positive ions produced by one electron at the anode or filament will produce one electron at the cathode or cylinder.

Let the ratio $\Delta R_x/\Delta R_p$ as previously defined be designated by "f." To account for the measured change in resistance, ΔR_x, the number of electrons passing through the applied potential difference per second would have to be a fraction "f" of the measured number. One electron, then, on the average would produce $(1-f)/f$ positive ions at the filament and $(1-f)/f$ positive ions would in turn produce on the average one electron at the cylinder wall. The number of electrons per positive ion liberated at the cathode is known as an "alternative second Townsend Coefficient."[18] The value for this coefficient is given by the relation

$$\gamma = f/1-f.$$

Using the average values for $1/f=\Delta R_p/\Delta R_x$ found in Tables III and IV we find the values for γ at a pressure of 3×10^{-6} mm Hg to be 0.40, 3.3, and 0.55 for temperatures 580°C, 280°C, and 20°C, respectively, and at a pressure of 8×10^{-6} mm Hg, they are 1.1, 2.5, 0.66 at the same temperatures. These values are averages at a field strength to pressure ratio, E/P, of the order of 10^{12} v/(cm mm Hg). Other experimental values for γ are not available at such high ratios of E/P as used here so that no comparisons can be made here. It must be remembered that these coefficients apply only to the surfaces used for this investigation.

Variations in resistance with applied field might have resulted because of other reasons such as a change in emissivity or a structural change in the wire itself. These changes are entirely possible, but an explanation of the results wholly on these changes would not account for the effects of the ionization currents, and it is seen that these can account for the observed changes. To detect changes due to other assumed reasons, one would have to reduce ionization currents to negligible amounts, and this can be done only in a vacuum of 10^{-9} mm Hg or better.

ACKNOWLEDGMENTS

I wish to express my thanks to Dr. E. Hutchisson and to Dr. C. S. Smith. I am also grateful to Dr. A. G. Worthing for his many helpful suggestions.

[17] W. P. Reid, Phys. Rev. **63**, 359 (1943).

[18] Leonard B. Loeb, reference 11, p. 687.

Letters to the Editor

Equivalent Circuits to Represent the Electromagnetic Field Equations

GABRIEL KRON
General Electric Company, Schenectady, New York

August 21, 1943

IT is known that for certain electromagnetic waves some of the characteristics of the wave propagation may be correctly described in terms of distributed inductances, capacitances, and resistances. This is commonly done, for example, in conventional transmission line analysis. Here it is the integrated effects (voltage and current) that are represented by the circuit and not the fields. For static fields, another example, the field distribution itself may be related to current or voltage distribution in a network of similar circuit elements. The general relation between electromagnetic waves and distributed constant networks has apparently not been investigated. The extent to which such networks may represent characteristics of various waves or indeed space in general as a medium for the propagation of any wave distribution, is apparently not known and is of considerable importance.

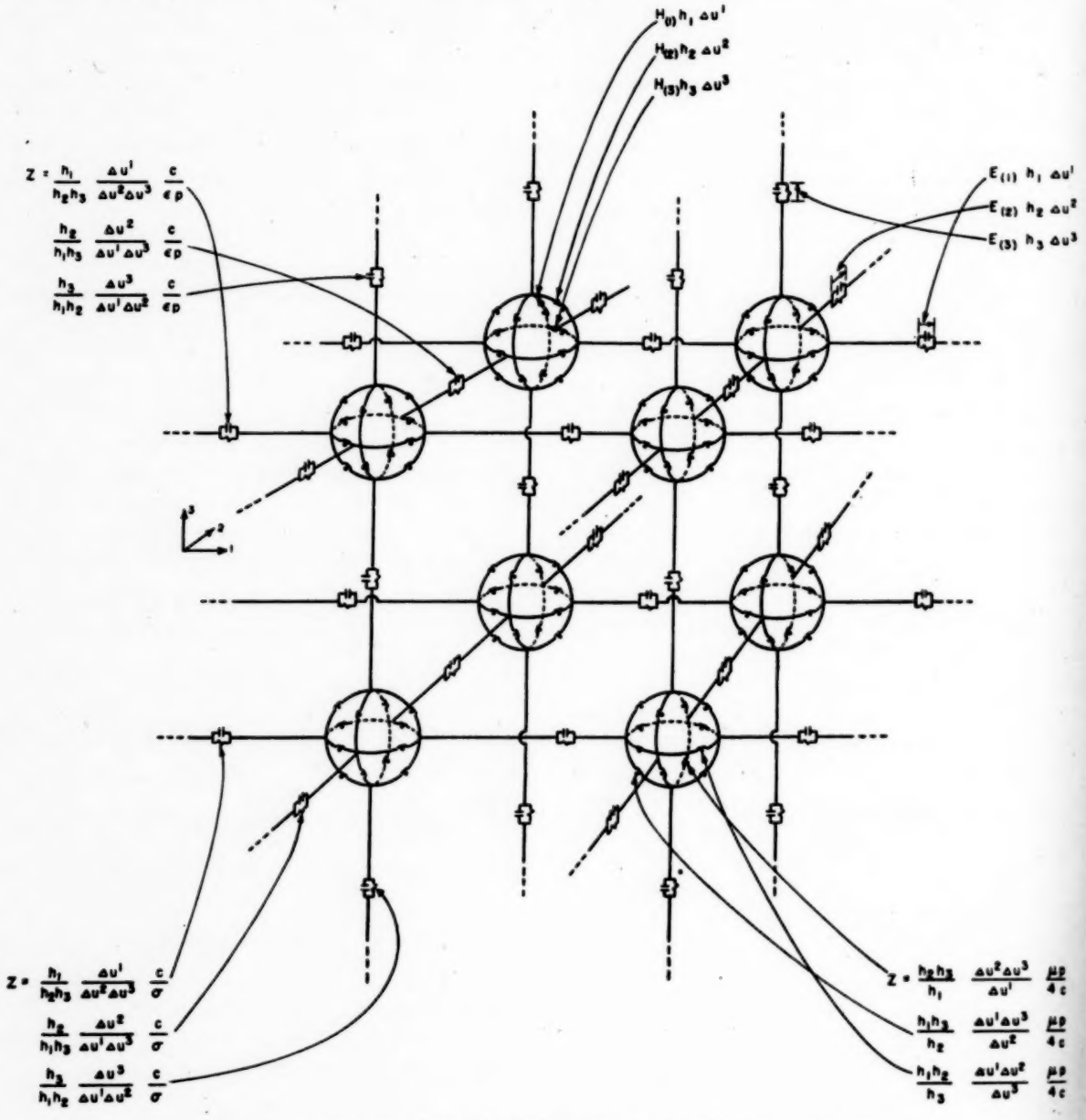
$H_{(1)}h_1\,\Delta u^1$
$H_{(2)}h_2\,\Delta u^2$
$H_{(3)}h_3\,\Delta u^3$
$Z = \frac{h_1}{h_2h_3}\,\frac{\Delta u^1}{\Delta u^2\Delta u^3}\,\frac{c}{\epsilon p}$
$\frac{h_2}{h_1h_3}\,\frac{\Delta u^2}{\Delta u^1\Delta u^3}\,\frac{c}{\epsilon p}$
$\frac{h_3}{h_1h_2}\,\frac{\Delta u^3}{\Delta u^1\Delta u^2}\,\frac{c}{\epsilon p}$
$E_{(1)}\,h_1\,\Delta u^1$
$E_{(2)}\,h_2\,\Delta u^2$
$E_{(3)}\,h_3\,\Delta u^3$
$Z = \frac{h_1}{h_2h_3}\,\frac{\Delta u^1}{\Delta u^2\Delta u^3}\,\frac{c}{\sigma}$
$\frac{h_2}{h_1h_3}\,\frac{\Delta u^2}{\Delta u^1\Delta u^3}\,\frac{c}{\sigma}$
$\frac{h_3}{h_1h_2}\,\frac{\Delta u^3}{\Delta u^1\Delta u^2}\,\frac{c}{\sigma}$
$Z = \frac{h_2h_3}{h_1}\,\frac{\Delta u^2\Delta u^3}{\Delta u^1}\,\frac{\mu p}{4c}$
$\frac{h_1h_3}{h_2}\,\frac{\Delta u^1\Delta u^3}{\Delta u^2}\,\frac{\mu p}{4c}$
$\frac{h_1h_2}{h_3}\,\frac{\Delta u^1\Delta u^2}{\Delta u^3}\,\frac{\mu p}{4c}$

FIG. 1. Transient equivalent circuit of the field equations of Maxwell for charge-free space.

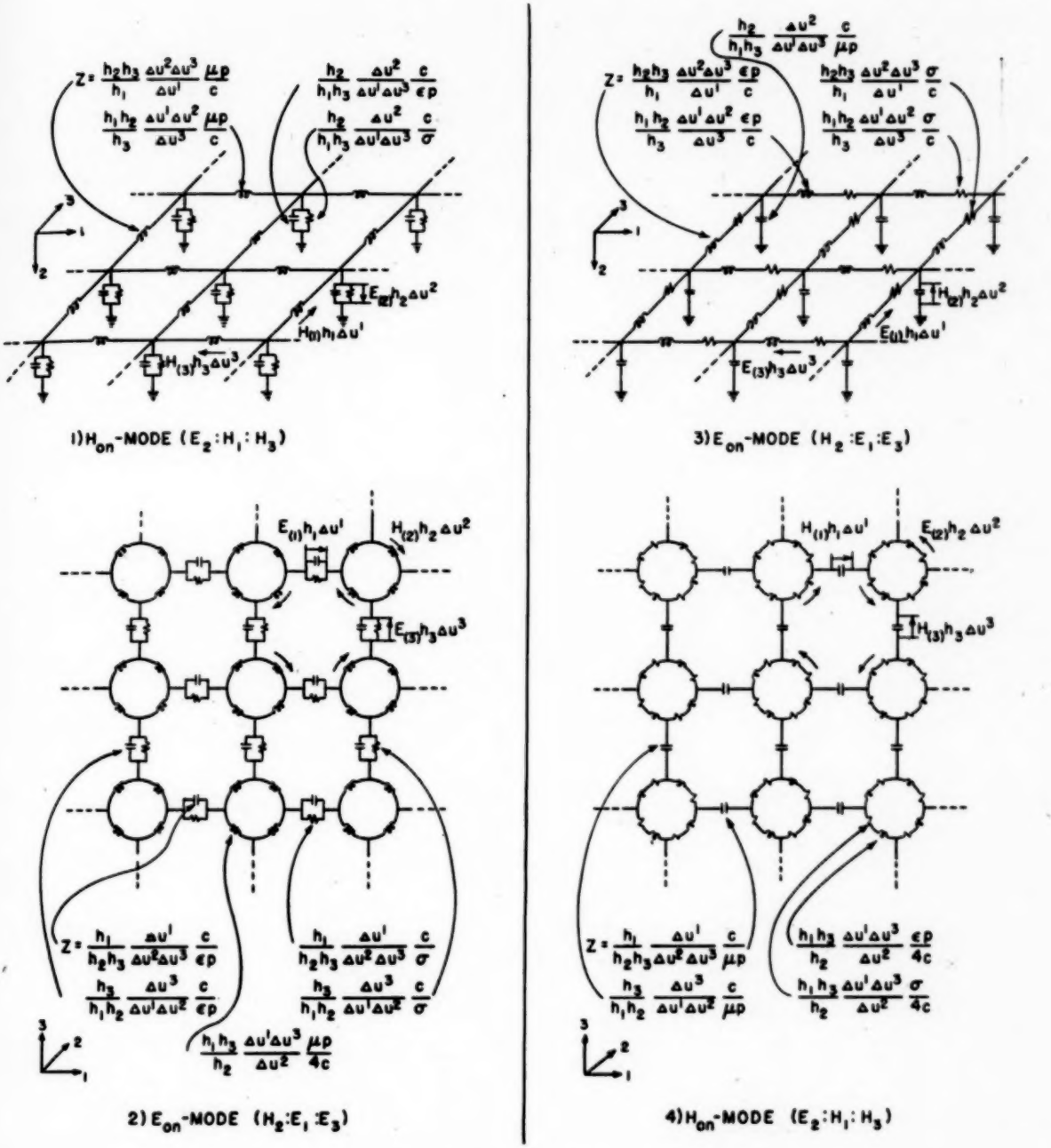

FIG. 2. Two sets of two-dimensional networks.

This has suggested that attempts be made to represent Maxwell's equations directly by equivalent circuits. A network which does this is shown in Fig. 1. In this network, which represents a charge-free space of permeability μ, dielectric constant ϵ, and conductivity σ, the electric and magnetic field components along the three directions 1, 2, 3 of the orthogonal curvilinear coordinates u_1, u_2, u_3, are represented by voltages and currents in impedance elements as indicated. (h_1, h_2, h_3 are the metrical coefficients and $p = \partial/\partial t$.) The values of these elements depend only upon μ, ϵ, σ, and the size of the infinitesimal cube of space being replaced. Thus the network represents space rather than any particular wave mode or frequency; the latter, as in reality, being determined by the boundary conditions.

For two-dimensional cases ($\partial/\partial u_2 = 0$), the three-dimensional network separates into two independent networks lying in one plane (Fig. 2). All networks shown are merely examples. Other equivalent networks have been obtained

which together with the derivations are expected to be the subject of a later paper.

On the Branching Ratio of Na^{22}

HANS WELTIN
University of California, Berkeley, California
August 2, 1943

LASLETT[1] has shown that Na^{22} may be formed by the bombardment of Mg with deuterons.

$$Mg^{24}+D\rightarrow Na^{22}+He^{4}. \quad (1)$$

Na^{22} emits positrons, and on the basis of the Fermi β-decay theory it can also decay by K capture. Lamb[2] has extended the calculations of Yukawa and Sakata to Uhlenbeck-Konopinski coupling. His calculations of the ratios of the number of nuclei excited to the number of positrons emitted are quoted here:

	Fermi	Uhlenbeck-Konopinski
$\Delta i=0$	1.2	4.7
$\Delta i=1$	2.1	30.4

Lamb suggested that the theory might be checked by measuring the amount of He produced in (1) and comparing it with the number of positrons emitted. Alvarez[3] indicated later that the theory might be checked equally well by comparing the amount of Ne with the number of positrons emitted according to

$$Na^{22}\rightarrow Ne^{22}+e^{+}. \quad (2)$$
$$Na^{22}+e^{-}\rightarrow Ne^{22}. \quad (3)$$

The latter method was used to obtain this ratio. A procedure for micro-gas analysis very similar to that developed by Paneth and Peters[4] made it possible to observe the pure Ne spectrum in a fine capillary and then to measure the gas. The number of positrons emitted was determined by comparing a known fraction of the total sample with a Segrè standard of uranium oxide, U_3O_8, by means of Geiger point counter and scale of 64. The average amount of Ne measured for a decay period of 58 days was found to be 3.8×10^{-6} cm³ N.P.T. The amount of Ne calculated from the number of positrons emitted was 1.2×10^{-6} cm³ N.P.T. Hence, the ratio of the number of nuclei excited to the number of positrons emitted is $3.8\times10^{-6}/1.2\times10^{-6}$, or 3.2. A comparison between this result and Lamb's calculations supports the Fermi theory, provided that the change in nuclear spin is $\Delta i=1$, as Lamb has suggested. In order to distinguish convincingly between $\Delta i=0$ and $\Delta i=1$, a stronger Na^{22} sample than the one available for these experiments would have to be employed.

I am indebted to Dr. Emilio Segrè for his very helpful discussions during the entire course of this research.

[1] L. J. Laslett, Phys. Rev. **50**, 388(A) (1936).
[2] W. E. Lamb, Jr., Phys. Rev. **50**, 388 (A) (1936).
[3] L. W. Alvarez, Phys. Rev. **54**, 486 (1938).
[4] F. Paneth and K. Peters, Zeits. f. physik. Chemie **134**, 353 (1928).